Engineering Analysis with Boundary Elements 164 (2024) 105762

Contents lists available at ScienceDirect

Engineering Analysis with Boundary Elements

journal homepage: www.elsevier.com/locate/enganabound

Free vibration analysis of laminated anisotropic doubly-curved shell structures reinforced with three-phase polymer/CNT/fiber material

Francesco Tornabene *, Matteo Viscoti, Rossana Dimitri

Department of Innovation Engineering, School of Engineering, University of Salento, 73100 Lecce, Italy

ARTICLE INFO

KEYWORDS:
Anisotropic materials
Carbon nanotubes
Doubly-curved shells
Equivalent single layer
Generalized differential quadrature method
Higher order theories

ABSTRACT

The present work investigates the vibrational response of laminated anisotropic doubly-curved shell structures reinforced with Carbon Nanotubes (CNTs) short fibers. The fundamental equations are derived from a curvilinear reference system of principal coordinates, employing the Equivalent Single Layer (ESL) methodology. Furthermore, a general variation in laminate thickness is considered. The unknown field variable is described using higher order theories through the unified formulation, taking into account a general interpolation of the unknown variables with Lagrange polynomials across the physical domain. The Hamiltonian Principle is adopted for the derivation of the dynamic equilibrium equations, which arediscretized numerically by using the Generalized Differential Quadrature (GDQ) method. In addition, an efficient isogeometric NURBS-based mapping is adopted for the distortion of the physical domain. The boundary conditions of the differential problem are modelled through a general distribution of linear elastic springs along the lateral surfaces of the three-dimensional doubly-curved solid. The theory is then applied to study the vibrational modes of structures with different curvatures and lamination schemes, taking into account a general distribution of CNTs along the thickness direction. The homogenized properties of CNTs layers are obtained from the Mori-Tanaka procedure, which accounts for the agglomeration effects of the dispersed nanofibers within the matrix. Unlike previous studies focusing on doubly-curved shells reinforced with composite materials and CNTs, the present formulation enables to derive the vibration characteristics of structures made of generally anisotropic materials with general orientations. Furthermore, the calibration of the parameters for the linear elastic springs' distribution leads to general external constraints within a single element, thus reducing the computational cost of the problem.

1. Introduction

New advances in many engineering fields are very often based on the adoption of structural elements with complex shape which usually exhibit a non-conventional static and dynamic behavior. Moreover, innovative materials with enhanced properties are frequently used [1]. When employing classical modelling techniques for components made of these materials, advanced formulations are required, typically of high computational cost, particularly for structures with curved geometries [2]. Moreover, an optimization process encompassing both topology and material selection is usually conducted, thus obtaining structures with non-conventional shapes [3]. Within this framework, the numerical implementation should use highly efficient numerical techniques to ensure stable and accurate results even with a limited number of Degrees of Freedom (DOFs). This approach facilitates iterative simulations and sensitivity analyses in a relatively reduced time.

The Finite Element Method (FEM), extensively discussed in Refs. [4,5] among others, is well-known for its capability to provide very accurate results in several case studies. According to the FEM approach, pre-determined shape functions are used to describe the unknown field variable within the physical domain, which is discretized into a finite number of elements. As a consequence, the DOFs of the discrete problem are defined in the nodes of a pre-determined grid, and the solution of the governing equations is thus obtained from an algebraic linear system. The mathematical properties of the selected shape functions can significantly affect the accuracy and stability of the solution, especially when dealing with complex geometries and materials [6,7]. Previous studies have demonstrated the importance of an accurate geometric description for the accuracy of solutions. For this reason, the Isogeometric Analysis (IGA) adopts, for the implementation of the shape functions, the same functions used in the Computer Aided Design (CAD) process when the geometry is defined [8]. Generally speaking,

* Corresponding author.
E-mail address: francesco.tornabene@unisalento.it (F. Tornabene).

https://doi.org/10.1016/j.enganabound.2024.105762
Received 10 January 2024; Received in revised form 3 April 2024; Accepted 27 April 2024
Available online 14 May 2024

Non-Uniform Rational Basis Spline (NURBS) curves are used to this end, due to their versatility and computational stability [9,10]. On the other hand, when classical FEM is adopted, this issue can be partially overcome by increasing the number of DOFs, even though in this way the computational effort and calculation time significantly increase. In contrast, IGA yields highly accurate results with a limited number of DOFs.

In order to reduce the computational effort, the three-dimensional problem is usually investigated using refined two-dimensional formulations [11-12]. The Equivalent Single Layer (ESL) and the Layer-Wise (LW) approaches [13-16] adopt a pre-determined set of thickness functions to describe the field variable along the normal direction of the structure. Classical two-dimensional approaches such as Classical Plate Theory (CPT) [17], First Order Shear Deformation Theory (FSDT) [18] and Third order shear deformation theory (TSDT) [19] are examples of ESL theories [20-23]. When the ESL is applied to doubly-curved shell structures, a three-dimensional solid of general shape is reduced to a reference surface located at its middle thickness, while the LW approach requires a reference surface for each layer of the structure. As demonstrated in Ref. [24], ESL theories can be seen as specific cases of LW theories, therefore a general approach can be followed for the development of the formulation. When analyzing structures with very complicated lamination schemes by using a two-dimensional model, a higher order expansion of the three-dimensional field variable should be taken into account along the shell thickness, thus adopting the Higher Order Shear Deformation Theories (HSDTs) [25-27]. In this way, complex deformations arising from the presence of softcore regions can be effectively modelled. When the ESL assumption is applied to laminated structures, the typical piecewise continuous distributions of displacements and stresses, known as zigzag effect, [28] must be considered. To this purpose, a highly efficient methodology was introduced for the first time in Refs. [29,30], where the zigzag deformation is described in terms of a discrete variation in the inclination of the in-plane variable distributions. Another interesting approach named Refined Zigzag Theory (RZT) has been demonstrated to be highly efficient and accurate, as presented in Refs. [31-33]. According to the RZT, the thickness functions assigned to in-plane displacement field components are defined in terms of the shear properties of the layers in the stacking sequence, while a uniform distribution is associated with the out-of-plane displacement component. However, this approach is based on the assumption of orthotropic behavior of each layer of the structure and thus cannot be applied to generally anisotropic materials. When using two-dimensional HSDTs, a key aspect is the unified formulation [34-36], which adopts a generalized expression of the field variable with an expansion up to any desired order. This enables the derivation of the fundamental equations for a generic order, followed by an assembly process to consider the complete expansion of the unknown variable.

The adoption of higher order theories becomes crucial when considering highly innovative materials into the model. As shown in Refs. [37,38], the adoption of HSDTs, together with zigzag functions, is particularly important when analyzing sandwich panels characterized by a core made of honeycomb cells and grid patterns. Furthermore, some studies must be mentioned regarding HSDT formulations for doubly-curved structures made of Functionally Graded Materials (FGMs) [39-42]. Generally speaking, FGMs belong to the category of granular composites, and find extensive application in the aerospace, among others, due to their excellent thermal properties and their good structural performances. These materials are composed two different constituent materials, namely Ceramic (C) and Metal (M). Various distributions of the two phases can be obtained along the thickness direction depending on the adopted manufacturing process. The equivalent properties of the FGM are derived from a homogenization procedure accounting for the mechanical properties of the two constituents [43]. The through-the-thickness distribution of the volume fractions can be modelled using various analytical expressions. The governing parameters of each distribution can, thus, influence the vibrational and buckling response of FGM structures, as extensively demonstrated in Refs. [44-45]. In addition, the porosity of FGM layers resulting from voids can be modelled with different approaches, allowing for the study of their effects on the overall structural response [46]. More specifically, various through-the-thickness distributions of material porosity can be achieved, including both even and uneven dispersions of voids within the structure [47].

When composite layers are considered, carbon or glass long fibers are usually adopted for the reinforcing phase [48]. These fibers are dispersed within an isotropic polymer matrix, and the obtained material turns out to be orthotropic. Engineering constants for such materials are usually determined through experimental tests and theoretical models. Different approaches are employed for the homogenization of composite materials, depending on the assumptions on the constitutive relationship of the reinforcing fibers [49-52]. On the other hand, the mechanical properties of the isotropic polymer matrix can be also enhanced with a dispersion of Carbon Nanotubes (CNTs) [53-56]. It should be recalled that a CNT nanofiber is made of one or more carbon concentric layers. In the first case, the Single-Walled Carbon Nanotubes (SWCNT) are obtained, otherwise Multi-Walled Carbon Nanotubes (MWCNT) nanofibers are considered [57-61]. As it is well-known, a crucial aspect of the structural performance of this heterogeneous material is the stress transfer between matrix and long fibers. When CNT nanofibers are adopted, a novel reinforcing phase is present in addition to long fibers which are associated to a higher material scale. As a result, the mechanical properties of the matrix are enhanced, and, consequently, a better interaction between the matrix and the reinforcing phase is obtained. For this reason, some possible application fields can be found in civil engineering, especially for the structural rehabilitation of existing structures, where composite reinforcements with long fibers which exhibit very high stiffness in a soft matrix, therefore, the dispersion of CNT nanofibers can enhance the interaction between the matrix and the reinforcing phase. Furthermore, three-phase-CNT composite materials can be adopted in mechanical engineering problems, particularly in studying the mechanical response of structural components of complex shape, which must exhibit a very high stiffness within a confined space. As a result, the adoption of CNTs mitigates cracking within the composite material and prevents splitting of long-fibers reinforcing phases, thus enhancing the overall structural performances. The methodology for deriving the equivalent elastic properties of this material must consider the distribution of CNTs within the matrix, as well as their orientation and waviness [62-65]. It is usually assumed that CNTs are randomly oriented within the layer under consideration, thus a non-homogeneous isotropic material is obtained with enhanced material properties. In contrast, when a specific orientation of CNT is present, material symmetries emerge [62]. The mechanical properties of a single CNT obtained from molecular dynamics simulations are thus combined with those of the isotropic polymer matrix with the Mori-Tanaka approach [66]. However, some remarks should be made on the CNT dispersed phase, when the agglomeration of nanofibers is considered [67-70]. When randomly oriented carbon fibers are modelled with a generalized distribution along the thickness direction, it is referred to the so-called Functionally Graded Carbon Nanotube (FG-CNT) layer [71-73].

As far as the boundary conditions of the problem is concerned, classical constraints are usually modelled within a weak formulation by eliminating the corresponding DOFs from the assembled discrete matrix. On the other hand, when a strong formulation is adopted, external constraints are obtained together with the fundamental equations through the evaluation of the various energetic contributions. This enables the assignment of prescribed values for the displacement field and stress components in the boundary regions of the physical domain. Moreover, non-conventional boundary conditions can be modelled using a general distribution of springs with linear elastic behavior along the edges of the physical domain [74,75]. The adoption of higher order theories allows one to distribute these springs along the four lateral

surfaces of the three-dimensional shell structure, accounting for a general distribution with in-plane and out-of-plane components. In this way, the calibration of the parameters of the distribution can even allow one to simulate a point constraint within a single continuum element [76-78].

The numerical solution of a differential system is usually derived employing various approaches based on the weighted residual procedure [79,80]. Several studies in literature show how an approximate solution can be obtained by selecting a proper set of shape functions for evaluating the unknown field variable. However, the closed-form solutions [81] can be obtained only if the number of DOFs is increased [82]. Furthermore, classical FEM procedures are based on the approximation of the field variable within the elements of a pre-determined mesh, therefore a smooth solution cannot be guaranteed a priori. In contrast, if a higher order interpolation is adopted along the entire physical domain, the present issue can be overcome [83-85].

A more efficient numerical solution can be more efficiently achieved by employing a spectral collocation approach [86]. Among these methods, the Generalized Differential Quadrature (GDQ) [87-91] stands out for its ability to obtain very accurate and stable results with a reduced computational cost. Based on the Weierstrass interpolation theorem, the GDQ method provides an effective discretization of the derivatives for a generic function. The GDQ technique has been adopted with success in very complicated applications like singularities models, fracture mechanics, curved structures, innovative materials, and arbitrarily-shaped domains [92-97]. Furthermore, the Generalized Integral Quadrature (GIQ) method, derived from considerations on the GDQ numerical technique, enables efficient numerical integrations with a high level of accuracy, even though a reduced number of grid nodes are used [98-101]. Since both the GDQ and GIQ are based on higher order interpolations of the unknown function, the best results are obtained when non-uniform grids are selected, unlike classical numerical approaches.

In the present work, a novel formulation based on higher order theories is presented for the free vibration analysis of laminated doubly-curved shell structures of arbitrary shape. The generalized displacement field is described using Lagrange interpolating polynomials starting from the values assumed by these quantities on a non-uniform two-dimensional discrete grid [102-104]. Unlike other previous studies focusing on the dynamic analysis of laminated doubly-curved shell structures with higher order theories, the present study investigates the dynamic response of shell laminated structures with generally anisotropic materials reinforced by a dispersion of CNTs. Furthermore, the study investigates the effects on the vibrational response of structures reinforced with nanofibers generally distributed along the thickness direction. The dispersion of these nanofibers within each layer is described using a five-parameters polynomial expression. Since the present formulation is a continuum-based model, the equivalent elastic properties of the three-dimensional material are derived using the well-known Mori-Tanaka procedure, while long fibers embedded within the matrix are homogenized using the Halpin-Tsai theoretical model. The fundamental equations of the dynamic problem, derived from the Hamiltonian Principle, are numerically solved with the GDQ method with a non-uniform two-dimensional computational grid.

A systematic series of examples is presented to validate the theory against numerical predictions obtained from complicated three-dimensional FEM models. After that, an extensive parametric investigation is conducted on structures with different curvatures and arbitrary shape, pointing out the influence of the FG-CNTs distribution on the dynamic response. The present formulation, integrated into the DiQuMASPAB software [105], offers an efficient two-dimensional model with three-dimensional capabilities for vibrational analysis of layered doubly-curved structures characterized by a continuum smooth distribution of constituent materials along their thickness, taking into account both symmetric and unsymmetric profiles of material dispersion.

2. Geometry description

A doubly-curved shell structure has a three-dimensional nature within the Euclidean space. For this reason, three parameters $\alpha_1,\alpha_2,\alpha_3$ are required so that the position vector of any point of the region under consideration, denoted by $\mathbf{R}$, is univocally identified. Referring to a global Cartesian system $Ox_1x_2x_3$, the following relation can be considered [12]:

$$\mathbf{R}(\alpha_1,\alpha_2,\alpha_3)=\bar{f}_1(\alpha_1,\alpha_2,\alpha_3)\mathbf{e}_1+\bar{f}_2(\alpha_1,\alpha_2,\alpha_3)\mathbf{e}_2+\bar{f}_3(\alpha_1,\alpha_2,\alpha_3)\mathbf{e}_3 \tag{1}$$

where $\bar{f}_1,\bar{f}_2,\bar{f}_3$ are continuous smooth functions with a single value for each $\alpha_1,\alpha_2,\alpha_3$, which are the curvilinear coordinates of the solid under consideration. Furthermore, $\mathbf{e}_1,\mathbf{e}_2,\mathbf{e}_3$ denote the unit vectors of the axes x_1,x_2,x_3, respectively.

In accordance with the ESL approach outlined in Ref. [12], a reference surface $\mathbf{r}(\alpha_1,\alpha_2)$ is introduced at the middle thickness $h(\alpha_1,\alpha_2)$ of the solid described in Eqn. (1), while the parameter α_3 represents the thickness axis ζ. On the other hand, α_1 and α_2 denote curvilinear coordinates aligned with the reference surface parametric lines. As a result, the position vector of the shell can be expressed as:

$$\mathbf{R}(\alpha_1,\alpha_2,\zeta)=\mathbf{r}(\alpha_1,\alpha_2)+\frac{h(\alpha_1,\alpha_2)}{2}z\,\mathbf{n}(\alpha_1,\alpha_2) \tag{2}$$

where $z=2\zeta/h(\alpha_1,\alpha_2)$ is a dimensionless quantity, with $z\in[-1,1]$. Furthermore, coordinates α_1,α_2 vary within the rectangular interval of extremes α_i^0,α_i^1 with $i=1,2$, namely $\left[\alpha_1^0,\alpha_1^1\right]\times\left[\alpha_2^0,\alpha_2^1\right]$. The thickness axis ζ is aligned at each point of the reference surface to its outward normal direction, whose unit vector $\mathbf{n}(\alpha_1,\alpha_2)$ is computed as follows [12]:

$$\mathbf{n}=\frac{\mathbf{r}_{,1}\times\mathbf{r}_{,2}}{\left|\mathbf{r}_{,1}\times\mathbf{r}_{,2}\right|} \tag{3}$$

In the previous relation, the symbols $\mathbf{r}_{,i}=\partial\mathbf{r}/\partial\alpha_i$ for $i=1,2$ denote the partial derivative of the reference surface equation with respect to the principal coordinates $\alpha_i=\alpha_1,\alpha_2$, whereas $\times$ stands for the well-known vector cross product. Nevertheless, the notation $\mathbf{r}_{,ij}=\partial^2\mathbf{r}/\left(\partial\alpha_i\partial\alpha_j\right)$ with $i,j=1,2$ is adopted for the identification of second-order partial derivatives of $\mathbf{r}(\alpha_1,\alpha_2)$. The principal radii of curvature of the shell $R_1(\alpha_1,\alpha_2)$ and $R_2(\alpha_1,\alpha_2)$, referred to α_1,α_2 directions, can be computed according to the following relations:

$$R_1=-\frac{\mathbf{r}_{,1}\cdot\mathbf{r}_{,1}}{\mathbf{r}_{,11}\cdot\mathbf{n}},\quad R_2=-\frac{\mathbf{r}_{,2}\cdot\mathbf{r}_{,2}}{\mathbf{r}_{,22}\cdot\mathbf{n}} \tag{4}$$

Furthermore, the Lamè parameters $A_1(\alpha_1,\alpha_2)$ and $A_2(\alpha_1,\alpha_2)$ are defined in each point of the reference surface as follows:

$$A_1=\sqrt{\mathbf{r}_{,1}\cdot\mathbf{r}_{,1}},\quad A_2=\sqrt{\mathbf{r}_{,2}\cdot\mathbf{r}_{,2}} \tag{5}$$

Referring to the outward normal direction, a useful scaling parameter $H_i(\alpha_1,\alpha_2,\zeta)$ can be defined, thus allowing to consider the effects of curvature in the model [12]:

$$H_i=1+\frac{\zeta}{R_i} \tag{6}$$

Starting from Eqn. (2), if the shell structure under consideration is composed of l laminae, the total thickness $h(\alpha_1,\alpha_2)$ is computed as the sum of the thickness $h_k(\alpha_1,\alpha_2)$ of each k-th layer, for $k=1,\ldots,l$:

$$h(\alpha_1,\alpha_2)=\sum_{k=1}^{l}h_k(\alpha_1,\alpha_2)=\sum_{k=1}^{l}\left(\zeta_{k+1}(\alpha_1,\alpha_2)-\zeta_k(\alpha_1,\alpha_2)\right) \tag{7}$$

where ζ_k,ζ_{k+1} denote the location of the bottom and the top faces of the k-th layer of the shell along the outward normal direction, respectively.

In the present study, a general profile of the shell thickness is modelled. To this end, normalized coordinates $\overline{\alpha}_1, \overline{\alpha}_2$ are introduced [12] along the shell principal directions, according to the following relations:

$$\overline{\alpha}_1 = \frac{\alpha_1 - \alpha_1^0}{\alpha_1^1 - \alpha_1^0}, \quad \overline{\alpha}_2 = \frac{\alpha_2 - \alpha_2^0}{\alpha_2^1 - \alpha_2^0} \tag{8}$$

Furthermore, the quantity $\widetilde{\alpha}_i = 1 - \overline{\alpha}_i$ for $i = 1, 2$ is conveniently defined. A general thickness variation law $\widehat{h}(\alpha_1, \alpha_2)$ is assessed starting from some univariate analytical expressions $\phi_i(\alpha_1, \alpha_2)$ for $i = 1, .., 4$, defined in terms of the position and shape parameters $\alpha_{im} \in [0, 1]$ and $n_i \in \mathbb{N}$, respectively, while $p_i \in \mathbb{R}$ denotes a power exponent [12]:

$$\begin{aligned}
\phi_1(\alpha_1, \alpha_2) &= \begin{cases} \overline{\alpha}_1^{\,p_1} \\ (\sin(\pi(n_1\overline{\alpha}_1 + \alpha_{1m})))^{p_1} \end{cases}, \quad \phi_2(\alpha_1, \alpha_2) = \begin{cases} \overline{\alpha}_2^{\,p_2} \\ (\sin(\pi(n_2\overline{\alpha}_2 + \alpha_{2m})))^{p_2} \end{cases} \\
\phi_3(\alpha_1, \alpha_2) &= \begin{cases} \widetilde{\alpha}_1^{\,p_3} \\ (\sin(\pi(n_3\widetilde{\alpha}_1 + \alpha_{3m})))^{p_3} \end{cases}, \quad \phi_4(\alpha_1, \alpha_2) = \begin{cases} \widetilde{\alpha}_2^{\,p_4} \\ (\sin(\pi(n_4\widetilde{\alpha}_2 + \alpha_{4m})))^{p_4} \end{cases}
\end{aligned} \tag{9}$$

In this way, a general variation of the thickness of a generic k-th layer within the physical domain $[\alpha_1^0, \alpha_1^1] \times [\alpha_2^0, \alpha_2^1]$ can be computed as [12]:

$$h_k(\alpha_1, \alpha_2) = h_k^0 \widehat{h}(\alpha_1, \alpha_2) = h_k^0 \left(1 + \overline{\delta} + \sum_{i=1}^{4} \delta_i \phi_i(\alpha_1, \alpha_2)\right) \tag{10}$$

where h_k^0 for $k = 1, ..., l$ is the reference thickness value, whereas $\overline{\delta}$ and δ_i are position and scaling parameters, respectively, for $i = 1, ..., 4$.

All these geometric quantities are defined in a two-dimensional grid of $I_N \times I_M$ nodes selected from the physical domain $[\alpha_1^0, \alpha_1^1] \times [\alpha_2^0, \alpha_2^1]$ of the shell under consideration. The generic coordinate of the node $(\alpha_{1f}, \alpha_{2g})$ with $f = 1, ..., I_N$ and $g = 1, ..., I_M$ of the grid at issue is given by the following relation:

$$\begin{aligned}
\alpha_{1f} &= \frac{\alpha_1^1 - \alpha_1^0}{r_{I_N} - r_1}(r_f - r_1) + \alpha_1^0 \\
\alpha_{2f} &= \frac{\alpha_2^1 - \alpha_2^0}{r_{I_M} - r_1}(r_g - r_1) + \alpha_2^0
\end{aligned} \tag{11}$$

where $r_f = r_1, ..., r_{I_N}$ and $r_g = r_1, ..., r_{I_M}$ depend on the selected point distribution. In the present work, the Legendre-Gauss-Lobatto (LGL) distribution is selected, since in some previous studies [12,85] its reliability has been checked when applied to higher order models with the weak form. The LGL distribution of I_P points is obtained finding the roots of the LGL polynomials, denoted by $LGL_{I_P+1}(\xi_r)$:

$$\begin{aligned}
LGL_{I_P+1}(\xi_r) &= (1 - \xi_r^2) A_{I_P-1}(\xi_r) \\
&= (1 - \xi_r^2) \frac{d}{d\xi_r}(L_{I_P}(\xi_r)) \quad \begin{array}{l} \text{for } I_P = I_N, I_M, \\ \text{for } r = 1, 2, \\ \text{for } \xi_r \in [-1, 1] \end{array}
\end{aligned} \tag{12}$$

where A_{I_P-1} and L_{I_P} are the Lobatto and Legendre polynomials, respectively. The Legendre polynomials are computed employing the following recursive formula, setting $L_1(\xi_r) = 1$ and $L_2(\xi_r) = \xi_r$:

$$L_{I_P}(\xi_r) = \frac{(2I_P - 3)\xi_r L_{I_P-1}(\xi_r) - (I_P - 2)L_{I_P-2}(\xi_r)}{I_P - 1} \quad \begin{array}{l} \text{for } I_P = I_N, I_M, \\ \text{for } r = 1, 2, \\ \text{for } \xi_r \in [-1, 1] \end{array} \tag{13}$$

3. Kinematic relations in the weak form

In this section the higher order assumption of the kinematic field variable is evaluated within the ESL framework. According to this methodology, a generalized expansion of the three-dimensional displacement field vector $\mathbf{U}^{(k)}(\alpha_1, \alpha_2, \zeta, t) = \left[U_1^{(k)} \; U_2^{(k)} \; U_3^{(k)}\right]^T$ up to the $(N + 1)$-th order is considered. More specifically, generalized thickness functions $F^{(k\tau)\alpha_1}, F^{(k\tau)\alpha_2}, F^{(k\tau)\alpha_3}$ are introduced for each $\tau = 0, ..., N + 1$, and the following expression is derived [24]:

$$\begin{bmatrix} U_1^{(k)} \\ U_2^{(k)} \\ U_3^{(k)} \end{bmatrix} = \sum_{\tau=0}^{N+1} \begin{bmatrix} F^{(k\tau)\alpha_1} & 0 & 0 \\ 0 & F^{(k\tau)\alpha_2} & 0 \\ 0 & 0 & F^{(k\tau)\alpha_3} \end{bmatrix} \begin{bmatrix} u_1^{(\tau)} \\ u_2^{(\tau)} \\ u_3^{(\tau)} \end{bmatrix} \tag{14}$$

Employing a compact notation, Eqn. (14) can be written as:

$$\mathbf{U}^{(k)}(\alpha_1, \alpha_2, \zeta, t) = \sum_{\tau=0}^{N+1} \mathbf{F}^{(k\tau)}(\zeta) \mathbf{u}^{(\tau)}(\alpha_1, \alpha_2, t) \tag{15}$$

The three-dimensional displacement field vector is, thus, expressed in terms of generalized displacement field components, which are collected, for each $\tau = 0, ..., N + 1$, in the vector $\mathbf{u}^{(\tau)}(\alpha_1, \alpha_2, t) = \left[u_1^{(\tau)} \; u_2^{(\tau)} \; u_3^{(\tau)}\right]^T$. This allows for a generalized axiomatic assumption of the displacement field components. Furthermore, classical approaches like the TSDT and FSDT can be considered in the model if the displacement field expansion is carefully selected. In the present work, thickness functions with a polynomial expression [12] are adopted for the description of the unknown field variable up to $\tau = N$, whereas the interlaminar issues are addressed in Eqn. (15) with the generalized zigzag function assigned to the $\tau = (N + 1)$-th kinematic expansion order:

$$F^{(k\tau)\alpha_i}(\zeta) = \begin{cases} \zeta^{\tau} & \text{for } \tau = 0, ..., N \\ (-1)^k z_k = (-1)^k \dfrac{2}{\zeta_{k+1} - \zeta_k}\zeta - \dfrac{\zeta_{k+1} + \zeta_k}{\zeta_{k+1} - \zeta_k} & \text{for } \tau = N + 1 \end{cases} \tag{16}$$

The nomenclature ED(Z) − N is conveniently introduced to identify the displacement field assumption within the higher order ESL model. In particular, E indicates that the ESL approach is adopted with an expansion up to the N-th order, whereas D means that a displacement-based formulation is developed. When the zigzag function is included within the thickness functions set, the symbol Z is used.

The unknown generalized displacement field components $u_1^{(\tau)}$, $u_2^{(\tau)}$, $u_3^{(\tau)}$ referred to a generic τ-th kinematic expansion order are described with generalized two-dimensional shape functions starting from the values assumed at the discrete nodes of Eqn. (11). The Lagrange interpolating polynomials $l_f(\alpha_1), l_g(\alpha_2)$ of degree $I_N - 1$ and $I_M - 1$, respectively, are adopted for the interpolation. Following the definition of Ref. [12], they assume the following aspect:

$$l_f(\alpha_1) = \frac{\prod_{i=1}^{I_N}(\alpha_1 - \alpha_{1i})}{(\alpha_1 - \alpha_{1f})\prod_{i=1,\ i\neq f}^{I_N}(\alpha_{1f} - \alpha_{1i})}, \quad l_g(\alpha_2) = \frac{\prod_{j=1}^{I_M}(\alpha_2 - \alpha_{2j})}{(\alpha_2 - \alpha_{2g})\prod_{j=1,\ j\neq g}^{I_M}(\alpha_{2g} - \alpha_{2j})} \tag{17}$$

The values assumed by the Lagrange polynomials on the discrete grid along α_1 and α_2 principal directions are I_N and I_M, respectively. It is useful to introduce the vectors $\mathbf{l}_{\alpha_1}$ and $\mathbf{l}_{\alpha_2}$ accounting for the values assumed by the Lagrange polynomials of Eqn. (17) in the discrete grid of I_N and I_M nodes, respectively:

$$\begin{aligned}\mathbf{l}_{\alpha_1} &= \begin{bmatrix} l_1(\alpha_1) & \dots & l_f(\alpha_1) & \dots & l_{I_N}(\alpha_1)\end{bmatrix}\\ \mathbf{l}_{\alpha_2} &= \begin{bmatrix} l_1(\alpha_2) & \dots & l_g(\alpha_2) & \dots & l_{I_M}(\alpha_2)\end{bmatrix}\end{aligned} \tag{18}$$

For the sake of completeness, in the following the vectors $\mathbf{l}^{(1)}_{\alpha_1}$ and $\mathbf{l}^{(1)}_{\alpha_2}$ of dimensions $1 \times I_N$ and $1 \times I_M$, respectively, account for the first order derivatives with respect to α_1 and α_2 of the Lagrange polynomials, setting $l^{(1)}_f(\alpha_1) = \partial l_f / \partial\alpha_1$ and $l^{(1)}_g(\alpha_2) = \partial l_g / \partial\alpha_2$ with $f = 1, \dots, I_N$ and $g = 1, \dots, I_M$:

$$\begin{aligned}\mathbf{l}^{(1)}_{\alpha_1} &= \begin{bmatrix} l^{(1)}_1(\alpha_1) & \dots & l^{(1)}_f(\alpha_1) & \dots & l^{(1)}_{I_N}(\alpha_1)\end{bmatrix}\\ \mathbf{l}^{(1)}_{\alpha_2} &= \begin{bmatrix} l^{(1)}_1(\alpha_2) & \dots & l^{(1)}_g(\alpha_2) & \dots & l^{(1)}_{I_M}(\alpha_2)\end{bmatrix}\end{aligned} \tag{19}$$

The generalized displacement field components $u^{(\tau)}_1(\alpha_1,\alpha_2,t)$, $u^{(\tau)}_2(\alpha_1,\alpha_2,t)$, $u^{(\tau)}_3(\alpha_1,\alpha_2,t)$ are thus expressed, for each τ-th kinematic expansion order, in terms of the values assumed in the two-dimensional grid introduced previously, denoted by $u^{(\tau)}_1(\alpha_{1f},\alpha_{2g},t)$, $u^{(\tau)}_2(\alpha_{1f},\alpha_{2g},t)$, $u^{(\tau)}_3(\alpha_{1f},\alpha_{2g},t)$:

$$\begin{bmatrix} u^{(\tau)}_1(\alpha_1,\alpha_2,t)\\ u^{(\tau)}_2(\alpha_1,\alpha_2,t)\\ u^{(\tau)}_3(\alpha_1,\alpha_2,t)\end{bmatrix} = \sum_{f=1}^{I_N}\sum_{g=1}^{I_M}\begin{bmatrix} l_f(\alpha_1)l_g(\alpha_2) & 0 & 0\\ 0 & l_f(\alpha_1)l_g(\alpha_2) & 0\\ 0 & 0 & l_f(\alpha_1)l_g(\alpha_2)\end{bmatrix}\begin{bmatrix} u^{(\tau)}_1(\alpha_{1f},\alpha_{2g},t)\\ u^{(\tau)}_2(\alpha_{1f},\alpha_{2g},t)\\ u^{(\tau)}_3(\alpha_{1f},\alpha_{2g},t)\end{bmatrix} \tag{20}$$

Employing a compact matrix notation, the following relation is obtained, where $\mathbf{N}^T$ is a matrix containing the generalized shape functions whereas $\overline{\mathbf{u}}^{(\tau)}(\alpha_{1f},\alpha_{2g},t)$ is a column vector of dimensions $(3I_NI_M) \times 1$ collecting the nodal kinematic unknowns [85]:

$$\mathbf{u}^{(\tau)} = \mathbf{N}^T\overline{\mathbf{u}}^{(\tau)} \tag{21}$$

The vector $\overline{\mathbf{u}}^{(\tau)}$ is assembled, for each $\tau = 0, \dots, N+1$, starting from the sub-vectors $\overline{\mathbf{u}}^{(\tau)}_i$ with $i = 1, 2, 3$ containing each generalized displacement field component $u^{(\tau)}_i$ evaluated in the discrete nodes $(\alpha_{1f},\alpha_{2g})$ with $f = 1, \dots, I_N$ and $g = 1, \dots, I_M$. In this way, the components of $\overline{\mathbf{u}}^{(\tau)}$, denoted by $u^{(\tau)}_{i(fg)}$ with $i = 1, 2, 3$, turn out to be the DOFs of the problem under consideration. To this purpose, a vectorization operation by-column [12] is conveniently introduced. If $\mathbf{A}$ denotes a generic matrix of dimensions $I_N \times I_M$, with generic element A_{ij}, a column vector $\overrightarrow{\mathbf{A}}$ of dimensions $I_NI_M \times 1$ can be introduced, defined as:

$$\overrightarrow{\mathbf{A}} = \mathrm{Vec}(\mathbf{A}) \ \Leftrightarrow\ A_k = \left(A_{ij}\right)_k \tag{22}$$

As it can be seen, the quantity $k = i + (j-1)I_N$ with $k = 1, \dots, I_NI_M$ is introduced so that a rearrangement of the matrix indexes i, j is performed. In this way, the vector $\overline{\mathbf{u}}^{(\tau)}$ looks as follows:

$$\overline{\mathbf{u}}^{(\tau)} = \begin{bmatrix}\overrightarrow{\mathbf{u}}^{(\tau)}_1\\ \overrightarrow{\mathbf{u}}^{(\tau)}_2\\ \overrightarrow{\mathbf{u}}^{(\tau)}_3\end{bmatrix} \tag{23}$$

where vectors $\overrightarrow{\mathbf{u}}^{(\tau)}_i = \overrightarrow{\mathbf{u}}^{(\tau)}_1, \overrightarrow{\mathbf{u}}^{(\tau)}_2, \overrightarrow{\mathbf{u}}^{(\tau)}_3$, defined by means of the vectorization operation of Eqn. (22), collect the values $u^{(\tau)}_{i(fg)} = u^{(\tau)}_{1(fg)}, u^{(\tau)}_{2(fg)}, u^{(\tau)}_{3(fg)}$ associated to the discrete grid points with $f = 1, \dots, I_N$ and $g = 1, \dots, I_M$:

$$\begin{aligned}\overrightarrow{\mathbf{u}}^{(\tau)}_i &= \mathrm{Vec}\left(\mathbf{u}^{(\tau)}_i\right)\\ &= \left[u^{(\tau)}_{i(11)} \ \cdots\ u^{(\tau)}_{i(I_N1)}\ u^{(\tau)}_{i(12)} \ \cdots\ u^{(\tau)}_{i(I_N2)}\ u^{(\tau)}_{i(1I_M)} \ \cdots\ u^{(\tau)}_{i(I_NI_M)}\right]^T \quad \text{for } i = 1,2,3\end{aligned} \tag{24}$$

Furthermore, a matrix $\mathbf{N}^T$ of dimensions $3 \times (3I_NI_M)$ is defined to collect the generalized shape functions, starting from the Kronecker product $\overline{\mathbf{N}}^T = \mathbf{l}_{\alpha_2} \otimes \mathbf{l}_{\alpha_1}$ of the vectors $\mathbf{l}_{\alpha_1}$ and $\mathbf{l}_{\alpha_2}$, according to Ref. [12]:

$$\mathbf{N}^T = \begin{bmatrix}\overline{\mathbf{N}}^T & 0 & 0\\ 0 & \overline{\mathbf{N}}^T & 0\\ 0 & 0 & \overline{\mathbf{N}}^T\end{bmatrix} = \begin{bmatrix}\mathbf{l}_{\alpha_2}\otimes\mathbf{l}_{\alpha_1} & 0 & 0\\ 0 & \mathbf{l}_{\alpha_2}\otimes\mathbf{l}_{\alpha_1} & 0\\ 0 & 0 & \mathbf{l}_{\alpha_2}\otimes\mathbf{l}_{\alpha_1}\end{bmatrix} \tag{25}$$

Substituting the generalized interpolation of Eqn. (21) in the higher order ESL model of Eqn. (15), the three-dimensional displacement field vector $\mathbf{U}^{(k)}(\alpha_1,\alpha_2,\zeta,t) = \left[U^{(k)}_1\ U^{(k)}_2\ U^{(k)}_3\right]^T$ is expressed as follows:

$$\mathbf{U}^{(k)}(\alpha_1,\alpha_2,\zeta,t) = \sum_{\tau=0}^{N+1}\mathbf{F}^{(k\tau)}\mathbf{u}^{(\tau)} = \sum_{\tau=0}^{N+1}\mathbf{F}^{(k\tau)}\mathbf{N}^T\overline{\mathbf{u}}^{(\tau)} \tag{26}$$

The kinematic relation for a doubly-curved shell solid is considered to express the three-dimensional strain vector defined in each k-th layer of the structure, denoted by $\boldsymbol{\varepsilon}^{(k)}(\alpha_1, \alpha_2, \zeta, t) = \left[\varepsilon^{(k)}_1\ \varepsilon^{(k)}_2\ \gamma^{(k)}_{12}\ \gamma^{(k)}_{13}\ \gamma^{(k)}_{23}\ \varepsilon^{(k)}_3\right]^T$, in terms of the vector $\mathbf{U}^{(k)}(\alpha_1,\alpha_2,\zeta,t)$ and a differential operator $\mathbf{D}$:

$$\boldsymbol{\varepsilon}^{(k)} = \mathbf{D}\,\mathbf{U}^{(k)} = \mathbf{D}_\zeta\left(\sum_{i=1}^{3}\mathbf{D}^{\alpha_i}_\Omega\right)\mathbf{U}^{(k)} \tag{27}$$

In the previous relation, the differential operator $\mathbf{D}$ is expressed in terms of the operators $\mathbf{D}_\zeta$ and $\mathbf{D}_\Omega^{\alpha_i} = \mathbf{D}_\Omega^{\alpha_1}, \mathbf{D}_\Omega^{\alpha_2}, \mathbf{D}_\Omega^{\alpha_3}$, accounting for the partial derivatives with respect to the thickness direction ζ and the principal coordinates α_1,α_2. In the following, an extended version of the operators at issue is reported:

$$\mathbf{D}_\zeta = \begin{bmatrix} \frac{1}{H_1} & 0 & 0 & 0 & 0 & 0 & 0 & 0 & 0 \\ 0 & \frac{1}{H_2} & 0 & 0 & 0 & 0 & 0 & 0 & 0 \\ 0 & 0 & \frac{1}{H_1} & \frac{1}{H_2} & 0 & 0 & 0 & 0 & 0 \\ 0 & 0 & 0 & 0 & \frac{1}{H_1} & 0 & \frac{\partial}{\partial\zeta} & 0 & 0 \\ 0 & 0 & 0 & 0 & 0 & \frac{1}{H_2} & 0 & \frac{\partial}{\partial\zeta} & 0 \\ 0 & 0 & 0 & 0 & 0 & 0 & 0 & 0 & \frac{\partial}{\partial\zeta} \end{bmatrix} \tag{28}$$

$$\begin{aligned} \mathbf{D}_\Omega^{\alpha_1} &= [\overline{\mathbf{D}}_\Omega^{\alpha_1}\ \mathbf{0}\ \mathbf{0}] \\ \mathbf{D}_\Omega^{\alpha_2} &= [\mathbf{0}\ \overline{\mathbf{D}}_\Omega^{\alpha_2}\ \mathbf{0}] \\ \mathbf{D}_\Omega^{\alpha_3} &= [\mathbf{0}\ \mathbf{0}\ \overline{\mathbf{D}}_\Omega^{\alpha_3}] \end{aligned} \tag{29}$$

where the sub-operators $\overline{\mathbf{D}}_\Omega^{\alpha_1}, \overline{\mathbf{D}}_\Omega^{\alpha_2}, \overline{\mathbf{D}}_\Omega^{\alpha_3}$ are defined as follows:

$$\begin{aligned} \overline{\mathbf{D}}_\Omega^{\alpha_1} &= \left[(\overline{\mathbf{D}}_\Omega^{\alpha_1})_1 \ \ (\overline{\mathbf{D}}_\Omega^{\alpha_1})_2 \ \ (\overline{\mathbf{D}}_\Omega^{\alpha_1})_3 \ \ (\overline{\mathbf{D}}_\Omega^{\alpha_1})_4 \ \ (\overline{\mathbf{D}}_\Omega^{\alpha_1})_5 \ \ (\overline{\mathbf{D}}_\Omega^{\alpha_1})_6 \ \ (\overline{\mathbf{D}}_\Omega^{\alpha_1})_7 \ \ (\overline{\mathbf{D}}_\Omega^{\alpha_1})_8 \ \ (\overline{\mathbf{D}}_\Omega^{\alpha_1})_9 \right]^T \\ \overline{\mathbf{D}}_\Omega^{\alpha_2} &= \left[(\overline{\mathbf{D}}_\Omega^{\alpha_2})_1 \ \ (\overline{\mathbf{D}}_\Omega^{\alpha_2})_2 \ \ (\overline{\mathbf{D}}_\Omega^{\alpha_2})_3 \ \ (\overline{\mathbf{D}}_\Omega^{\alpha_2})_4 \ \ (\overline{\mathbf{D}}_\Omega^{\alpha_2})_5 \ \ (\overline{\mathbf{D}}_\Omega^{\alpha_2})_6 \ \ (\overline{\mathbf{D}}_\Omega^{\alpha_2})_7 \ \ (\overline{\mathbf{D}}_\Omega^{\alpha_2})_8 \ \ (\overline{\mathbf{D}}_\Omega^{\alpha_2})_9 \right]^T \\ \overline{\mathbf{D}}_\Omega^{\alpha_3} &= \left[(\overline{\mathbf{D}}_\Omega^{\alpha_3})_1 \ \ (\overline{\mathbf{D}}_\Omega^{\alpha_3})_2 \ \ (\overline{\mathbf{D}}_\Omega^{\alpha_3})_3 \ \ (\overline{\mathbf{D}}_\Omega^{\alpha_3})_4 \ \ (\overline{\mathbf{D}}_\Omega^{\alpha_3})_5 \ \ (\overline{\mathbf{D}}_\Omega^{\alpha_3})_6 \ \ (\overline{\mathbf{D}}_\Omega^{\alpha_3})_7 \ \ (\overline{\mathbf{D}}_\Omega^{\alpha_3})_8 \ \ (\overline{\mathbf{D}}_\Omega^{\alpha_3})_9 \right]^T \end{aligned} \tag{30}$$

In the previous relation, quantities $(\overline{\mathbf{D}}_\Omega^{\alpha_i})_j$ for $i = 1, 2, 3$ and $j = 1, ..., 9$, read as:

$$\begin{aligned} (\overline{\mathbf{D}}_\Omega^{\alpha_1})_1 = (\overline{\mathbf{D}}_\Omega^{\alpha_2})_3 = (\overline{\mathbf{D}}_\Omega^{\alpha_3})_5 = \frac{1}{A_1}\frac{\partial}{\partial\alpha_1},\ (\overline{\mathbf{D}}_\Omega^{\alpha_1})_4 = (\overline{\mathbf{D}}_\Omega^{\alpha_2})_2 = (\overline{\mathbf{D}}_\Omega^{\alpha_3})_6 = \frac{1}{A_2}\frac{\partial}{\partial\alpha_2}, \\ (\overline{\mathbf{D}}_\Omega^{\alpha_1})_3 = (\overline{\mathbf{D}}_\Omega^{\alpha_2})_1 = -\frac{1}{A_1A_2}\frac{\partial A_1}{\partial\alpha_2},\ (\overline{\mathbf{D}}_\Omega^{\alpha_1})_2 = -(\overline{\mathbf{D}}_\Omega^{\alpha_2})_4 = \frac{1}{A_1A_2}\frac{\partial A_2}{\partial\alpha_1}, \\ (\overline{\mathbf{D}}_\Omega^{\alpha_1})_5 = -(\overline{\mathbf{D}}_\Omega^{\alpha_3})_1 = -\frac{1}{R_1},\ (\overline{\mathbf{D}}_\Omega^{\alpha_2})_6 = -(\overline{\mathbf{D}}_\Omega^{\alpha_3})_2 = -\frac{1}{R_2},\ (\overline{\mathbf{D}}_\Omega^{\alpha_1})_7 = (\overline{\mathbf{D}}_\Omega^{\alpha_2})_8 = (\overline{\mathbf{D}}_\Omega^{\alpha_3})_9 = 1, \\ (\overline{\mathbf{D}}_\Omega^{\alpha_1})_6 = (\overline{\mathbf{D}}_\Omega^{\alpha_1})_8 = (\overline{\mathbf{D}}_\Omega^{\alpha_1})_9 = (\overline{\mathbf{D}}_\Omega^{\alpha_2})_5 = (\overline{\mathbf{D}}_\Omega^{\alpha_2})_7 = (\overline{\mathbf{D}}_\Omega^{\alpha_2})_9 = (\overline{\mathbf{D}}_\Omega^{\alpha_3})_3 = (\overline{\mathbf{D}}_\Omega^{\alpha_3})_4 = (\overline{\mathbf{D}}_\Omega^{\alpha_3})_7 = (\overline{\mathbf{D}}_\Omega^{\alpha_3})_8 = 0 \end{aligned} \tag{31}$$

The kinematic relations of Eqn. (27) referred to a three-dimensional solid are embedded in the present higher order ESL model of Eqn. (26) by means of the operator $\mathbf{Z}^{(k\tau)\alpha_i} = \mathbf{D}_\zeta F^{(k\tau)\alpha_i}$, as follows [12]:

$$\boldsymbol{\varepsilon}^{(k)} = \sum_{\tau=0}^{N+1}\sum_{i=1}^{3} \mathbf{D}_\zeta \mathbf{D}_\Omega^{\alpha_i} \mathbf{F}^{(k\tau)} \mathbf{u}^{(\tau)} = \sum_{\tau=0}^{N+1}\sum_{i=1}^{3} \mathbf{Z}^{(k\tau)\alpha_i} \mathbf{D}_\Omega^{\alpha_i} \mathbf{u}^{(\tau)} = \sum_{\tau=0}^{N+1}\sum_{i=1}^{3} \mathbf{Z}^{(k\tau)\alpha_i} \boldsymbol{\varepsilon}^{(\tau)\alpha_i} \tag{32}$$

where the generalized displacement field vector $\boldsymbol{\varepsilon}^{(\tau)\alpha_i} = \left[\varepsilon_1^{(\tau)\alpha_i}\ \varepsilon_2^{(\tau)\alpha_i}\ \gamma_1^{(\tau)\alpha_i}\ \gamma_2^{(\tau)\alpha_i}\ \gamma_{13}^{(\tau)\alpha_i}\ \gamma_{23}^{(\tau)\alpha_i}\ \omega_{13}^{(\tau)\alpha_i}\ \omega_{23}^{(\tau)\alpha_i}\ \varepsilon_3^{(\tau)\alpha_i}\right]^T$ is defined in each point of the reference surface, for each τ-th kinematic expansion order, taking into account the generalized interpolation with Lagrange polynomials according to Eqn. (21):

$$\boldsymbol{\varepsilon}^{(\tau)\alpha_i} = \mathbf{D}_\Omega^{\alpha_i} \mathbf{u}^{(\tau)} = \mathbf{D}_\Omega^{\alpha_i} \mathbf{N}^T \overline{\mathbf{u}}^{(\tau)} = \mathbf{B}^{\alpha_i} \overline{\mathbf{u}}^{(\tau)} \tag{33}$$

where

$$\begin{aligned} \mathbf{B}_\Omega^{\alpha_1} &= [\overline{\mathbf{B}}_\Omega^{\alpha_1}\ \mathbf{0}\ \mathbf{0}] \\ \mathbf{B}_\Omega^{\alpha_2} &= [\mathbf{0}\ \overline{\mathbf{B}}_\Omega^{\alpha_2}\ \mathbf{0}] \\ \mathbf{B}_\Omega^{\alpha_3} &= [\mathbf{0}\ \mathbf{0}\ \overline{\mathbf{B}}_\Omega^{\alpha_3}] \end{aligned} \tag{34}$$

Finally, the operators $\overline{\mathbf{B}}^{\alpha_i} = \overline{\mathbf{B}}^{\alpha_1}, \overline{\mathbf{B}}^{\alpha_2}, \overline{\mathbf{B}}^{\alpha_3}$ of dimensions $9 \times (I_N I_M)$ are computed in the following by means of the Kronecker product, according to the extensive procedure reported in Ref. [85]:

$$\overline{\mathbf{B}}^{\alpha_1} = \begin{bmatrix} \frac{1}{A_1}\mathbf{l}_{\alpha_2} \otimes \mathbf{l}^{(1)}_{\alpha_1} \\ \frac{1}{A_1A_2}\frac{\partial A_2}{\partial \alpha_1}\mathbf{l}_{\alpha_2} \otimes \mathbf{l}_{\alpha_1} \\ -\frac{1}{A_1A_2}\frac{\partial A_1}{\partial \alpha_2}\mathbf{l}_{\alpha_2} \otimes \mathbf{l}_{\alpha_1} \\ \frac{1}{A_2}\mathbf{l}^{(1)}_{\alpha_2} \otimes \mathbf{l}_{\alpha_1} \\ -\frac{1}{R_1}\mathbf{l}_{\alpha_2} \otimes \mathbf{l}_{\alpha_1} \\ 0 \\ \mathbf{l}_{\alpha_2} \otimes \mathbf{l}_{\alpha_1} \\ 0 \\ 0 \end{bmatrix}, \quad \overline{\mathbf{B}}^{\alpha_2} = \begin{bmatrix} \frac{1}{A_1A_2}\frac{\partial A_1}{\partial \alpha_2}\mathbf{l}_{\alpha_2} \otimes \mathbf{l}_{\alpha_1} \\ \frac{1}{A_2}\mathbf{l}^{(1)}_{\alpha_2} \otimes \mathbf{l}_{\alpha_1} \\ \frac{1}{A_1}\mathbf{l}_{\alpha_2} \otimes \mathbf{l}^{(1)}_{\alpha_1} \\ -\frac{1}{A_1A_2}\frac{\partial A_2}{\partial \alpha_1}\mathbf{l}_{\alpha_2} \otimes \mathbf{l}_{\alpha_1} \\ 0 \\ -\frac{1}{R_2}\mathbf{l}_{\alpha_2} \otimes \mathbf{l}_{\alpha_1} \\ 0 \\ \mathbf{l}_{\alpha_2} \otimes \mathbf{l}_{\alpha_1} \\ 0 \end{bmatrix}, \quad \overline{\mathbf{B}}^{\alpha_3} = \begin{bmatrix} \frac{1}{R_1}\mathbf{l}_{\alpha_2} \otimes \mathbf{l}_{\alpha_1} \\ \frac{1}{R_2}\mathbf{l}_{\alpha_2} \otimes \mathbf{l}_{\alpha_1} \\ 0 \\ 0 \\ \frac{1}{A_1}\mathbf{l}_{\alpha_2} \otimes \mathbf{l}^{(1)}_{\alpha_1} \\ \frac{1}{A_2}\mathbf{l}^{(1)}_{\alpha_2} \otimes \mathbf{l}_{\alpha_1} \\ 0 \\ 0 \\ \mathbf{l}_{\alpha_2} \otimes \mathbf{l}_{\alpha_1} \end{bmatrix} \tag{35}$$

4. Constitutive relations

In this section, the constitutive model is presented of an arbitrary layer of the doubly-curved shell made of smart innovative materials within the present higher order ESL model. To this purpose, a linear elastic behavior with generally anisotropic material symmetry is considered. On the other hand, classical orthotropic layers are obtained as a particular case of a generally anisotropic material, whereas for CNT nanofibers are derived by means of an efficient homogenization procedure. The following three-dimensional constitutive relationship is considered for a generic k-th layer of the shell with $k = 1, ..., l$, being $\boldsymbol{\sigma}^{(k)}(\alpha_1, \alpha_2, \zeta, t) = \left[\sigma_1^{(k)} \ \sigma_2^{(k)} \ \tau_{12}^{(k)} \ \tau_{13}^{(k)} \ \tau_{23}^{(k)} \ \sigma_3^{(k)}\right]^T$ the three-dimensional stress vector and $\boldsymbol{\varepsilon}^{(k)}(\alpha_1, \alpha_2, \zeta, t) = \left[\varepsilon_1^{(k)} \ \varepsilon_2^{(k)} \ \gamma_{12}^{(k)} \ \gamma_{13}^{(k)} \ \gamma_{23}^{(k)} \ \varepsilon_3^{(k)}\right]^T$ the three-dimensional strain vector [11]:

$$\begin{bmatrix} \sigma_1^{(k)} \\ \sigma_2^{(k)} \\ \tau_{12}^{(k)} \\ \tau_{13}^{(k)} \\ \tau_{23}^{(k)} \\ \sigma_3^{(k)} \end{bmatrix} = \begin{bmatrix} \overline{E}_{11}^{(k)} & \overline{E}_{12}^{(k)} & \overline{E}_{16}^{(k)} & \overline{E}_{14}^{(k)} & \overline{E}_{15}^{(k)} & \overline{E}_{13}^{(k)} \\ \overline{E}_{12}^{(k)} & \overline{E}_{22}^{(k)} & \overline{E}_{26}^{(k)} & \overline{E}_{24}^{(k)} & \overline{E}_{25}^{(k)} & \overline{E}_{23}^{(k)} \\ \overline{E}_{16}^{(k)} & \overline{E}_{26}^{(k)} & \overline{E}_{66}^{(k)} & \overline{E}_{46}^{(k)} & \overline{E}_{56}^{(k)} & \overline{E}_{36}^{(k)} \\ \overline{E}_{14}^{(k)} & \overline{E}_{24}^{(k)} & \overline{E}_{46}^{(k)} & \overline{E}_{44}^{(k)} & \overline{E}_{45}^{(k)} & \overline{E}_{34}^{(k)} \\ \overline{E}_{15}^{(k)} & \overline{E}_{25}^{(k)} & \overline{E}_{56}^{(k)} & \overline{E}_{45}^{(k)} & \overline{E}_{55}^{(k)} & \overline{E}_{35}^{(k)} \\ \overline{E}_{13}^{(k)} & \overline{E}_{23}^{(k)} & \overline{E}_{36}^{(k)} & \overline{E}_{34}^{(k)} & \overline{E}_{35}^{(k)} & \overline{E}_{33}^{(k)} \end{bmatrix} \begin{bmatrix} \varepsilon_1^{(k)} \\ \varepsilon_2^{(k)} \\ \gamma_{12}^{(k)} \\ \gamma_{13}^{(k)} \\ \gamma_{23}^{(k)} \\ \varepsilon_3^{(k)} \end{bmatrix} \quad \Leftrightarrow \quad \boldsymbol{\sigma}^{(k)} = \overline{\mathbf{E}}^{(k)}\boldsymbol{\varepsilon}^{(k)} \tag{36}$$

for $k = 1, ..., l$. In the previous relation, $\overline{E}_{ij}^{(k)}$ for $i, j = 1, ..., 6$ are the homogenized elastic stiffness constants. They are referred to the geometric reference system $O'\alpha_1\alpha_2\zeta$ of principal coordinates introduced in Eqn. (2). On the other hand, it is convenient to provide the constitutive behavior of each layer with respect to the so-called material reference system, denoted by $O'\alpha_1^{(k)}\alpha_2^{(k)}\zeta$, which is intended to be rotated by an angle $\vartheta^{(k)}$ with respect to the geometric reference system. The following relation should be considered [11]:

$$\begin{bmatrix} \widehat{\sigma}_1^{(k)} \\ \widehat{\sigma}_2^{(k)} \\ \widehat{\tau}_{12}^{(k)} \\ \widehat{\tau}_{13}^{(k)} \\ \widehat{\tau}_{23}^{(k)} \\ \widehat{\sigma}_3^{(k)} \end{bmatrix} = \begin{bmatrix} E_{11}^{(k)} & E_{12}^{(k)} & E_{16}^{(k)} & E_{14}^{(k)} & E_{15}^{(k)} & E_{13}^{(k)} \\ E_{12}^{(k)} & E_{22}^{(k)} & E_{26}^{(k)} & E_{24}^{(k)} & E_{25}^{(k)} & E_{23}^{(k)} \\ E_{16}^{(k)} & E_{26}^{(k)} & E_{66}^{(k)} & E_{46}^{(k)} & E_{56}^{(k)} & E_{36}^{(k)} \\ E_{14}^{(k)} & E_{24}^{(k)} & E_{46}^{(k)} & E_{44}^{(k)} & E_{45}^{(k)} & E_{34}^{(k)} \\ E_{15}^{(k)} & E_{25}^{(k)} & E_{56}^{(k)} & E_{45}^{(k)} & E_{55}^{(k)} & E_{35}^{(k)} \\ E_{13}^{(k)} & E_{23}^{(k)} & E_{36}^{(k)} & E_{34}^{(k)} & E_{35}^{(k)} & E_{33}^{(k)} \end{bmatrix} \begin{bmatrix} \widehat{\varepsilon}_1^{(k)} \\ \widehat{\varepsilon}_2^{(k)} \\ \widehat{\gamma}_{12}^{(k)} \\ \widehat{\gamma}_{13}^{(k)} \\ \widehat{\gamma}_{23}^{(k)} \\ \widehat{\varepsilon}_3^{(k)} \end{bmatrix} \quad \Leftrightarrow \quad \widehat{\boldsymbol{\sigma}}^{(k)} = \mathbf{E}^{(k)}\widehat{\boldsymbol{\varepsilon}}^{(k)} \tag{37}$$

for $k = 1, ..., l$. In this way, the elastic constants $E_{ij}^{(k)}$ with $i, j = 1, ..., 6$ can be easily obtained from a homogenization procedure or from experimental tests.

When the layer under consideration is characterized by an orthotropic behavior, the well-known engineering constants are provided, namely the elastic moduli $E_1^{(k)}, E_2^{(k)}, E_3^{(k)}$, the shear moduli $G_{12}^{(k)}, G_{13}^{(k)}, G_{23}^{(k)}$ and the Poisson's coefficients $\nu_{12}^{(k)}, \nu_{13}^{(k)}, \nu_{23}^{(k)}$. The complete expression of constants $E_{ij}^{(k)} = C_{ij}^{(k)}$ occurring in the three-dimensional stiffness matrix $\mathbf{E}^{(k)}$ of Eqn. (37) can be found in Appendix I.

As a matter of fact, when the ESL generalized assumption of Eqn. (14) considers a higher order displacement field, the well-known three-dimensional elastic stiffness constants $E_{ij}^{(k)} = C_{ij}^{(k)}$ should be considered, whereas the so-called reduced elastic coefficients $E_{ij}^{(k)} = Q_{ij}^{(k)}$ with $i, j = 1, ..., 6$ should be considered for a uniform distribution assumptions of the out-of-plane displacement field. The quantities at issue are computed from the following relation:

$$Q_{ij}^{(k)} = C_{ij}^{(k)} - \frac{C_{j3}^{(k)}C_{i3}^{(k)}}{C_{33}^{(k)}} \quad \begin{matrix} \text{for} \ \ i,j = 1, ..., 6, \\ \text{for} \ \ k = 1, ..., l \end{matrix} \tag{38}$$

Starting from Eqn. (37), the rotated elastic stiffness matrix $\overline{\mathbf{E}}^{(k)}$ is obtained, for each k-th layer, by means of a rotation matrix $\mathbf{T}^{(k)} =$

$\mathbf{T}^{(k)}(\vartheta^{(k)})$ dependent on the material orientation angle $\vartheta^{(k)}$, as explained in Ref. [11]:

$$\overline{\mathbf{E}}^{(k)} = \mathbf{T}^{(k)}\mathbf{E}^{(k)}\left(\mathbf{T}^{(k)}\right)^{T} \quad \text{for} \quad k = 1, ..., l \tag{39}$$

Once the elastic constitutive relationship of Eqn. (36) is defined for each layer of the shell, a two-dimensional homogenized stiffness matrix is provided within the higher order ESL model so that the entire lamination scheme is taken into account. More specifically, a generalized constitutive relationship is derived by means of the computation of the elastic strain energy Φ which relates, for each τ-th kinematic order, the generalized strain vector $\boldsymbol{\varepsilon}^{(\tau)\alpha_i}(\alpha_1, \alpha_2, t) = \left[\varepsilon_1^{(\tau)\alpha_i}\ \varepsilon_2^{(\tau)\alpha_i}\ \gamma_1^{(\tau)\alpha_i}\ \gamma_2^{(\tau)\alpha_i}\ \gamma_{13}^{(\tau)\alpha_i}\ \gamma_{23}^{(\tau)\alpha_i}\ \omega_{13}^{(\tau)\alpha_i}\ \omega_{23}^{(\tau)\alpha_i}\ \varepsilon_3^{(\tau)\alpha_i}\right]^T$ introduced in Eqn. (33) to the generalized vector of stress resultants $\mathbf{S}^{(\tau)\alpha_i}(\alpha_1, \alpha_2, t) = \left[N_1^{(\tau)\alpha_i}\ N_2^{(\tau)\alpha_i}\ N_{12}^{(\tau)\alpha_i}\ N_{21}^{(\tau)\alpha_i}\ T_1^{(\tau)\alpha_i}\ T_2^{(\tau)\alpha_i}\ P_1^{(\tau)\alpha_i}\ P_2^{(\tau)\alpha_i}\ S_3^{(\tau)\alpha_i}\right]^T$ located on the reference surface of the shell. Finally, the relation reported in the following is obtained [12]:

$$\mathbf{S}^{(\tau)\alpha_i} = \sum_{\eta=0}^{N+1}\sum_{j=1}^{3}\mathbf{A}^{(\tau\eta)\alpha_i\alpha_j}\boldsymbol{\varepsilon}^{(\tau)\alpha_i} = \sum_{\eta=0}^{N+1}\sum_{j=1}^{3}\mathbf{A}^{(\tau\eta)\alpha_i\alpha_j}\mathbf{D}_{\Omega}^{\alpha_i}\mathbf{N}^{T}\overline{\mathbf{u}}^{(\tau)} \tag{40}$$

where the matrix $\mathbf{A}^{(\tau\eta)\alpha_i\alpha_j}$ looks in an extended form as follows:

$$\mathbf{A}^{(\tau\eta)\alpha_i\alpha_j} = \left[\begin{array}{cccccc|ccc}
A_{11(20)}^{(\tau\eta)[00]\alpha_i\alpha_j} & A_{12(11)}^{(\tau\eta)[00]\alpha_i\alpha_j} & A_{16(20)}^{(\tau\eta)[00]\alpha_i\alpha_j} & A_{16(11)}^{(\tau\eta)[00]\alpha_i\alpha_j} & A_{14(20)}^{(\tau\eta)[00]\alpha_i\alpha_j} & A_{15(11)}^{(\tau\eta)[00]\alpha_i\alpha_j} & A_{14(10)}^{(\tau\eta)[01]\alpha_i\alpha_j} & A_{15(10)}^{(\tau\eta)[01]\alpha_i\alpha_j} & A_{13(10)}^{(\tau\eta)[01]\alpha_i\alpha_j} \\
A_{12(11)}^{(\tau\eta)[00]\alpha_i\alpha_j} & A_{22(02)}^{(\tau\eta)[00]\alpha_i\alpha_j} & A_{26(11)}^{(\tau\eta)[00]\alpha_i\alpha_j} & A_{26(02)}^{(\tau\eta)[00]\alpha_i\alpha_j} & A_{24(11)}^{(\tau\eta)[00]\alpha_i\alpha_j} & A_{25(02)}^{(\tau\eta)[00]\alpha_i\alpha_j} & A_{24(01)}^{(\tau\eta)[01]\alpha_i\alpha_j} & A_{25(01)}^{(\tau\eta)[01]\alpha_i\alpha_j} & A_{23(01)}^{(\tau\eta)[01]\alpha_i\alpha_j} \\
A_{16(20)}^{(\tau\eta)[00]\alpha_i\alpha_j} & A_{26(11)}^{(\tau\eta)[00]\alpha_i\alpha_j} & A_{66(20)}^{(\tau\eta)[00]\alpha_i\alpha_j} & A_{66(11)}^{(\tau\eta)[00]\alpha_i\alpha_j} & A_{46(20)}^{(\tau\eta)[00]\alpha_i\alpha_j} & A_{56(11)}^{(\tau\eta)[00]\alpha_i\alpha_j} & A_{46(10)}^{(\tau\eta)[01]\alpha_i\alpha_j} & A_{56(10)}^{(\tau\eta)[01]\alpha_i\alpha_j} & A_{36(10)}^{(\tau\eta)[01]\alpha_i\alpha_j} \\
A_{16(11)}^{(\tau\eta)[00]\alpha_i\alpha_j} & A_{26(02)}^{(\tau\eta)[00]\alpha_i\alpha_j} & A_{66(11)}^{(\tau\eta)[00]\alpha_i\alpha_j} & A_{66(02)}^{(\tau\eta)[00]\alpha_i\alpha_j} & A_{46(11)}^{(\tau\eta)[00]\alpha_i\alpha_j} & A_{56(02)}^{(\tau\eta)[00]\alpha_i\alpha_j} & A_{46(01)}^{(\tau\eta)[01]\alpha_i\alpha_j} & A_{56(01)}^{(\tau\eta)[01]\alpha_i\alpha_j} & A_{36(01)}^{(\tau\eta)[01]\alpha_i\alpha_j} \\
A_{14(20)}^{(\tau\eta)[00]\alpha_i\alpha_j} & A_{24(11)}^{(\tau\eta)[00]\alpha_i\alpha_j} & A_{46(20)}^{(\tau\eta)[00]\alpha_i\alpha_j} & A_{46(11)}^{(\tau\eta)[00]\alpha_i\alpha_j} & A_{44(20)}^{(\tau\eta)[00]\alpha_i\alpha_j} & A_{45(11)}^{(\tau\eta)[00]\alpha_i\alpha_j} & A_{44(10)}^{(\tau\eta)[01]\alpha_i\alpha_j} & A_{45(10)}^{(\tau\eta)[01]\alpha_i\alpha_j} & A_{34(10)}^{(\tau\eta)[01]\alpha_i\alpha_j} \\
A_{15(11)}^{(\tau\eta)[00]\alpha_i\alpha_j} & A_{25(02)}^{(\tau\eta)[00]\alpha_i\alpha_j} & A_{56(11)}^{(\tau\eta)[00]\alpha_i\alpha_j} & A_{56(02)}^{(\tau\eta)[00]\alpha_i\alpha_j} & A_{45(11)}^{(\tau\eta)[00]\alpha_i\alpha_j} & A_{55(02)}^{(\tau\eta)[00]\alpha_i\alpha_j} & A_{45(01)}^{(\tau\eta)[01]\alpha_i\alpha_j} & A_{55(01)}^{(\tau\eta)[01]\alpha_i\alpha_j} & A_{35(01)}^{(\tau\eta)[01]\alpha_i\alpha_j} \\
\hline
A_{14(10)}^{(\tau\eta)[10]\alpha_i\alpha_j} & A_{24(01)}^{(\tau\eta)[10]\alpha_i\alpha_j} & A_{46(10)}^{(\tau\eta)[10]\alpha_i\alpha_j} & A_{46(01)}^{(\tau\eta)[10]\alpha_i\alpha_j} & A_{44(10)}^{(\tau\eta)[10]\alpha_i\alpha_j} & A_{45(01)}^{(\tau\eta)[10]\alpha_i\alpha_j} & A_{44(00)}^{(\tau\eta)[11]\alpha_i\alpha_j} & A_{45(00)}^{(\tau\eta)[11]\alpha_i\alpha_j} & A_{34(00)}^{(\tau\eta)[11]\alpha_i\alpha_j} \\
A_{15(10)}^{(\tau\eta)[10]\alpha_i\alpha_j} & A_{25(01)}^{(\tau\eta)[10]\alpha_i\alpha_j} & A_{56(10)}^{(\tau\eta)[10]\alpha_i\alpha_j} & A_{56(01)}^{(\tau\eta)[10]\alpha_i\alpha_j} & A_{45(10)}^{(\tau\eta)[10]\alpha_i\alpha_j} & A_{55(01)}^{(\tau\eta)[10]\alpha_i\alpha_j} & A_{45(00)}^{(\tau\eta)[11]\alpha_i\alpha_j} & A_{55(00)}^{(\tau\eta)[11]\alpha_i\alpha_j} & A_{35(00)}^{(\tau\eta)[11]\alpha_i\alpha_j} \\
A_{13(10)}^{(\tau\eta)[10]\alpha_i\alpha_j} & A_{23(01)}^{(\tau\eta)[10]\alpha_i\alpha_j} & A_{36(10)}^{(\tau\eta)[10]\alpha_i\alpha_j} & A_{36(01)}^{(\tau\eta)[10]\alpha_i\alpha_j} & A_{34(10)}^{(\tau\eta)[10]\alpha_i\alpha_j} & A_{35(01)}^{(\tau\eta)[10]\alpha_i\alpha_j} & A_{34(00)}^{(\tau\eta)[11]\alpha_i\alpha_j} & A_{35(00)}^{(\tau\eta)[11]\alpha_i\alpha_j} & A_{33(00)}^{(\tau\eta)[11]\alpha_i\alpha_j}
\end{array}\right] \tag{41}$$

If the notations $F_{\tau}^{\alpha_i} = \partial^0 F_{\tau}^{\alpha_i}/\partial\zeta^0$ and $F_{\eta}^{\alpha_j} = \partial^0 F_{\eta}^{\alpha_j}/\partial\zeta^0$ for the identification of the thickness functions with their derivative of zero-th order are adopted, the general component of $\mathbf{A}^{(\tau\eta)\alpha_i\alpha_j}$ can be computed with a single condensed relation as follows [20]:

$$A_{nm\,(pq)}^{(\tau\eta)[fg]\alpha_i\alpha_j} = \sum_{k=1}^{l}\int_{\zeta_k}^{\zeta_{k+1}}\overline{B}_{nm}^{(k)}\frac{\partial^f F_{\eta}^{\alpha_j}}{\partial\zeta^f}\frac{\partial^g F_{\tau}^{\alpha_i}}{\partial\zeta^g}\frac{H_1H_2}{H_1^pH_2^q}d\zeta \quad \begin{array}{l}\text{for } \tau,\eta = 0,1,2,...,N,N+1 \\ \text{for } n,m = 1,2,3,4,5,6 \\ \text{for } p,q = 0,1,2 \\ \text{for } \alpha_i,\alpha_j = \alpha_1,\alpha_2,\alpha_3 \\ \text{for } f,g = 0,1\end{array} \tag{42}$$

The integral occurring in the previous relation accounts for a general variation of the integration interval so that the effect of the thickness variation is considered. Furthermore, the higher order generalized stiffness constants are dependent on the selection of the thickness function, as well as the change of curvature within the physical domain. The three-dimensional elastic constitutive behavior of each lamina is taken into account by means of coefficient $\overline{B}_{nm}^{(k)} = \overline{E}_{nm}^{(k)}$ with $n, m = 1, ..., 6$. In case of lower order theories which do not take into account the deformation contributions coming from shear forces, the so-called shear correction factor $\kappa(\zeta)$ is adopted so that this issue is easily overcome in an approximate way:

$$\overline{B}_{nm}^{(k)} = \begin{cases}\overline{E}_{nm}^{(k)} & \text{for} \quad n,m = 1,2,3,6 \\ \kappa(\zeta)\overline{E}_{nm}^{(k)} & \text{for} \quad n,m = 4,5\end{cases} \tag{43}$$

In the present work, the value $\kappa(\zeta) = 5/6$ has been assumed.

Finally, the generalized higher order constitutive relation of Eqn. (40) is rearranged so that the stress resultant vector $\mathbf{S}^{(\tau)\alpha_i}$ is explicitly expressed, for each $\tau = 0, ..., N + 1$, in terms of the generalized displacement field vector $\mathbf{u}^{(\tau)}$. Introducing the unified formulation of the unknown field variable of Eqn. (15), the following relation can be derived [76]:

$$\begin{bmatrix} N_1^{(\tau)\alpha_i} \\ N_2^{(\tau)\alpha_i} \\ N_{12}^{(\tau)\alpha_i} \\ N_{21}^{(\tau)\alpha_i} \\ T_1^{(\tau)\alpha_i} \\ T_2^{(\tau)\alpha_i} \\ P_1^{(\tau)\alpha_i} \\ P_2^{(\tau)\alpha_i} \\ S_3^{(\tau)\alpha_i} \end{bmatrix} = \sum_{\eta=0}^{N+1} \begin{bmatrix} O_{11}^{(\tau\eta)\alpha_i\alpha_1} & O_{21}^{(\tau\eta)\alpha_i\alpha_2} & O_{31}^{(\tau\eta)\alpha_i\alpha_3} \\ O_{12}^{(\tau\eta)\alpha_i\alpha_1} & O_{22}^{(\tau\eta)\alpha_i\alpha_2} & O_{32}^{(\tau\eta)\alpha_i\alpha_3} \\ O_{13}^{(\tau\eta)\alpha_i\alpha_1} & O_{23}^{(\tau\eta)\alpha_i\alpha_2} & O_{33}^{(\tau\eta)\alpha_i\alpha_3} \\ O_{14}^{(\tau\eta)\alpha_i\alpha_1} & O_{24}^{(\tau\eta)\alpha_i\alpha_2} & O_{34}^{(\tau\eta)\alpha_i\alpha_3} \\ O_{15}^{(\tau\eta)\alpha_i\alpha_1} & O_{25}^{(\tau\eta)\alpha_i\alpha_2} & O_{35}^{(\tau\eta)\alpha_i\alpha_3} \\ O_{16}^{(\tau\eta)\alpha_i\alpha_1} & O_{26}^{(\tau\eta)\alpha_i\alpha_2} & O_{36}^{(\tau\eta)\alpha_i\alpha_3} \\ O_{17}^{(\tau\eta)\alpha_i\alpha_1} & O_{27}^{(\tau\eta)\alpha_i\alpha_2} & O_{37}^{(\tau\eta)\alpha_i\alpha_3} \\ O_{18}^{(\tau\eta)\alpha_i\alpha_1} & O_{28}^{(\tau\eta)\alpha_i\alpha_2} & O_{38}^{(\tau\eta)\alpha_i\alpha_3} \\ O_{19}^{(\tau\eta)\alpha_i\alpha_1} & O_{29}^{(\tau\eta)\alpha_i\alpha_2} & O_{39}^{(\tau\eta)\alpha_i\alpha_3} \end{bmatrix} \begin{bmatrix} u_1^{(\eta)} \\ u_2^{(\eta)} \\ u_3^{(\eta)} \end{bmatrix}$$

$$= \sum_{\eta=0}^{N+1} \begin{bmatrix} O_{11}^{(\tau\eta)\alpha_i\alpha_1} & O_{21}^{(\tau\eta)\alpha_i\alpha_2} & O_{31}^{(\tau\eta)\alpha_i\alpha_3} \\ O_{12}^{(\tau\eta)\alpha_i\alpha_1} & O_{22}^{(\tau\eta)\alpha_i\alpha_2} & O_{32}^{(\tau\eta)\alpha_i\alpha_3} \\ O_{13}^{(\tau\eta)\alpha_i\alpha_1} & O_{23}^{(\tau\eta)\alpha_i\alpha_2} & O_{33}^{(\tau\eta)\alpha_i\alpha_3} \\ O_{14}^{(\tau\eta)\alpha_i\alpha_1} & O_{24}^{(\tau\eta)\alpha_i\alpha_2} & O_{34}^{(\tau\eta)\alpha_i\alpha_3} \\ O_{15}^{(\tau\eta)\alpha_i\alpha_1} & O_{25}^{(\tau\eta)\alpha_i\alpha_2} & O_{35}^{(\tau\eta)\alpha_i\alpha_3} \\ O_{16}^{(\tau\eta)\alpha_i\alpha_1} & O_{26}^{(\tau\eta)\alpha_i\alpha_2} & O_{36}^{(\tau\eta)\alpha_i\alpha_3} \\ O_{17}^{(\tau\eta)\alpha_i\alpha_1} & O_{27}^{(\tau\eta)\alpha_i\alpha_2} & O_{37}^{(\tau\eta)\alpha_i\alpha_3} \\ O_{18}^{(\tau\eta)\alpha_i\alpha_1} & O_{28}^{(\tau\eta)\alpha_i\alpha_2} & O_{38}^{(\tau\eta)\alpha_i\alpha_3} \\ O_{19}^{(\tau\eta)\alpha_i\alpha_1} & O_{29}^{(\tau\eta)\alpha_i\alpha_2} & O_{39}^{(\tau\eta)\alpha_i\alpha_3} \end{bmatrix} \begin{bmatrix} \overline{\mathbf{N}}^T \overrightarrow{\mathbf{u}}_1^{(\eta)} \\ \overline{\mathbf{N}}^T \overrightarrow{\mathbf{u}}_2^{(\eta)} \\ \overline{\mathbf{N}}^T \overrightarrow{\mathbf{u}}_3^{(\eta)} \end{bmatrix} \tag{44}$$

The complete expression of the generalized coefficients $O_{kr}^{(\tau\eta)\alpha_i\alpha_j}$ with $i, j, k = 1, 2, 3$ and $r = 1, \ldots, 9$ is reported in Appendix II. Note that Eqn. (44) is a key aspect for the assessment of non-conventional boundary conditions with a three-dimensional connotation for the present continuum-based two-dimensional model.

Volume Element (RVE), denoted by W_r, is intended as the sum of the volume W_r^m for the scattered CNT nanofibers and that one for the CNTs spherical inclusions W_r^{in}:

$$W_r = W_r^m + W_r^{in} \tag{46}$$

In this way, the total volume of the unit cell W can be computed as:

$$W = W_r + W_m \tag{47}$$

The definitions of volume fractions of the matrix and CNTs, denoted by V_m and V_r, respectively, are reported in the following:

$$V_r = \frac{W_r}{W}, \quad V_m = \frac{W_m}{W} = 1 - V_r \tag{48}$$

In the present work, the volume fraction of CNTs $V_r = V_r(\zeta)$ is computed in terms of the two contributions V_r^* and $V_C^* = V_C^*(\zeta)$. The first one depends on the CNT mass fraction w_r and of the densities ρ_m,ρ_r of the matrix and the CNTs, respectively, whereas V_C^* denotes a smooth variation along the thickness of the layer [12]:

$$V_r(\zeta) = V_r^* V_C^*(\zeta) = V_r^* \left(V_C(\zeta) + f_p \right) \tag{49}$$

being f_p an arbitrary constant. The volume fraction contribution V_r^* is computed by the following expression:

$$V_r^* = \left(\frac{\rho_r}{w_r \rho_m} - \frac{\rho_r}{\rho_m} + 1 \right)^{-1} \tag{50}$$

On the other hand, the contribution $V_C^{(k)} = V_C^{(k)}(\zeta)$ is defined for the generic k-th layer of the stacking sequence with a five-parameter polynomial expression with exponent $p^{(k)} \geq 0$ and with parameters $a^{(k)}, b^{(k)}, c^{(k)}, d^{(k)} \in \mathbb{R}$. More specifically, two different profiles are considered, as follows [12]:

$$\begin{aligned} &\mathrm{FGM}_{PM\ \left(a^{(k)}/b^{(k)}/c^{(k)}/d^{(k)}/p^{(k)}\right)}^{CNT}: \quad V_C^{(k)}(\zeta) = \left(d^{(k)} - a^{(k)} \left(\frac{\zeta_{k+1} - \zeta}{h_k} \right) + b^{(k)} \left(\frac{\zeta_{k+1} - \zeta}{h_k} \right)^{c^{(k)}} \right)^{p^{(k)}} \\ &\mathrm{FGM}_{CNT\ \left(a^{(k)}/b^{(k)}/c^{(k)}/d^{(k)}/p^{(k)}\right)}^{PM}: \quad V_C^{(k)}(\zeta) = \left(d^{(k)} - a^{(k)} \left(\frac{\zeta - \zeta_k}{h_k} \right) + b^{(k)} \left(\frac{\zeta - \zeta_k}{h_k} \right)^{c^{(k)}} \right)^{p^{(k)}} \end{aligned} \tag{51}$$

5. Homogenized properties of a CNT composite layer

At this point, the equivalent elastic properties are derived for a composite layer reinforced with a dispersion of CNTs within the matrix, taking into account the effects of the agglomeration of the dispersed nanofibers (Fig. 1). The procedure consists in two different steps: in a first stage, the equivalent elastic properties of both the hybrid matrix and the inclusions are evaluated separately. Then, the equivalent elastic properties of the homogenized continuum layer are derived.

According to the main results of Ref. [12], it is assumed that straight CNT fibers are dispersed with random orientation in an isotropic matrix, being w_r the mass fraction of CNTs and w_m the mass fraction of the matrix:

$$w_r = \frac{M_r}{M_r + M_m}, \quad w_m = \frac{M_m}{M_r + M_m} = 1 - w_r \tag{45}$$

setting M_r and M_m the mass of CNTs and the matrix, respectively. If a random dispersion of CNT is considered, the mechanical behavior of the homogenized material turns out to be isotropic in absence of preferential orientations. Moreover, the total volume of CNTs within the Reference

The first distribution is adopted if CNTs are concentrated at the top of the k-th layer, whereas the second one is used when CNTs are concentrated at the lower side of the k-th lamina.

The agglomeration of the nanofibers within the isotropic matrix is taken into account by means of the agglomeration parameters μ_1 and μ_2, defined as [12]:

$$\mu_1 = \frac{W_{in}}{W}, \quad \mu_2 = \frac{W_r^{in}}{W_r} \tag{52}$$

As it is shown in Fig. 1, when μ_1 is equal to 1, no agglomeration can be seen because all CNTs are dispersed in the matrix. On the other hand, for the case $\mu_2 = 1$, no scattered nanofibers are present because all of them are located within the spherical inclusions.

As it has been shown in other works, a single CNT fiber can be considered as transversely isotropic, with the isotropy plane orthogonal to its long axis. In the following, the constitutive relationship for a single CNT fiber is reported with respect to its material symmetry axes $\hat{x}_1, \hat{x}_2, \hat{x}_3$ [12]:

$$\begin{bmatrix} \widehat{\sigma}^r_1 \\ \widehat{\sigma}^r_2 \\ \widehat{\tau}^r_{12} \\ \widehat{\tau}^r_{13} \\ \widehat{\tau}^r_{23} \\ \widehat{\sigma}^r_3 \end{bmatrix} = \begin{bmatrix} n_r & l_r & 0 & 0 & 0 & l_r \\ l_r & k_r+m_r & 0 & 0 & 0 & k_r-m_r \\ 0 & 0 & p_r & 0 & 0 & 0 \\ 0 & 0 & 0 & p_r & 0 & 0 \\ 0 & 0 & 0 & 0 & m_r & 0 \\ l_r & k_r-m_r & 0 & 0 & 0 & k_r+m_r \end{bmatrix} \begin{bmatrix} \widehat{\varepsilon}^r_1 \\ \widehat{\varepsilon}^r_2 \\ \widehat{\gamma}^r_{12} \\ \widehat{\gamma}^r_{13} \\ \widehat{\gamma}^r_{23} \\ \widehat{\varepsilon}^r_3 \end{bmatrix} \tag{53}$$

being k_r,l_r,m_r,n_r,p_r the five independent Hill's moduli of the transversely isotropic material. In the same way, the independent engineering constants $E^r_1, E^r_2, E^r_3, \nu^r_{12}, \nu^r_{13}, \nu^r_{23}, G^r_{12}, G^r_{13}, G^r_{23}$ of the material presented in the previous equation are computed as follows:

$$\begin{aligned} E^r_1 &= n_r - \frac{l_r^2}{k_r}, \quad E^r_2 = E^r_3 = \frac{4m_r(k_r n_r - l_r^2)}{k_r n_r - l_r^2 + m_r n_r} \\ \nu^r_{12} &= \nu^r_{13} = \frac{l_r}{2k_r}, \quad \nu^r_{23} = \frac{n_r(k_r - m_r) - l_r^2}{n_r(k_r + m_r) - l_r^2} \\ G^r_{12} &= G^r_{13} = p_r, \quad G^r_{23} = \frac{E^r_2}{2(1+\nu^r_{23})} \end{aligned} \tag{54}$$

setting G_{in},G_{out} the shear moduli and K_{in},K_{out} the bulk moduli of the CNT inclusions (*in*) and of the hybrid matrix (*out*), respectively. The Poisson's coefficient occurring in Eqns. (56)-(57), denoted by ν_{out}, is calculated as follows:

$$\nu_{out}(\zeta) = \frac{3K_{out} - 2G_{out}}{6K_{out} + 2G_{out}} \tag{58}$$

The shear and bulk moduli G_{in},G_{out},K_{in},K_{out} occurring in Eqn. (56) and Eqn. (57) are calculated from the following relations:

$$\begin{aligned} K_{in}(\zeta) &= K_m + \frac{V_r \mu_2 (\delta_r - 3K_m \alpha_r)}{3(\mu_1 - V_r \mu_2 + V_r \mu_2 \alpha_r)} \\ K_{out}(\zeta) &= K_m + \frac{V_r (1-\mu_2)(\delta_r - 3K_m \alpha_r)}{3(1-\mu_1 - V_r(1-\mu_2) + V_r(1-\mu_2)\alpha_r)} \end{aligned} \tag{59}$$

$$\begin{aligned} G_{in}(\zeta) &= G_m + \frac{V_r \mu_2 (\eta_r - 2G_m \beta_r)}{2(\mu_1 - V_r \mu_2 + V_r \mu_2 \beta_r)} \\ G_{out}(\zeta) &= G_m + \frac{V_r (1-\mu_2)(\eta_r - 2G_m \beta_r)}{2(1-\mu_1 - V_r(1-\mu_2) + V_r(1-\mu_2)\beta_r)} \end{aligned} \tag{60}$$

where quantities α_r,β_r,δ_r,η_r, referred to the CNT single fiber, read as:

$$\begin{aligned} \alpha_r &= \frac{3(K_m + G_m) + k_r + l_r}{3(G_m + k_r)} \\ \beta_r &= \frac{4G_m + 2k_r + l_r}{15(G_m + k_r)} + \frac{4G_m}{5(G_m + p_r)} + \frac{2(G_m(3K_m + G_m) + G_m(3K_m + 7G_m))}{5G_m(3K_m + G_m) + 5m_r(3K_m + 7G_m)} \\ \delta_r &= \frac{n_r + 2l_r}{3} + \frac{(2k_r + l_r)(3K_m + G_m - l_r)}{3(G_m + k_r)} \\ \eta_r &= \frac{2}{15}(n_r - l_r) + \frac{8G_m p_r}{5(G_m + p_r)} + \frac{2(k_r - l_r)(2G_m + l_r)}{15(G_m + k_r)} + \frac{8m_r G_m(3K_m + 4G_m)}{15K_m(m_r + G_m) + 5G_m(7m_r + G_m)} \end{aligned} \tag{61}$$

The mechanical properties of the isotropic matrix with CNTs dispersed nanofibers are denoted by E_m,ν_m,ρ_m, which are the elastic modulus, the Poisson's ratio and the density, respectively. The corresponding shear modulus G_m and bulk modulus K_m are easily derived from the relations reported in the following:

$$G_m = \frac{E_m}{2(1+\nu_m)}, \quad K_m = \frac{E_m}{3(1-2\nu_m)} \tag{55}$$

The estimation of the equivalent properties of the hybrid matrix is performed with some relations derived in Ref. [49] starting from the Mori-Tanaka procedure. Accordingly, the homogenized bulk modulus $K^*_m(\zeta)$ and shear modulus $G^*_m(\zeta)$ of the matrix reinforced with randomly dispersed nanofibers can be computed as [12]:

$$K^*_m(\zeta) = K_{out} + \frac{K_{out}\mu_1 \left(\frac{K_{in}}{K_{out}} - 1\right)}{1 + (1-\mu_1)\left(\frac{K_{in}}{K_{out}} - 1\right)\frac{1+\nu_{out}}{3-3\nu_{out}}} \tag{56}$$

$$G^*_m(\zeta) = G_{out} + \frac{G_{out}\mu_1 \left(\frac{G_{in}}{G_{out}} - 1\right)}{1 + (1-\mu_1)\left(\frac{G_{in}}{G_{out}} - 1\right)\frac{8-10\nu_{out}}{15-15\nu_{out}}} \tag{57}$$

As it has been shown in Ref. [12], if a random dispersion of CNTs is assumed, the matrix reinforced with CNTs turns out to be isotropic. Following the Mori-Tanaka scheme, the elastic modulus $E^*_m(\zeta)$ and the Poisson's ratio $\nu^*_m(\zeta)$ are computed in terms of the bulk modulus $K^*_m = K^*_m(\zeta)$ of Eqn. (56) and the shear modulus $G^*_m = G^*_m(\zeta)$ of Eqn. (57):

$$E^*_m(\zeta) = \frac{9K^*_m G^*_m}{3K^*_m + G^*_m} \tag{62}$$

$$\nu^*_m(\zeta) = \frac{3K^*_m - 2G^*_m}{6K^*_m + 2G^*_m} \tag{63}$$

On the other hand, the density $\rho^*_m(\zeta)$ of the CNT hybrid matrix is derived by means of the well-known rule of mixture:

$$\rho^*_m(\zeta) = (\rho_r - \rho_m)V_r(\zeta) + \rho_m \tag{64}$$

setting $V_r(\zeta)$ the volume fraction of the CNT fibers of density ρ_r dispersed in the matrix of density ρ_m.

When the improved isotropic CNT matrix is reinforced also with transversely isotropic long fibers, the homogenization procedure also embeds the so-called Halpin-Tsai model. For this case, a uniform through-the-thickness distribution is considered for the CNT volume fraction, namely $V_C^{(k)} = 1$. The first step consists in the evaluation of the

Hill's elastic moduli of long fibers, namely k_f,l_f,m_f,n_f,p_f, according to the following expressions [12]:

$$\begin{aligned} k_f &= \frac{E^f_2}{2\left(1-\nu^f_{23}-2\nu^f_{12}\nu^f_{21}\right)} \\ l_f &= 2\nu^f_{12}k_f \\ m_f &= \frac{1-\nu^f_{23}-2\nu^f_{12}\nu^f_{21}}{1+\nu^f_{23}}k_f \\ n_f &= 2\left(1-\nu^f_{23}\right)\frac{E^f_1}{E^f_2}k_f \\ p_f &= G^f_{12} \end{aligned} \tag{65}$$

In the same way, the Hill's moduli of the matrix reinforced with agglomerated CNTs, denoted by $k^*_m, l^*_m, m^*_m, n^*_m, p^*_m$, are computed as:

$$\begin{aligned} k^*_m &= \frac{E^*_m}{2(1+\nu^*_m)(1-2\nu^*_m)} \\ l^*_m &= 2\nu^*_m k^*_m \\ m^*_m &= (1-2\nu^*_m)k^*_m \\ n^*_m &= 2(1-\nu^*_m)k^*_m \\ p^*_m &= (1-2\nu^*_m)k^*_m \end{aligned} \tag{66}$$

According to the Halpin-Tsai model, the orthotropic engineering constants $E^{(k)}_1, E^{(k)}_2, E^{(k)}_3, \nu^{(k)}_{12}, \nu^{(k)}_{13}, \nu^{(k)}_{23}, G^{(k)}_{12}, G^{(k)}_{13}, G^{(k)}_{23}$ of the CNT composite material are derived for the k-th layer by means of the following expressions:

$$\begin{aligned} E^{(k)}_1 &= n - \frac{l^2}{k} \\ E^{(k)}_2 &= E^{(k)}_3 = \frac{4m(kn-l^2)}{kn-l^2+mn} \\ \nu^{(k)}_{12} &= \nu^{(k)}_{13} = \frac{l}{2k} \\ \nu^{(k)}_{23} &= \frac{n(k-m)-l^2}{n(k+m)-l^2} \\ G^{(k)}_{12} &= G^{(k)}_{13} = p \\ G^{(k)}_{23} &= m \end{aligned} \tag{67}$$

where k, l, m, n, p are the Hill moduli of the overall composite material. These elastic constants are computed starting from those referred to long fibers (65) and those related to the hybrid matrix (66):

$$\begin{aligned} k &= \frac{k^*_m(k_f+m^*_m)V^*_m + k_f(k^*_m+m^*_m)V_f}{(k_f+m^*_m)V^*_m + (k^*_m+m^*_m)V_f} \\ l &= V_f l_f + V^*_m l^*_m + \frac{l_f-l^*_m}{k_f-k^*_m}\left(k - V_f k_f - V^*_m k^*_m\right) \\ m &= m^*_m \frac{2V_f m_f(k^*_m+m^*_m) + 2V^*_m m_f m^*_m + V^*_m k^*_m(m_f+m^*_m)}{2V_f m^*_m(k^*_m+m^*_m) + 2V^*_m m_f m^*_m + V^*_m k^*_m(m_f+m^*_m)} \\ n &= V_f n_f + V^*_m n^*_m + \left(\frac{l_f-l^*_m}{k_f-k^*_m}\right)^2\left(k - V_f k_f - V^*_m k^*_m\right) \\ p &= \frac{\left(p_f+p^*_m\right)p^*_m V^*_m + 2p_f p^*_m V_f}{\left(p_f+p^*_m\right)V^*_m + 2p^*_m V_f} \end{aligned} \tag{68}$$

The volume fraction of long fibers V_f is derived once the corresponding mass fraction w_f is provided:

$$V_f = \left(\frac{\rho_f}{w_f\rho^*_m} - \frac{\rho_f}{\rho^*_m} + 1\right)^{-1} \tag{69}$$

6. General boundary conditions

An efficient methodology is now presented for the assessment of non-conventional boundary conditions in the present higher order continuum model. To this purpose, a distribution of linear elastic springs of stiffness $k^{(k)\alpha^m_j}_{if}$ for $i = 1, 2, 3, j = 1, 2$ and $m = 0, 1$ are enforced along the lateral surfaces of the three-dimensional solid. Then, the computation of the virtual work associated to the springs under consideration is adopted for the derivation of the generalized stress resultants which are in turn included in the assembled governing equations. Referring to the two sides of the three-dimensional shell associated to the boundaries with $\alpha_1 = \alpha^m_1$ for $m = 0, 1$, the stresses $\overline{\sigma}^{(k)}_1$, $\overline{\tau}^{(k)}_{12}$ and $\overline{\tau}^{(k)}_{13}$ are induced at each k-th layer, reading as:

$$\begin{aligned} \overline{\sigma}^{(k)}_1(\alpha^m_1,\alpha_2,\zeta,t) &= -k^{(k)\alpha^m_1}_{1f}\widetilde{f}(\alpha^m_1,\alpha_2)\overline{\lambda}(\zeta)U^{(k)}_1(\alpha^m_1,\alpha_2,\zeta,t) \\ \overline{\tau}^{(k)}_{12}(\alpha^m_1,\alpha_2,\zeta,t) &= -k^{(k)\alpha^m_1}_{2f}\widetilde{f}(\alpha^m_1,\alpha_2)\overline{\lambda}(\zeta)U^{(k)}_2(\alpha^m_1,\alpha_2,\zeta,t) \\ \overline{\tau}^{(k)}_{13}(\alpha^m_1,\alpha_2,\zeta,t) &= -k^{(k)\alpha^m_1}_{3f}\widetilde{f}(\alpha^m_1,\alpha_2)\overline{\lambda}(\zeta)U^{(k)}_3(\alpha^m_1,\alpha_2,\zeta,t) \end{aligned} \tag{70}$$

with $\alpha_2 \in \left[\alpha^0_2, \alpha^1_2\right]$ In the same way, the lateral surfaces of the three-dimensional shell located at $\alpha_2 = \alpha^m_2$ for $m = 0, 1$ are subjected to the boundary stresses $\overline{\tau}^{(k)}_{12}$, $\overline{\sigma}^{(k)}_2$ and $\overline{\tau}^{(k)}_{23}$, setting $\alpha_1 \in \left[\alpha^0_1, \alpha^1_1\right]$:

$$\begin{aligned} \overline{\tau}^{(k)}_{12}(\alpha_1,\alpha^m_2,\zeta,t) &= -k^{(k)\alpha^m_2}_{1f}\widetilde{f}(\alpha_1,\alpha^m_2)\overline{\lambda}(\zeta)U^{(k)}_1(\alpha_1,\alpha^m_2,\zeta,t) \\ \overline{\sigma}^{(k)}_2(\alpha_1,\alpha^m_2,\zeta,t) &= -k^{(k)\alpha^m_2}_{2f}\widetilde{f}(\alpha_1,\alpha^m_2)\overline{\lambda}(\zeta)U^{(k)}_2(\alpha_1,\alpha^m_2,\zeta,t) \\ \overline{\tau}^{(k)}_{23}(\alpha_1,\alpha^m_2,\zeta,t) &= -k^{(k)\alpha^m_2}_{3f}\widetilde{f}(\alpha_1,\alpha^m_2)\overline{\lambda}(\zeta)U^{(k)}_3(\alpha_1,\alpha^m_2,\zeta,t) \end{aligned} \tag{71}$$

In the previous relations, a general distribution of springs is considered, characterized by in-plane components $\widetilde{f}(\alpha^m_1,\alpha_2)$ and $\widetilde{f}(\alpha^m_1,\alpha_2)$. Furthermore, an out-of-plane general dispersion is modelled, denoted by $\overline{\lambda}(\zeta)$, accounting for a constant ($\overline{\lambda} = 1$), a linear ($\overline{\lambda} = 2\zeta/h$) and a parabolic ($\overline{\lambda} = 1 - (2\zeta/h)^2$) through-the-thickness stiffness variation. As far as the in-plane spring distribution is concerned, in-plane univariate analytical expressions are provided in terms of dimensionless coordinates $\overline{\alpha}_i = \overline{\xi} \in [0,1]$ and $\widetilde{\alpha}_i = \widetilde{\xi} \in [0,1]$, according to their definition reported in Eqn. (8). In particular, a Double-Weibull (D) and a Super elliptic (S) expression are considered for $\widetilde{f}$. They are defined in terms of a power exponent p and two position parameters $\overline{\xi}_m, \widetilde{\xi}_m \in [0,1]$ [12]:

$$\widetilde{f}(\xi) = \begin{cases} 1 - \left(e^{-\left(\frac{\overline{\xi}}{\overline{\xi}_m}\right)^p} - e^{-\left(\frac{\widetilde{\xi}}{\widetilde{\xi}_m}\right)^p}\right) & \text{Double} - \text{Weibull} \\ e^{-\frac{1}{2}\left(\frac{\overline{\xi}-\widetilde{\xi}_m}{\widetilde{\xi}_m}\right)} & \text{Super elliptic} \end{cases} \tag{72}$$

The boundary stresses of Eqns. (70)-(71) are embedded in the present ESL model in terms of induced generalized stress resultants $\overline{\mathbf{S}}^{(\tau)}_{\alpha_1}(\alpha^m_1,\alpha_2,t) = \left[\overline{N}^{(\tau)\alpha_1}_1\ \overline{N}^{(\tau)\alpha_2}_{12}\ \overline{T}^{(\tau)\alpha_3}_1\right]^T$ and $\overline{\mathbf{S}}^{(\tau)}_{\alpha_2}(\alpha_1,\alpha^m_2,t) = \left[\overline{N}^{(\tau)\alpha_1}_{21}\ \overline{N}^{(\tau)\alpha_2}_2\ \overline{T}^{(\tau)\alpha_3}_2\right]^T$. The components of $\overline{\mathbf{S}}^{(\tau)}_{\alpha_1}$ read as [12]:

$$\begin{aligned} \overline{N}^{(\tau)\alpha_1}_1(\alpha^m_1,\alpha_2,t) &= \sum_{k=1}^{l}\int_{\zeta_k}^{\zeta_{k+1}} \overline{\sigma}^{(k)}_1 F^{(k\tau)\alpha_1} H_2 d\zeta \\ \overline{N}^{(\tau)\alpha_2}_{12}(\alpha^m_1,\alpha_2,t) &= \sum_{k=1}^{l}\int_{\zeta_k}^{\zeta_{k+1}} \overline{\tau}^{(k)}_{12} F^{(k\tau)\alpha_2} H_2 d\zeta \quad \begin{matrix}\text{for } m = 0,1 \\ \text{for } \alpha_2 \in \left[\alpha^0_2,\alpha^1_2\right]\end{matrix} \\ \overline{T}^{(\tau)\alpha_3}_1(\alpha^m_1,\alpha_2,t) &= \sum_{k=1}^{l}\int_{\zeta_k}^{\zeta_{k+1}} \overline{\tau}^{(k)}_{13} F^{(k\tau)\alpha_3} H_2 d\zeta \end{aligned} \tag{73}$$

In the same way, the generalized stress resultants $\overline{N}_{21}^{(\tau)\alpha_1}, \overline{N}_{2}^{(\tau)\alpha_2}, \overline{T}_{2}^{(\tau)\alpha_3}$ account for the stresses outlined in Eqn. (71):

$$\begin{aligned}
\overline{N}_{21}^{(\tau)\alpha_1}(\alpha_1,\alpha_2^m,t) &= \sum_{k=1}^{l}\int_{\zeta_k}^{\zeta_{k+1}} \overline{\tau}_{12}^{(k)}\overline{\lambda}F^{(k\tau)\alpha_1}H_1 d\zeta \\
\overline{N}_{2}^{(\tau)\alpha_2}(\alpha_1,\alpha_2^m,t) &= \sum_{k=1}^{l}\int_{\zeta_k}^{\zeta_{k+1}} \overline{\sigma}_{2}^{(k)}\overline{\lambda}F^{(k\tau)\alpha_2}H_1 d\zeta \qquad \begin{matrix}\text{for } m=0,1\\ \text{for } \alpha_1\in[\alpha_1^0,\alpha_1^1]\end{matrix} \\
\overline{T}_{2}^{(\tau)\alpha_3}(\alpha_1,\alpha_2^m,t) &= \sum_{k=1}^{l}\int_{\zeta_k}^{\zeta_{k+1}} \overline{\tau}_{23}^{(k)}\overline{\lambda}F^{(k\tau)\alpha_3}H_1 d\zeta
\end{aligned} \tag{74}$$

Introducing in Eqns. (73)-(74) the ESL expression of the generalized stresses of Eqn. (44), the following relations are obtained:

$$\begin{aligned}
\begin{bmatrix}\overline{N}_{1}^{(\tau)\alpha_1}\\ \overline{N}_{12}^{(\tau)\alpha_2}\\ \overline{T}_{1}^{(\tau)\alpha_3}\end{bmatrix} &= -\sum_{\eta+0}^{N+1}\begin{bmatrix} K_{b1(2)\alpha_1^m}^{(\tau\eta)\alpha_1} & 0 & 0\\ 0 & K_{b1(2)\alpha_1^m}^{(\tau\eta)\alpha_2} & 0\\ 0 & 0 & K_{b3(2)\alpha_1^m}^{(\tau\eta)\alpha_1}\end{bmatrix}\begin{bmatrix}u_1^{(\eta)}\\ u_2^{(\eta)}\\ u_3^{(\eta)}\end{bmatrix} \\
&= -\sum_{\eta=0}^{N+1}\mathbf{K}_{b(1)\alpha_1^m}^{(\tau\eta)}\mathbf{u}^{(\eta)} \quad \begin{matrix}\text{for} & m=0,1\\ \text{for} & \alpha_2\in[\alpha_2^0,\alpha_2^1]\end{matrix}
\end{aligned} \tag{75}$$

$$\begin{aligned}
\delta\Phi &= \sum_{\tau=0}^{N+1}\sum_{i=1}^{3}\int_{\alpha_1}\int_{\alpha_2}\left(\delta\varepsilon^{(\tau)\alpha_i}\right)^T\mathbf{S}^{(\tau)\alpha_i}A_1A_2 d\alpha_1 d\alpha_2 = \\
&= \sum_{\tau=0}^{N+1}\sum_{\eta=0}^{N+1}\sum_{i=1}^{3}\sum_{j=1}^{3}\int_{\alpha_1}\int_{\alpha_2}\left[\delta\left(\mathbf{D}_{\Omega}^{\alpha_i}\mathbf{u}^{(\tau)}\right)\right]^T\mathbf{A}^{(\tau\eta)\alpha_i\alpha_j}\mathbf{D}_{\Omega}^{\alpha_j}\mathbf{u}^{(\eta)}A_1A_2 d\alpha_1 d\alpha_2 = \\
&= \sum_{\tau=0}^{N+1}\sum_{\eta=0}^{N+1}\sum_{i=1}^{3}\sum_{j=1}^{3}\int_{\alpha_1}\int_{\alpha_2}\left(\mathbf{D}_{\Omega}^{\alpha_i}\mathbf{N}^T\delta\overline{\mathbf{u}}^{(\tau)}\right)^T\mathbf{A}^{(\tau\eta)\alpha_i\alpha_j}\left(\mathbf{D}_{\Omega}^{\alpha_j}\mathbf{N}^T\overline{\mathbf{u}}^{(\eta)}\right)A_1A_2 d\alpha_1 d\alpha_2 = \\
&= \sum_{\tau=0}^{N+1}\sum_{\eta=0}^{N+1}\delta\overline{\mathbf{u}}^{(\tau)T}\left(\sum_{i=1}^{3}\sum_{j=1}^{3}\int_{\alpha_1}\int_{\alpha_2}\left(\mathbf{D}_{\Omega}^{\alpha_i}\mathbf{N}^T\right)^T\mathbf{A}^{(\tau\eta)\alpha_i\alpha_j}\left(\mathbf{D}_{\Omega}^{\alpha_j}\mathbf{N}^T\right)A_1A_2 d\alpha_1 d\alpha_2\right)\overline{\mathbf{u}}^{(\eta)} = \\
&= \sum_{\tau=0}^{N+1}\sum_{\eta=0}^{N+1}\delta\overline{\mathbf{u}}^{(\tau)T}\overline{\mathbf{K}}_s^{(\tau\eta)}\overline{\mathbf{u}}^{(\eta)}
\end{aligned} \tag{79}$$

$$\begin{aligned}
\begin{bmatrix}\overline{N}_{21}^{(\tau)\alpha_1}\\ \overline{N}_{2}^{(\tau)\alpha_2}\\ \overline{T}_{2}^{(\tau)\alpha_3}\end{bmatrix} &= -\sum_{\eta+0}^{N+1}\begin{bmatrix} K_{b1(2)\alpha_2^m}^{(\tau\eta)\alpha_1} & 0 & 0\\ 0 & K_{b1(2)\alpha_2^m}^{(\tau\eta)\alpha_2} & 0\\ 0 & 0 & K_{b3(1)\alpha_2^m}^{(\tau\eta)\alpha_3}\end{bmatrix}\begin{bmatrix}u_1^{(\eta)}\\ u_2^{(\eta)}\\ u_3^{(\eta)}\end{bmatrix} \\
&= -\sum_{\eta=0}^{N+1}\mathbf{K}_{b(1)\alpha_2^m}^{(\tau\eta)}\mathbf{u}^{(\eta)} \quad \begin{matrix}\text{for} & m=0,1\\ \text{for} & \alpha_1\in[\alpha_2^0,\alpha_1^1]\end{matrix}
\end{aligned} \tag{76}$$

The generalized stiffnesses $K_{bi(p)\alpha_n^m}^{(\tau\eta)\alpha_i}$ with $m = 0, 1$, $n = 1, 2$ and $p = 1, 2$, are computed by means of the following relation for each $\tau, \eta = 0, ..., N + 1$ and $i = 1, 2, 3$ [12]:

$$K_{bi(p)\alpha_n^m}^{(\tau\eta)\alpha_i} = \sum_{k=1}^{l}\int_{\zeta_k}^{\zeta_{k+1}} k_{if}^{(k)\alpha_n^m}F_{\eta}^{\alpha_i}F_{\tau}^{\alpha_i}H_p d\zeta \tag{77}$$

7. Governing equations

In the present section, a methodology is applied to derive the dynamic equilibrium equations for a doubly-curved shell structure. The procedure in hand is based on the Hamiltonian Principle [12] accounting for the virtual variation of the elastic strain energy $\delta\Phi$, the kinetic energy δT, and the virtual work, denoted by δL_{eb}, of boundary springs distributed along the lateral surfaces. After that, the fundamental relations for the problem under consideration are derived if the ESL higher order kinematic relations based on Eqn. (26) are considered, as well as the generalized elastic constitutive relationship reported in Eqn. (40).

Referring to a generic time interval $[t_1,t_2]$, a stationary configuration of the system is derived from the following relation:

$$\int_{t_1}^{t_2}(\delta\Phi - \delta T + \delta L_{eb})dt = 0 \tag{78}$$

The computation of the virtual variation of the elastic strain energy is performed starting from the three-dimensional elasticity theory. Introducing the ESL kinematic assumption of Eqn. (26), an expression in terms of the generalized stress resultant vector $\mathbf{S}^{(\tau)\alpha_i}$ and the generalized strain vector $\boldsymbol{\varepsilon}^{(\tau)\alpha_i}$ with $\tau = 0, ..., N + 1$ and $i = 1, 2, 3$ is provided, as follows [12]:

The generalized strain vector is expressed in terms of the discrete generalized displacement field vector $\overline{\mathbf{u}}^{(\tau)}$ of Eqn. (23), which is not involved in the integration along α_1,α_2 coordinates occurring in the previous equation. On the other hand, such computations are performed thanks to the generalized shape functions matrix $\mathbf{N}^T$. A key aspect consists in the generalized stiffness matrix $\overline{\mathbf{K}}_s^{(\tau\eta)}$ of dimensions $(3I_NI_M) \times (3I_NI_M)$ for each τ, η-th kinematic expansion order. Employing a compact notation, it gives [12]:

$$\begin{aligned}\overline{\mathbf{K}}_s^{(\tau\eta)} &= \sum_{i=1}^{3}\sum_{j=1}^{3}\int_{\alpha_1}\int_{\alpha_2}\left(\mathbf{D}_{\Omega}^{\alpha_i}\mathbf{N}^T\right)^T\mathbf{A}^{(\tau\eta)\alpha_i\alpha_j}\left(\mathbf{D}_{\Omega}^{\alpha_j}\mathbf{N}^T\right)A_1A_2d\alpha_1d\alpha_2 \\ &= \sum_{i=1}^{3}\sum_{j=1}^{3}\int_{\alpha_1}\int_{\alpha_2}\left(\mathbf{B}^{\alpha_i}\right)^T\mathbf{A}^{(\tau\eta)\alpha_i\alpha_j}\mathbf{B}^{\alpha_j}A_1A_2d\alpha_1d\alpha_2\end{aligned} \tag{80}$$

where $\overline{\mathbf{B}}^{\alpha_i} = \overline{\mathbf{D}}_{\Omega}^{\alpha_i}\overline{\mathbf{N}}^T$ are matrices of dimensions $9 \times (I_N I_M)$. The higher order weak stiffness matrix $\overline{\mathbf{K}}_s^{(\tau\eta)}$ is more conveniently expressed in expanded form as follows:

$$\overline{\mathbf{K}}_s^{(\tau\eta)} = \int_{\alpha_1}\int_{\alpha_2}\begin{bmatrix}\overline{\mathbf{K}}_s^{(\tau\eta)\alpha_1\alpha_1} & \overline{\mathbf{K}}_s^{(\tau\eta)\alpha_1\alpha_2} & \overline{\mathbf{K}}_s^{(\tau\eta)\alpha_1\alpha_3}\\ \overline{\mathbf{K}}_s^{(\tau\eta)\alpha_2\alpha_1} & \overline{\mathbf{K}}_s^{(\tau\eta)\alpha_2\alpha_2} & \overline{\mathbf{K}}_s^{(\tau\eta)\alpha_2\alpha_3}\\ \overline{\mathbf{K}}_s^{(\tau\eta)\alpha_3\alpha_1} & \overline{\mathbf{K}}_s^{(\tau\eta)\alpha_3\alpha_2} & \overline{\mathbf{K}}_s^{(\tau\eta)\alpha_3\alpha_3}\end{bmatrix}A_1A_2d\alpha_1d\alpha_2 \tag{81}$$

setting $\overline{\mathbf{K}}_s^{(\tau\eta)\alpha_i\alpha_j} = \left(\overline{\mathbf{B}}^{\alpha_i}\right)^T\mathbf{A}^{(\tau\eta)\alpha_i\alpha_j}\overline{\mathbf{B}}^{\alpha_j}$. In Ref. [85] the interested reader can find the complete expression for all terms occurring in Eqn. (81). In the same way, the virtual variation of the kinetic energy δT of Eqn. (78) is computed starting from the following relation [12]:

$$\delta T = -\sum_{\tau=0}^{N+1}\int_{\alpha_1}\int_{\alpha_2}\left(\delta\mathbf{u}^{(\tau)}\right)^T\left(\sum_{\eta=0}^{N+1}\mathbf{M}^{(\tau\eta)}\ddot{\mathbf{u}}^{(\eta)}\right)A_1A_2d\alpha_1d\alpha_2 \tag{82}$$

Introducing the generalized interpolation of the unknown field variable of Eqn. (21), δT is expressed in weak form in terms of the generalized discrete vectors $\overline{\mathbf{u}}_1^{(\tau)}, \overline{\mathbf{u}}_2^{(\tau)}, \overline{\mathbf{u}}_3^{(\tau)}$ as follows:

$$\begin{aligned}\delta T = &-\sum_{\tau=0}^{N+1}\int_{\alpha_1}\int_{\alpha_2}\left(\left(\overline{\mathbf{N}}^T\delta\overline{\mathbf{u}}_1^{(\tau)}\right)^T\left(\sum_{\eta=0}^{N+1}I_0^{(\tau\eta)\alpha_1\alpha_1}\overline{\mathbf{N}}^T\ddot{\overline{\mathbf{u}}}_1^{(\eta)}\right)+\left(\overline{\mathbf{N}}^T\delta\overline{\mathbf{u}}_2^{(\tau)}\right)^T\left(\sum_{\eta=0}^{N+1}I_0^{(\tau\eta)\alpha_2\alpha_2}\overline{\mathbf{N}}^T\ddot{\overline{\mathbf{u}}}_2^{(\eta)}\right)+\right.\\ &\left.+\left(\overline{\mathbf{N}}^T\delta\overline{\mathbf{u}}_3^{(\tau)}\right)^T\left(\sum_{\eta=0}^{N+1}I_0^{(\tau\eta)\alpha_3\alpha_3}\overline{\mathbf{N}}^T\ddot{\overline{\mathbf{u}}}_3^{(\eta)}\right)\right)A_1A_2d\alpha_1d\alpha_2 = \\ = &-\sum_{\tau=0}^{N+1}\int_{\alpha_1}\int_{\alpha_2}\left(\left(\delta\overline{\mathbf{u}}_1^{(\tau)}\right)^T\left(\sum_{\eta=0}^{N+1}\overline{\mathbf{N}}I_0^{(\tau\eta)\alpha_1\alpha_1}\overline{\mathbf{N}}^T\right)\ddot{\overline{\mathbf{u}}}_1^{(\eta)}+\left(\delta\overline{\mathbf{u}}_2^{(\tau)}\right)^T\left(\sum_{\eta=0}^{N+1}\overline{\mathbf{N}}I_0^{(\tau\eta)\alpha_2\alpha_2}\overline{\mathbf{N}}^T\right)\ddot{\overline{\mathbf{u}}}_2^{(\eta)}+\right.\\ &\left.+\left(\delta\overline{\mathbf{u}}_3^{(\tau)}\right)^T\left(\sum_{\eta=0}^{N+1}\overline{\mathbf{N}}I_0^{(\tau\eta)\alpha_3\alpha_3}\overline{\mathbf{N}}^T\right)\ddot{\overline{\mathbf{u}}}_3^{(\eta)}\right)A_1A_2d\alpha_1d\alpha_2 = \\ = &-\sum_{\tau=0}^{N+1}\sum_{\eta=0}^{N+1}\left(\delta\overline{\mathbf{u}}^{(\tau)}\right)^T\mathbf{M}^{(\tau\eta)}\ddot{\overline{\mathbf{u}}}^{(\eta)}\end{aligned} \tag{83}$$

The higher order inertial terms $I_0^{(\tau\eta)\alpha_i\alpha_j} = I_0^{(\tau\eta)\alpha_1\alpha_1}, I_0^{(\tau\eta)\alpha_2\alpha_2}, I_0^{(\tau\eta)\alpha_3\alpha_3}$ are computed, for each $\tau, \eta = 0, ..., N+1$, as follows [12]:

$$I_0^{(\tau\eta)\alpha_i\alpha_j} = \sum_{k=1}^{l}\int_{\zeta_k}^{\zeta_{k+1}}\rho^{(k)}F^{(k\tau)\alpha_i}F^{(k\eta)\alpha_j}H_1H_2d\zeta \quad \begin{matrix}\text{for } i,j=1,2,3,\\ \text{for } \tau,\eta=0,...,N+1\end{matrix} \tag{84}$$

Moreover, the higher order mass matrix $\mathbf{M}^{(\tau\eta)}$ is introduced in Eqn. (83) for each $\tau, \eta = 0, ..., N+1$. In the following, the extended definition of the matrix at issue can be found:

$$\mathbf{M}^{(\tau\eta)} = \int_{\alpha_1}\int_{\alpha_2}\begin{bmatrix}\mathbf{M}^{(\tau\eta)\alpha_1\alpha_2} & \mathbf{M}^{(\tau\eta)\alpha_1\alpha_2} & \mathbf{M}^{(\tau\eta)\alpha_1\alpha_3}\\ \mathbf{M}^{(\tau\eta)\alpha_2\alpha_1} & \mathbf{M}^{(\tau\eta)\alpha_2\alpha_2} & \mathbf{M}^{(\tau\eta)\alpha_2\alpha_3}\\ \mathbf{M}^{(\tau\eta)\alpha_3\alpha_1} & \mathbf{M}^{(\tau\eta)\alpha_3\alpha_2} & \mathbf{M}^{(\tau\eta)\alpha_3\alpha_3}\end{bmatrix}A_1A_2d\alpha_1d\alpha_2 \tag{85}$$

where $\mathbf{M}^{(\tau\eta)\alpha_i\alpha_j} = \overline{\mathbf{N}}I_0^{(\tau\eta)\alpha_i\alpha_j}\overline{\mathbf{N}}^T$ for $i = j$, whereas $\mathbf{M}^{(\tau\eta)\alpha_i\alpha_j} = \mathbf{0}$ for $i \neq j$. The virtual work δL_{eb} induced by the springs located at the lateral surfaces of the shell consists in two contributions δL_{eb1} and δL_{eb2} coming from the generalized stress resultants $\overline{\mathbf{S}}_{\alpha_1}^{(\tau)}$ and $\overline{\mathbf{S}}_{\alpha_2}^{(\tau)}$, defined in Eqns. (75)-(76) [12]:

$$\delta L_{eb} = \delta L_{eb1} + \delta L_{eb2} = \sum_{\tau=0}^{N+1}\left(\oint_{\alpha_2}\left(\delta\mathbf{u}^{(\tau)}\right)^T\overline{\mathbf{S}}_{\alpha_1}^{(\tau)}A_2\alpha_2 + \oint_{\alpha_1}\left(\delta\mathbf{u}^{(\tau)}\right)^T\overline{\mathbf{S}}_{\alpha_2}^{(\tau)}A_1\alpha_1\right) \tag{86}$$

Introducing, for each $\tau = 0, ..., N+1$, the higher order interpolation (21) of the generalized kinematic field variable $\mathbf{u}^{(\tau)}$, the following generalized stress resultant vectors $\overline{\mathbf{Q}}_{\alpha_1}^{(\tau)}$ and $\overline{\mathbf{Q}}_{\alpha_2}^{(\tau)}$ of dimensions $(3I_N I_M) \times 1$ can be defined:

$$\begin{aligned}\delta L_{eb} = \delta L_{eb1} + \delta L_{eb2} &= \sum_{\tau=0}^{N+1}\left[\left(\delta\overline{\mathbf{u}}^{(\tau)}\right)^T\left(\overline{\mathbf{Q}}_{\alpha_1}^{(\tau)} + \overline{\mathbf{Q}}_{\alpha_2}^{(\tau)}\right)\right] = \\ &= \sum_{\tau=0}^{N+1}\left(\left(\delta\overline{\mathbf{u}}^{(\tau)}\right)^T\oint_{\alpha_2}\begin{bmatrix}\overline{\mathbf{N}}\overline{N}_1^{(\tau)\alpha_1}\\ \overline{\mathbf{N}}\overline{N}_{12}^{(\tau)\alpha_2}\\ \overline{\mathbf{N}}\overline{T}_1^{(\tau)\alpha_3}\end{bmatrix}A_2\alpha_2 + \left(\delta\overline{\mathbf{u}}^{(\tau)}\right)^T\oint_{\alpha_1}\begin{bmatrix}\overline{\mathbf{N}}\overline{N}_{21}^{(\tau)\alpha_1}\\ \overline{\mathbf{N}}\overline{N}_2^{(\tau)\alpha_2}\\ \overline{\mathbf{N}}\overline{T}_2^{(\tau)\alpha_3}\end{bmatrix}A_1\alpha_1\right)\end{aligned} \tag{87}$$

Finally, the following relation is obtained for δL_{eb}, if Eqns. (75)-(76) are substituted in Eqn. (87) [12]:

$$\delta L_{eb} = \sum_{\tau=0}^{N+1} \left(\delta \overline{\mathbf{u}}^{(\tau)}\right)^T \sum_{\eta=0}^{N+1} \left[\sum_{m=0}^{1} \left(\int_{\alpha_2} \boldsymbol{N}\boldsymbol{K}_{b(1)\alpha_2^m}^{(\tau\eta)} \mathbf{N}^{\mathrm{T}} A_2 \alpha_2 + \int_{\alpha_1} \boldsymbol{N}\boldsymbol{K}_{b(1)\alpha_1^m}^{(\tau\eta)} \mathbf{N}^T A_1 \alpha_1 \right) \right] \overline{\mathbf{u}}^{(\eta)} = \sum_{\tau=0}^{N+1} \left(\delta \overline{\mathbf{u}}^{(\tau)}\right)^T \sum_{\eta=0}^{N+1} \mathbf{K}_b^{(\tau\eta)} \overline{\mathbf{u}}^{(\eta)} \tag{88}$$

Introducing the elastic strain energy of Eqn. (79) and kinetic energy of Eqn. (83) in the Hamiltonian Principle of Eqn. (78), the final form of the fundamental governing equations is derived for a generic $\tau = 0, ..., N + 1$:

$$\begin{aligned} \sum_{\eta=0}^{N+1} \mathbf{K}^{(\tau\eta)} \overline{\mathbf{u}}^{(\eta)} + \sum_{\eta=0}^{N+1} \mathbf{M}^{(\tau\eta)} \ddot{\overline{\mathbf{u}}}^{(\eta)} = \mathbf{0} \quad \Leftrightarrow \quad & \sum_{\eta=0}^{N+1} \left(\overline{\mathbf{K}}_s^{(\tau\eta)} - \overline{\mathbf{K}}_b^{(\tau\eta)} \right) \overline{\mathbf{u}}^{(\eta)} \\ & + \sum_{\eta=0}^{N+1} \mathbf{M}^{(\tau\eta)} \ddot{\overline{\mathbf{u}}}^{(\eta)} \\ & = \mathbf{0} \end{aligned} \tag{89}$$

The interested reader can find in Ref. [12] an extended expression of the coefficients of matrices $\overline{\mathbf{K}}_s^{(\tau\eta)}$ and $\mathbf{M}^{(\tau\eta)}$.

Rearranging Eqn. (89) so that all kinematic expansion orders are taken into account, the assembled version of the governing equations are obtained:

$$\begin{bmatrix} \mathbf{K}^{(00)} & \mathbf{K}^{(01)} & \cdots & \mathbf{K}^{(0(N))} & \mathbf{K}^{(0(N+1))} \\ \mathbf{K}^{(10)} & \mathbf{K}^{(11)} & \cdots & \mathbf{K}^{(1(N))} & \mathbf{K}^{(1(N+1))} \\ \vdots & \vdots & \ddots & \vdots & \vdots \\ \mathbf{K}^{((N)0)} & \mathbf{K}^{((N)1)} & \cdots & \mathbf{K}^{((N)(N))} & \mathbf{K}^{((N)(N+1))} \\ \mathbf{K}^{((N+1)0)} & \mathbf{K}^{((N+1)1)} & \cdots & \mathbf{K}^{((N+1)(N))} & \mathbf{K}^{((N+1)(N+1))} \end{bmatrix} \begin{bmatrix} \overline{\mathbf{u}}^{(0)} \\ \overline{\mathbf{u}}^{(1)} \\ \vdots \\ \overline{\mathbf{u}}^{(N)} \\ \overline{\mathbf{u}}^{(N+1)} \end{bmatrix} + \\ + \begin{bmatrix} \mathbf{M}^{(00)} & \mathbf{M}^{(01)} & \cdots & \mathbf{M}^{(0(N))} & \mathbf{M}^{(0(N+1))} \\ \mathbf{M}^{(10)} & \mathbf{M}^{(11)} & \cdots & \mathbf{M}^{(1(N))} & \mathbf{M}^{(1(N+1))} \\ \vdots & \vdots & \ddots & \vdots & \vdots \\ \mathbf{M}^{((N)0)} & \mathbf{M}^{((N)1)} & \cdots & \mathbf{M}^{((N)(N))} & \mathbf{M}^{((N)(N+1))} \\ \mathbf{M}^{((N+1)0)} & \mathbf{M}^{((N+1)1)} & \cdots & \mathbf{M}^{((N+1)(N))} & \mathbf{M}^{((N+1)(N+1))} \end{bmatrix} \begin{bmatrix} \ddot{\overline{\mathbf{u}}}^{(0)} \\ \ddot{\overline{\mathbf{u}}}^{(1)} \\ \vdots \\ \ddot{\overline{\mathbf{u}}}^{(N)} \\ \ddot{\overline{\mathbf{u}}}^{(N+1)} \end{bmatrix} = \begin{bmatrix} \mathbf{0} \\ \mathbf{0} \\ \vdots \\ \mathbf{0} \\ \mathbf{0} \end{bmatrix} \end{bmatrix} \tag{90}$$

The fundamental relations are now arranged so that the free vibration analysis can be performed. Referring to a generic τ-th kinematic expansion order, harmonic solutions are selected from those coming from Eqn. (89). To this purpose, the following definition is considered for the discrete generalized displacement field vector $\overline{\mathbf{u}}^{(\tau)}$:

$$\overline{\mathbf{u}}^{(\tau)}\left(\alpha_{1f}, \alpha_{2g}, t\right) = \overline{\mathbf{U}}^{(\tau)}\left(\alpha_{1f}, \alpha_{2g}\right) e^{i\omega t} \tag{91}$$

where ω is the circular frequency so that $\omega = 2\pi f$, whereas $\overline{\mathbf{U}}^{(\tau)}$ denotes the generalized mode shape column vector of dimensions $(3I_N I_M) \times 1$, defined for each $\tau = 0, ..., N + 1$ according to the same procedure outlined in Eqn. (23) for vector $\overline{\mathbf{u}}^{(\tau)}$. Substituting Eqn. (91) in the higher order fundamental relations of Eqn. (89), it gives:

$$\sum_{\eta=0}^{N+1} \mathbf{K}^{(\tau\eta)} \overline{\mathbf{U}}^{(\eta)} = \omega^2 \sum_{\eta=0}^{N+1} \mathbf{M}^{(\tau\eta)} \overline{\mathbf{U}}^{(\eta)} \tag{92}$$

The final assembled form of the fundamental equations accounting for the two-dimensional $I_N \times I_M$ computational grid and kinematic field expansion from $\tau = 0$ up to $\tau = N + 1$ looks as follows:

$$\boldsymbol{K}\boldsymbol{\delta} = \omega^2 \boldsymbol{M}\boldsymbol{\delta} \tag{93}$$

being $\boldsymbol{\delta}$ the column vector of dimensions $(3(N + 2)I_N I_M) \times 1$ collecting the DOFs of the problem, whereas $\mathbf{K}$ and $\mathbf{M}$ are the assembled form of the stiffness and mass matrix, respectively, of dimensions $(3(N + 2)I_N I_M) \times (3(N + 2)I_N I_M)$. It is convenient to arrange Eqn. (93) so that the DOFs related to the boundary region of the computational domain, collected in the sub-vector $\boldsymbol{\delta}_b$, are separated from the remaining ones arranged in the sub-vector $\boldsymbol{\delta}_d$. One gets [91]:

$$\left[\begin{array}{c|c} \mathbf{K}_{bb} & \mathbf{K}_{bd} \\ \hline \mathbf{K}_{db} & \mathbf{K}_{dd} \end{array}\right] \left[\begin{array}{c} \boldsymbol{\delta}_b \\ \hline \boldsymbol{\delta}_d \end{array}\right] = \omega^2 \left[\begin{array}{c|c} \mathbf{0} & \mathbf{0} \\ \hline \mathbf{0} & \mathbf{M}_{dd} \end{array}\right] \left[\begin{array}{c} \boldsymbol{\delta}_b \\ \hline \boldsymbol{\delta}_d \end{array}\right] \tag{94}$$

where $\boldsymbol{\delta} = [\boldsymbol{\delta}_b \boldsymbol{\delta}_d]^T$. In this way, a more efficient algebraic system comes out from the application of a static condensation, whereas prescribed DOFs vector $\boldsymbol{\delta}_b$ related to the boundaries is not considered in the computation. If the symbol $\mathbf{I}$ denotes an identity matrix of proper dimensions, Eqn. (94) becomes:

$$\left(\mathbf{M}_{dd}^{-1}\left(\mathbf{K}_{dd} - \mathbf{K}_{db}\mathbf{K}_{bb}^{-1}\mathbf{K}_{bd}\right) - \omega^2 \mathbf{I}\right)\boldsymbol{\delta}_d = 0 \tag{95}$$

8. Numerical implementation

In the present section, the fundamental relations, derived in weak form, are solved numerically employing the GDQ method. According to this numerical technique, the derivative of a generic order of a function is expressed as a linear combination of the values assumed by the function itself in a discrete set of nodes. Referring to a univariate smooth function $f = f(x)$ defined in a closed interval $[a, b]$, the derivative of a generic n-th order in a generic point $x = x_i$ of the grid at issue made of I_Q nodes is computed as [91]:

$$\left.\frac{\partial^n f(x)}{\partial x^n}\right|_{x=x_i} \cong \sum_{j=1}^{I_Q} \varsigma_{ij}^{(n)} f(x_j) \tag{96}$$

where $f(x_j)$ is the values assumed by the function in the node x_j of the grid with $j = 1, ..., I_Q$, whereas $\varsigma_{ij}^{(n)}$ are the GDQ weighting coefficients for the derivative of n-th order, setting $i, j = 1, ..., I_Q$. The GDQ weighting coefficients are calculated with the recursive expression derived from the Weierstrass interpolation theorem [91]:

$$\begin{aligned} \varsigma_{ij}^{(1)} &= \frac{\mathscr{L}^{(1)}(x_i)}{(x_i - x_j)\mathscr{L}^{(1)}(x_j)} = \frac{\prod_{k=1, k\neq i}^{N} (x_i - x_k)}{(x_i - x_j) \prod_{k=1, k\neq j}^{N} (x_j - x_k)} && \text{for } i \neq j \\ \varsigma_{ij}^{(n)} &= n\left(\varsigma_{ij}^{(1)}\varsigma_{ii}^{(n-1)} - \frac{\varsigma_{ij}^{(n-1)}}{x_i - x_j}\right) && \text{for } i \neq j, \quad n > 1 \\ \varsigma_{ii}^{(n)} &= -\sum_{j=1 j\neq i}^{N} \varsigma_{ij}^{(n)} && \text{for } i = j, \quad \forall n \end{aligned} \tag{97}$$

being $\mathscr{L}^{(1)}(x_i), \mathscr{L}^{(1)}(x_j)$ the first order derivative of the Lagrange

interpolating polynomials evaluated at points x_i and x_j with $i, j = 1, ..., I_Q$.

Moving from the GDQ numerical technique, the numerical integration is here performed by means of the GIQ method [91]. Following a similar procedure of Eqn. (96), the integral of a generic univariate smooth function $f = f(x)$ with $x \in [a, b]$ restricted to a closed interval $[x_i, x_j]$ is evaluated in terms of a linear combination of values $f(x_k)$ assumed by f in a discrete number of points x_k with $k = 1, ..., I_Q$:

$$\int_{x_i}^{x_j} f(x)dx = \sum_{k=1}^{I_Q} w_k^{ij} f(x_k) = \sum_{k=1}^{I_Q} (w_{jk} - w_{ik}) f(x_k) \tag{98}$$

The GIQ coefficients w_{ik}, w_{jk} are conveniently collected in a matrix $\mathbf{W}$ of dimensions $I_Q \times I_Q$. They are derived from the matrix $\bar{\varsigma}^{\zeta(1)}$ collecting the GDQ shifted coefficients of the first order derivative denoted by $\bar{\varsigma}_{ij}^{\zeta(1)}$ with $i, j = 1, ..., I_Q$, defined as follows [91]:

$$\begin{aligned} \bar{\varsigma}_{ij}^{\zeta(1)} &= \frac{x_i - \varepsilon}{x_j - \varepsilon} \varsigma_{ij}^{\zeta(1)} \qquad \text{for } i \neq j \\ \bar{\varsigma}_{ij}^{\zeta(1)} &= \varsigma_{ii}^{\zeta(1)} + \frac{1}{x_i - \varepsilon} \qquad \text{for } i = j \end{aligned} \tag{99}$$

where the value $\varepsilon = 1 \times 10^{-10}$ has been assumed. As it has been shown in Ref. [91], the matrix of the GIQ coefficients is derived from the inversion of $\bar{\varsigma}^{\zeta(1)}$:

$$\mathbf{W} = \left(\bar{\varsigma}^{\zeta(1)}\right)^{-1} \tag{100}$$

9. Governing equations for aribtrarily-shaped domains

The formulation presented in the manuscript is based on a parametric description of the reference surface of the shell in terms of curvilinear principal coordinates. In this way, a rectangular physical domain comes out. When arbitrarily-shaped shell structures are considered, a parametrization of $\mathbf{r}$ is not provided, and a mapping of the physical domain is performed. In this way, the distorted domain under consideration is turned into a squared dimensionless parent element, described by means of ξ_1 and ξ_2 coordinates, which are expressed in terms of α_1,α_2 so that $(\xi_1,\xi_2) \in [-1, +1] \times [-1, +1]$. To this end, the generalized blending functions $\alpha_1(\xi_1,\xi_2)$ and $\alpha_2(\xi_1,\xi_2)$ are introduced [12]:

$$\begin{bmatrix} \alpha_1(\xi_1, \xi_2) \\ \alpha_2(\xi_1, \xi_2) \end{bmatrix} = \begin{bmatrix} \bar{\mathbf{b}} & \mathbf{0} \\ \mathbf{0} & \bar{\mathbf{b}} \end{bmatrix} \begin{bmatrix} \bar{\mathbf{B}} & \mathbf{0} \\ \mathbf{0} & \bar{\mathbf{B}} \end{bmatrix} \begin{bmatrix} \tilde{\alpha}_1 \\ \tilde{\alpha}_2 \end{bmatrix} \tag{101}$$

being $\tilde{\boldsymbol{\alpha}}_i = [\bar{\boldsymbol{\alpha}}_i \quad \boldsymbol{\alpha}_i]^T$ for $i = 1, 2$ a vector containing the geometric description $\bar{\boldsymbol{\alpha}}_i, \boldsymbol{\alpha}_i$ of the edges and the corners of the physical domain, respectively. More specifically, the corners locations $(\alpha_{1(q)},\alpha_{2(q)})$ with $q = 1, ..., 4$ are arranged so that $\boldsymbol{\alpha}_i = [\alpha_{i(1)} \quad \alpha_{i(2)} \quad \alpha_{i(3)} \quad \alpha_{i(4)}]^T$ with $i = 1, 2$, whereas the vector $\bar{\boldsymbol{\alpha}}_i = [\bar{\alpha}_{i(1)}(\xi_1) \quad \bar{\alpha}_{i(2)}(\xi_2) \quad \bar{\alpha}_{i(3)}(\xi_1) \quad \bar{\alpha}_{i(4)}(\xi_2)]^T$ for $i = 1, 2$ accounts for the location of the four edges of the structure within the physical domain, denoted by $(\bar{\alpha}_{1(p)}, \bar{\alpha}_{2(p)})$ for $p = 1, ..., 4$. In addition, the operators $\bar{\mathbf{b}}$ and $\bar{\mathbf{B}}$ occurring in Eqn. (101) read as:

$$\bar{\mathbf{b}} = [\mathbf{b} \quad \mathbf{b}], \quad \bar{\mathbf{B}} = \begin{bmatrix} \frac{1}{2}\mathbf{I} & \mathbf{0} \\ \mathbf{0} & -\frac{1}{4}\mathbf{B} \end{bmatrix} \tag{102}$$

where $\mathbf{I}$ is the identity matrix, whereas $\mathbf{b}$ and $\mathbf{B}$ are defined as follows:

$$\mathbf{b} = [(1 - \xi_2) \quad (1 + \xi_1) \quad (1 + \xi_2) \quad (1 - \xi_1)]$$
$$\mathbf{B} = \begin{bmatrix} (1 - \xi_1) & 0 & 0 & 0 \\ 0 & (1 - \xi_2) & 0 & 0 \\ 0 & 0 & (1 + \xi_1) & 0 \\ 0 & 0 & 0 & (1 + \xi_2) \end{bmatrix} \tag{103}$$

Starting from Eqn. (101), first order derivatives with respect to α_1,α_2 are expressed in terms of those with respect to the natural coordinates ξ_1,ξ_2 [12]:

$$\begin{bmatrix} \frac{\partial}{\partial \alpha_1} \\ \frac{\partial}{\partial \alpha_2} \end{bmatrix} = \begin{bmatrix} \frac{\partial \xi_1}{\partial \alpha_1} & \frac{\partial \xi_2}{\partial \alpha_1} \\ \frac{\partial \xi_1}{\partial \alpha_2} & \frac{\partial \xi_2}{\partial \alpha_2} \end{bmatrix} \begin{bmatrix} \frac{\partial}{\partial \xi_1} \\ \frac{\partial}{\partial \xi_2} \end{bmatrix} = \begin{bmatrix} \xi_{1,\alpha_1} & \xi_{2,\alpha_1} \\ \xi_{1,\alpha_2} & \xi_{2,\alpha_2} \end{bmatrix} \begin{bmatrix} \frac{\partial}{\partial \xi_1} \\ \frac{\partial}{\partial \xi_2} \end{bmatrix} \tag{104}$$

Since a one-to-one relation is assessed between natural and principal coordinates, the partial first order derivation with respect to ξ_1,ξ_2 can be written in terms of α_1,α_2 with the well-known chain rule:

$$\begin{bmatrix} \frac{\partial}{\partial \xi_1} \\ \frac{\partial}{\partial \xi_2} \end{bmatrix} = \begin{bmatrix} \frac{\partial \alpha_1}{\partial \xi_1} & \frac{\partial \alpha_2}{\partial \xi_1} \\ \frac{\partial \alpha_1}{\partial \xi_2} & \frac{\partial \alpha_2}{\partial \xi_2} \end{bmatrix} \begin{bmatrix} \frac{\partial}{\partial \alpha_1} \\ \frac{\partial}{\partial \alpha_2} \end{bmatrix} = \mathbf{J} \begin{bmatrix} \frac{\partial}{\partial \alpha_1} \\ \frac{\partial}{\partial \alpha_2} \end{bmatrix} \tag{105}$$

being $\mathbf{J}$ the Jacobian operator of the coordinate transformation under consideration:

$$\det(\mathbf{J}) = \frac{\partial \alpha_1}{\partial \xi_1} \frac{\partial \alpha_2}{\partial \xi_2} - \frac{\partial \alpha_2}{\partial \xi_1} \frac{\partial \alpha_1}{\partial \xi_2} \tag{106}$$

If $\det(\mathbf{J}) \neq 0$, Eqn. (105) can be inverted, setting $\mathbf{J}^{-1}$ the inverse Jacobian matrix [12]:

$$\begin{aligned} \begin{bmatrix} \frac{\partial}{\partial \alpha_1} \\ \frac{\partial}{\partial \alpha_2} \end{bmatrix} &= \mathbf{J}^{-1} \begin{bmatrix} \frac{\partial}{\partial \xi_1} \\ \frac{\partial}{\partial \xi_2} \end{bmatrix} = \begin{bmatrix} \frac{\partial \xi_1}{\partial \alpha_1} & \frac{\partial \xi_2}{\partial \alpha_1} \\ \frac{\partial \xi_1}{\partial \alpha_2} & \frac{\partial \xi_2}{\partial \alpha_2} \end{bmatrix} \begin{bmatrix} \frac{\partial}{\partial \xi_1} \\ \frac{\partial}{\partial \xi_2} \end{bmatrix} \\ &= \frac{1}{\det(\mathbf{J})} \begin{bmatrix} \frac{\partial \alpha_2}{\partial \xi_2} & -\frac{\partial \alpha_2}{\partial \xi_1} \\ -\frac{\partial \alpha_1}{\partial \xi_2} & \frac{\partial \alpha_1}{\partial \xi_1} \end{bmatrix} \begin{bmatrix} \frac{\partial}{\partial \xi_1} \\ \frac{\partial}{\partial \xi_2} \end{bmatrix} \end{aligned} \tag{107}$$

The following definitions are introduced if Eqn. (105) and Eqn. (107) are compared to each other:

$$\begin{aligned} \xi_{1,\alpha_1} &= \frac{1}{\det(\mathbf{J})} \frac{\partial \alpha_2}{\partial \xi_2}, \quad \xi_{2,\alpha_1} = -\frac{1}{\det(\mathbf{J})} \frac{\partial \alpha_2}{\partial \xi_1} \\ \xi_{1,\alpha_2} &= -\frac{1}{\det(\mathbf{J})} \frac{\partial \alpha_1}{\partial \xi_2}, \quad \xi_{2,\alpha_2} = \frac{1}{\det(\mathbf{J})} \frac{\partial \alpha_1}{\partial \xi_1} \end{aligned} \tag{108}$$

In the same way, the second order derivatives can be easily studied.

Regarding the four edges of the distorted domain, NURBS curves are adopted for their geometric descriptions along the physical domain. If a curvilinear coordinate $u \in [a, b]$ with $a, b \in \mathbb{R}$ is adopted, a NURBS curve is defined by means of a set $\mathbf{P}_i$ for $i = 1, ..., n$ of n control points [8-9]:

$$\mathbf{C}(u) = \frac{\sum_{i=0}^{n} N_{i,p}(u) w_i \mathbf{P}_i}{\sum_{i=0}^{n} N_{i,p}(u) w_i} \tag{109}$$

where w_i are proper weighting coefficients, whereas $N_{i,p}(u)$ with $i = 0, ..., n$ are B-Spline basis functions of degree p defined in the interval $[a, b] = [0, 1]$. These functions are calculated from a recursive procedure, taking into account a knot vector $\boldsymbol{\Omega} = \left[\underbrace{a, \cdots, a}_{p+1}, u_{p+1}, \cdots, u_{m-p-1}, \underbrace{b, \cdots, b}_{p+1}\right]$ of m breakpoint.

A local reference system of unit vectors $\mathbf{n}_n$, $\mathbf{n}_s$, $\mathbf{n}_\zeta$ is now introduced to define general boundary conditions along the mapped edges of the structure, in terms of their cosine directors with respect to the shell principal reference system [12]:

$$\begin{aligned}\mathbf{n}_n &= [n_{n1}\ \ n_{n2}\ \ n_{n3}]^T,\\ \mathbf{n}_s &= [n_{s1}\ \ n_{s2}\ \ n_{s3}]^T,\\ \mathbf{n}_\zeta &= [n_{\zeta 1}\ \ n_{\zeta 2}\ \ n_{\zeta 3}]^T\end{aligned} \tag{110}$$

If unit vectors under consideration are selected so that $\mathbf{n}_\zeta = \mathbf{n}$ and $\mathbf{n}_n$, $\mathbf{n}_s$ are the normal and tangential directions of a generic curve lying on the shell reference surface $\mathbf{r}(\alpha_1,\alpha_2)$, the definitions n_{n3},n_{s3},$n_{\zeta 1}$,$n_{\zeta 2} = 0$ and $n_{\zeta 3} = 1$ are introduced.

The higher order kinematic field variable $\mathbf{u}^{(\tau)} = \left[u_1^{(\tau)}\ u_2^{(\tau)}\ u_3^{(\tau)}\right]^T$ referred to a generic τ-th expansion order, defined with respect to the shell principal directions α_1,α_2,ζ is now described with respect to the local reference system of unit vectors $\mathbf{n}_s$, $\mathbf{n}_n$ and $\mathbf{n}_\zeta$ defined by Eqn. (110), leading to the new higher order displacement field components, denoted by $u_n^{(\tau)}, u_s^{(\tau)}, u_\zeta^{(\tau)}$:

$$\begin{bmatrix} u_n^{(\tau)} \\ u_s^{(\tau)} \\ u_\zeta^{(\tau)} \end{bmatrix} = \begin{bmatrix} n_{n1} & n_{n2} & 0 \\ n_{s1} & n_{s2} & 0 \\ 0 & 0 & 1 \end{bmatrix} \begin{bmatrix} u_1^{(\tau)} \\ u_2^{(\tau)} \\ u_3^{(\tau)} \end{bmatrix} \quad \text{for} \quad \tau = 0, \ldots, N+1 \tag{111}$$

In the same way, the higher order generalized stress resultants $N_1^{(\tau)\alpha_1}$, $N_2^{(\tau)\alpha_1}$, $N_{12}^{(\tau)\alpha_1}$, $N_{21}^{(\tau)\alpha_1}$, $T_1^{(\tau)\alpha_3}$, $T_2^{(\tau)\alpha_3}$ are employed to introduce the quantities $N_n^{(\tau)\alpha_1}$, $N_{ns}^{(\tau)\alpha_2}$ and $T_\zeta^{(\tau)\alpha_3}$ defined in the local coordinate system of Eqn. (110) according to the following transformation:

$$\begin{aligned} N_n^{(\tau)\alpha_1} &= N_1^{(\tau)\alpha_1} n_{n1}^2 + N_2^{(\tau)\alpha_1} n_{n2}^2 + N_{12}^{(\tau)\alpha_1} n_{n1} n_{n2} + N_{21}^{(\tau)\alpha_1} n_{n1} n_{n2} \\ N_{ns}^{(\tau)\alpha_2} &= N_1^{(\tau)\alpha_2} n_{n1} n_{s1} + N_2^{(\tau)\alpha_2} n_{n2} n_{s2} + N_{12}^{(\tau)\alpha_2} n_{n1} n_{s2} + N_{21}^{(\tau)\alpha_2} n_{n2} n_{s1} \\ T_\zeta^{(\tau)\alpha_3} &= T_1^{(\tau)\alpha_3} n_{n1} + T_2^{(\tau)\alpha_3} n_{n2} \end{aligned} \tag{112}$$

When the generalized blending functions of Eqn. (101) are adopted, the generalized stiffness matrix introduced in Eqn. (81) and the mass matrix of Eqn. (85) assume the following aspect [12]:

$$\begin{aligned} \overline{\mathbf{K}}_s^{(\tau\eta)} &= \int_{-1}^{1}\int_{-1}^{1} \begin{bmatrix} \overline{\mathbf{K}}_s^{(\tau\eta)\alpha_1\alpha_1} & \overline{\mathbf{K}}_s^{(\tau\eta)\alpha_1\alpha_2} & \overline{\mathbf{K}}_s^{(\tau\eta)\alpha_1\alpha_3} \\ \overline{\mathbf{K}}_s^{(\tau\eta)\alpha_2\alpha_1} & \overline{\mathbf{K}}_s^{(\tau\eta)\alpha_2\alpha_2} & \overline{\mathbf{K}}_s^{(\tau\eta)\alpha_2\alpha_3} \\ \overline{\mathbf{K}}_s^{(\tau\eta)\alpha_3\alpha_1} & \overline{\mathbf{K}}_s^{(\tau\eta)\alpha_3\alpha_2} & \overline{\mathbf{K}}_s^{(\tau\eta)\alpha_3\alpha_3} \end{bmatrix} A_1 A_2 \det(\mathbf{J}) d\xi_1 d\xi_2 \\ \mathbf{M}^{(\tau\eta)} &= \int_{-1}^{1}\int_{-1}^{1} \begin{bmatrix} \mathbf{M}^{(\tau\eta)\alpha_1\alpha_1} & \mathbf{M}^{(\tau\eta)\alpha_1\alpha_2} & \mathbf{M}^{(\tau\eta)\alpha_1\alpha_3} \\ \mathbf{M}^{(\tau\eta)\alpha_2\alpha_1} & \mathbf{M}^{(\tau\eta)\alpha_2\alpha_2} & \mathbf{M}^{(\tau\eta)\alpha_2\alpha_3} \\ \mathbf{M}^{(\tau\eta)\alpha_3\alpha_1} & \mathbf{M}^{(\tau\eta)\alpha_3\alpha_2} & \mathbf{M}^{(\tau\eta)\alpha_3\alpha_3} \end{bmatrix} A_1 A_2 \det(\mathbf{J}) d\xi_1 d\xi_2 \end{aligned} \tag{113}$$

Another key factor for the assessment of boundary conditions on a mapped domain is the evaluation of the length $L_{(i)}$ of its four edges ($i = 1$, ..., 4). To this purpose, the expression of the length of a generic curve lying on the reference surface $\mathbf{r}(\alpha_1,\alpha_2)$ is adopted for $j = 1, 2$ [12]:

$$L_{(i)} = \int_{-1}^{1} \sqrt{A_1^2 \left(\frac{d\alpha_1}{d\xi_j}\right)^2 + A_2^2 \left(\frac{d\alpha_2}{d\xi_j}\right)^2}\, d\xi_j \tag{114}$$

Furthermore, the higher order boundary stress vector $\overline{\mathbf{Q}}_{n(i)}^{(\tau)}$ with $i = 1$, ..., 4 is computed along the edges of the mapped domain in terms of the generalized stress resultants $N_n^{(\tau)\alpha_1}$, $N_{ns}^{(\tau)\alpha_2}$, $T_\zeta^{(\tau)\alpha_3}$. If $ds_{n(i)}$ identifies the curvilinear abscissa of the i-th shell edge, the following expression comes out [12]:

$$\overline{\mathbf{Q}}_{n(i)}^{(\tau)} = \int_0^{L_{(i)}} \begin{bmatrix} \overline{\mathbf{N}}\overline{\mathbf{N}}_n^{(\tau)\alpha_1} \\ \overline{\mathbf{N}}\overline{\mathbf{N}}_{ns}^{(\tau)\alpha_2} \\ \overline{\mathbf{N}}\overline{\mathbf{T}}_\zeta^{(\tau)\alpha_3} \end{bmatrix} ds_{n(i)} = \int_{-1}^{1} \begin{bmatrix} \overline{\mathbf{N}}\overline{\mathbf{N}}_n^{(\tau)\alpha_1} \\ \overline{\mathbf{N}}\overline{\mathbf{N}}_{ns}^{(\tau)\alpha_2} \\ \overline{\mathbf{N}}\overline{\mathbf{T}}_\zeta^{(\tau)\alpha_3} \end{bmatrix} \frac{L_{(i)}}{2} d\eta_{(i)} \tag{115}$$

where $\eta_{(i)} \in [-1, 1]$ is the dimensionless parameter employed for the geometric description of the curve at issue.

When the generalized boundary stresses of Eqn. (115) are applied to edges of the physical domain, a useful nomenclature is adopted, defined as:

$$\begin{array}{ccccc} \text{West edge (W)} & \rightarrow & \xi_2 = -1 & \rightarrow & (\alpha_1,\alpha_2) = \left(\overline{\alpha}_{1(1)}(\xi_1), \overline{\alpha}_{2(1)}(\xi_1)\right) \\ \text{South edge (S)} & \rightarrow & \xi_1 = 1 & \rightarrow & (\alpha_1,\alpha_2) = \left(\overline{\alpha}_{1(2)}(\xi_2), \overline{\alpha}_{2(2)}(\xi_2)\right) \\ \text{East edge (E)} & \rightarrow & \xi_2 = 1 & \rightarrow & (\alpha_1,\alpha_2) = \left(\overline{\alpha}_{1(3)}(\xi_1), \overline{\alpha}_{2(3)}(\xi_1)\right) \\ \text{North edge (N)} & \rightarrow & \xi_1 = -1 & \rightarrow & (\alpha_1,\alpha_2) = \left(\overline{\alpha}_{1(4)}(\xi_2), \overline{\alpha}_{2(4)}(\xi_2)\right) \end{array} \tag{116}$$

10. Applications and results

Some numerical examples are now presented, where the proposed formulation is applied to derive the natural frequencies of some laminated structures reinforced by CNTs. These numerical predictions are compared to the results obtained from some three-dimensional Finite Element simulations to assess the accuracy of the present two-dimensional formulation. More specifically, FEM models are developed using commercial software, employing a mesh made up of C3D20 brick parabolic elements.

Structures of various curvatures are considered, each of them characterized by a general thickness variation according to Eqn. (10). Furthermore, a generalized mapping of the physical domain is applied as described in Eqn. (101), enabling the study of structures of various shape with the present model. The lamination schemes considered in the examples account for different numbers of layers with various material symmetries and softcore behavior. Furthermore, some laminae are characterized by a smooth variation of the material properties, coming from dispersed and agglomerated FG-CNTs. On the other hand, the CNT composite layers are obtained from an isotropic matrix [49] of density $\rho_m = 1150\text{kg/m}^3$. Its mechanical properties are expressed in terms of the elastic modulus $E_m = 2.1\text{GPa}$ and Poisson ratio $\nu_m = 0.34$. The elastic constitutive behavior of the CNT particles adopted in the simulations is described in terms of the Hill's elastic moduli, according to the notation in Eqn. (53). Table 1 provides the mechanical properties of SWCNT nanofibers with armchair configuration for different values of the chiral indexes (n, n). Throughout all simulations presented in the manuscript, the value $n = 10$ has been adopted.

In Fig. 2a parametric investigation on the homogenized elastic properties of a CNT composite material is performed. Glass [49] long fibers of density $\rho_f = 2491.191\text{kg/m}^3$ with a mass concentration equal to $w_f = 0.85$ are adopted, as happens in all CNT composite layers considered in the present study, characterized by an elastic modulus equal to $E^f_1 = E^f_2 = E^f_3 = E^f = 73.084$ GPa and a Poisson coefficient $\nu^f_{12} = \nu^f_{13} = \nu^f_{13} = \nu^f = 0.22$. The elastic properties of the equivalent orthotropic material are evaluated for various CNT concentrations. In the first column the agglomeration parameter μ_1 is set equal to 0.25, while in the second column the value $\mu_2 = 1$ is assumed. The introduction of CNT agglomerated nanofibers leads to an increased elastic modulus along α_1 and of $E_2 = E_3$, while the Poisson coefficients decrease. A similar behavior is seen when μ_1 is varied. Furthermore, μ_1 turns out to be a higher sensitivity parameter than μ_2 for the CNT composite material under considerations as a smoother variation of the material properties is found.

In Table 2 and Table 3, a rectangular plate laminated with generally anisotropic materials is studied. The geometric and mechanical properties are reported in Fig. 3. As it can be seen, the GDQ model is developed starting from a two-dimensional grid of $I_N \times I_M = 25 \times 25$ nodes based on the LGL distribution, while the 3D FEM simulations are calculated on a structured mesh with parabolic brick elements. The structure under consideration is obtained from the superimposition of five layers of arbitrary orientation. More specifically, the two laminae of trigonal material ($\rho^{(k)} = 2649\ \text{kg}/\text{m}^3$) are characterized by the

following three-dimensional stiffness matrix, according to the nomenclature outlined in Eqn. (37), setting $E_{ij}^{(k)} = C_{ij}^{(k)}$ with $i, j = 1, ..., 6$ [105]:

$$\begin{bmatrix} C_{11}^{(k)} & C_{12}^{(k)} & C_{16}^{(k)} & C_{14}^{(k)} & C_{15}^{(k)} & C_{13}^{(k)} \\ C_{12}^{(k)} & C_{22}^{(k)} & C_{26}^{(k)} & C_{24}^{(k)} & C_{25}^{(k)} & C_{23}^{(k)} \\ C_{16}^{(k)} & C_{26}^{(k)} & C_{66}^{(k)} & C_{46}^{(k)} & C_{56}^{(k)} & C_{36}^{(k)} \\ C_{14}^{(k)} & C_{24}^{(k)} & C_{46}^{(k)} & C_{44}^{(k)} & C_{45}^{(k)} & C_{34}^{(k)} \\ C_{15}^{(k)} & C_{25}^{(k)} & C_{56}^{(k)} & C_{45}^{(k)} & C_{55}^{(k)} & C_{35}^{(k)} \\ C_{13}^{(k)} & C_{23}^{(k)} & C_{36}^{(k)} & C_{34}^{(k)} & C_{35}^{(k)} & C_{33}^{(k)} \end{bmatrix} = \begin{bmatrix} 86.74 & 6.99 & 0 & 0 & -17.91 & 11.91 \\ 6.99 & 86.74 & 0 & 0 & 17.91 & 11.91 \\ 0 & 0 & 39.88 & 0 & 0 & 0 \\ 0 & 0 & 0 & 57.94 & 0 & 0 \\ -17.91 & 17.91 & 0 & 0 & 57.94 & 0 \\ 11.91 & 11.91 & 0 & 0 & 0 & 107.2 \end{bmatrix} \text{GPa} \quad (117)$$

Mode frequencies and shapes are evaluated for various configurations of the CNT composite layers. In all cases, a long fiber percentage equal to $w_f = 0.85$ is considered, and the vibrational response is evaluated for different values of the agglomeration parameters μ_1,μ_2. More specifically, Table 2 presents the results obtained varying the parameter μ_1 with $\mu_2 = 1$, while Table 3 reports the numerical results for the case $\mu_1 = 0.7$. As illustrated in Fig. 4, an increased mass concentration of CNT nanofibers leads to higher vibration frequencies in all modes for any value of μ_1,μ_2. Furthermore, when the CNT composite layer exclusively consists of agglomerated nanofibers within the isotropic matrix, a significative increase in the natural frequencies is seen, particularly for the first and the second mode, for the same value of w_r. In addition, when $\mu_2 = 1$, the natural frequencies are independent on the CNT concentration w_r for lower μ_1 values, as visible in Fig. 4 and Table 3. This behavior can be explained from a physical perspective remembering that when $\mu_2 = 1$, a complete agglomeration of nanofibers is obtained, therefore an increase in the CNTs mass fraction does not vary the configuration of the inclusions within the isotropic matrix. In this example, all the results obtained from the present formulation are calculated employing the EDZ4 displacement field assumption according to Eqn. (15). The selection of the higher order theory considers the case $w_r = 0.2$ and $w_r = 0.4$ for all investigated configurations of the agglomeration effect in the CNT layers. In particular, the mode frequencies are calculated using a computationally demanding 3D FEM simulation, pointing out the accuracy, stability and numerical efficiency of the two-dimensional formulation of the present study.

Finally, the first nine mode shape vectors have been calculated for the case characterized by a complete absence of dispersed CNT particles, as they are all agglomerated in particles inside the matrix ($\mu_1 = \mu_2 = 1$). As depicted in Fig. 5, where a three-dimensional reconstruction of the first nine mode shapes is presented, the employment of a higher order displacement field expansion enables the prediction of both bending and stretching deflections, as well as the coupling between different deformation contributions. In fact, from a physical point of view, the stretching effect can be found in lamination schemes where the stiffness of the layers are very different from that of the adjacent ones.

Next example aims to determine the most suitable displacement field assumption for the dynamic analysis of structures reinforced with CNTs when curvatures are introduced. For this purpose, a fully-clamped (CCCC) laminated doubly-curved hyperbolic paraboloid is considered, maintaining the same lamination scheme as in the previous example. The geometric representation of the reference surface of the structure is performed employing a parametrization with curvilinear principal coordinates, as shown in Fig. 6. The validation of the higher order theory is conducted in Table 4 for two different values of the CNT mass concentration. All simulations are performed setting $\mu_2 = 1$, while different values of the agglomeration parameter μ_1 are considered. The results obtained from a 3D FEM model are reported for each reference configuration of the CNT composite layer, and the unified formulation is employed to derive the natural frequencies are derived using different field variable assumptions along the thickness direction. In particular, the solution is provided from simulations based on FSDT and TSDT, as well as the ED4 and EDZ4 theory. The results obtained from finite element simulations are reproduced with a high level of accuracy for the structure under consideration when a higher order displacement field assumption is employed, along with the generalized zigzag function introduced in Eqn. (16). Once it has been shown that the EDZ4 theory accurately predicts the 3D FEM results, in Fig. 7 the first nine mode shapes are derived for the hyperbolic paraboloid under consideration. These mode shapes are calculated using the EDZ4 displacement field assumption for a CNT concentration equal to $w_r = 0.2$, taking into account the values 0.75 and 1 for the agglomeration parameters μ_1 and μ_2, respectively.

Once the present higher order model is validated with respect to the homogenization method and the selection of the higher order theory, numerical investigations are conducted to investigate the influence of the distribution of CNT nanofibers within the lamination scheme. A laminated catenoid of arbitrary shape is thus introduced, characterized by two external anisotropic layers with general orientation and a central isotropic core made of a hybrid matrix and a variation of the CNT volume fraction distribution. The mapping of the physical domain is performed with the generalized blending functions of Eqn. (101), taking into account the geometric description with NURBS curves of its four edges, which are defined in terms of knots, weights and control points, as reported in Fig. 8. The structure is constrained with a Super elliptic in-plane distribution of linear elastic springs, while a constant profile of springs is assumed in the out-of-plane direction. The two external isotropic layers [105] of density $\rho^{(k)} = 7750$ kg /m^3 are made of triclinic material, whose three-dimensional stiffness matrix (37) looks as follows:

$$\begin{bmatrix} C_{11}^{(k)} & C_{12}^{(k)} & C_{16}^{(k)} & C_{14}^{(k)} & C_{15}^{(k)} & C_{13}^{(k)} \\ C_{12}^{(k)} & C_{22}^{(k)} & C_{26}^{(k)} & C_{24}^{(k)} & C_{25}^{(k)} & C_{23}^{(k)} \\ C_{16}^{(k)} & C_{26}^{(k)} & C_{66}^{(k)} & C_{46}^{(k)} & C_{56}^{(k)} & C_{36}^{(k)} \\ C_{14}^{(k)} & C_{24}^{(k)} & C_{46}^{(k)} & C_{44}^{(k)} & C_{45}^{(k)} & C_{34}^{(k)} \\ C_{15}^{(k)} & C_{25}^{(k)} & C_{56}^{(k)} & C_{45}^{(k)} & C_{55}^{(k)} & C_{35}^{(k)} \\ C_{13}^{(k)} & C_{23}^{(k)} & C_{36}^{(k)} & C_{34}^{(k)} & C_{35}^{(k)} & C_{33}^{(k)} \end{bmatrix} = \begin{bmatrix} 98.84 & 53.92 & 0.03 & 1.05 & -0.1 & 50.78 \\ 53.92 & 99.19 & 0.03 & 0.55 & -0.18 & 50.87 \\ 0.03 & 0.03 & 22.55 & -0.04 & 0.25 & 0.02 \\ 1.05 & 0.55 & -0.04 & 21.1 & 0.07 & 1.03 \\ -0.1 & -0.18 & 0.25 & 0.07 & 21.14 & -0.18 \\ 50.78 & 50.87 & 0.02 & 1.03 & -0.18 & 87.23 \end{bmatrix} \text{GPa} \quad (118)$$

The through-the-thickness variation of the volume fraction of CNT in the central core of the structure is described in terms of the five-parameters FG-CNT expression of Eqn. (51) so that nanofibers are concentrated at the top surface of the layer under consideration. In Table 5 and in Table 6 an extended parametric investigation is conducted, focusing on the effects on mode frequencies and the corresponding mode shapes arising from the FG-CNT agglomeration parameters. Different values of the power FGM parameter p used in Eqn. (51) are considered to examine the influence of the variation of the material through-the-thickness distribution. A 3D FEM solution is provided for the case characterized by $p = +\infty$ where the volume fraction of CNTs is equal to zero, thus validating the results of the investigation. The greatest variation in the results is evident for lower values of p, where a decrease in natural frequencies is seen, except for the case $\mu_2 = 1$ where an increase of natural frequencies occur. In fact, from a physical point of view, it should be remembered that lower values of the p parameter means that a higher concentration of CNTs can be found along the thickness direction of the shell, therefore the reinforcement efficiency is

more evident. Referring to Table 5, the greatest variation of the results can be traced in the case of higher values of μ_1, while in Table 6 it is shown that a significative variation of the natural frequencies occurs for all configuration of the agglomeration of nanofibers. The sensitivity of the parameters of the FGM distribution is illustrated in Fig. 9, where it is shown that for p values between 0 and 5, the redistribution of the FGM material stiffness and density significantly influences the natural frequencies. On the other hand, for higher values of these parameters, a smaller variation in the dynamic properties is seen if compared to the structure with an unreinforced core, in fact a stabilization of the frequency values can be traced as the parameter p increases.

In Fig. 10 the three-dimensional representation of the first mode shapes for the catenoid is provided, calculated under the assumption of EDZ4 higher order theory.

The next numerical investigations point out the influence of the agglomeration parameters on a doubly-curved structure containing FG-CNTs layers. A mapped helicoid of arbitrary shape and variable thickness is presented, as reported in Fig. 11. In particular, a general thickness variation is modelled according to Eqn. (10), employing a power function and a sinusoidal analytical expression. The lamination scheme consists of three layers of the trigonal material introduced in Eqn. (117) and two cores made of an isotropic matrix reinforced with agglomerated FG-CNTs. Boundary conditions are enforced on the structure through a Super elliptic dispersion (72) of linear springs along the lateral surfaces of the three-dimensional doubly-curved solid. The CNT distributions are calibrated according to Eqn. (51) so that in one layer the nanofibers are concentrated near the bottom surface, while in the other one they are located at the top surface.

In Table 7, the first ten mode frequencies are reported for different values of μ_1, while $\mu_2 = 1$ is fixed. Furthermore, various shapes of CNT distribution are investigated by setting different values of p. The presence of agglomerated CNTs increases the values of the first ten natural frequencies for each considered configuration of FGM distributions. As outlined in Fig. 12, the highest increase in natural frequencies can be observed for a constant distribution ($p = 0$) of CNT nanofibers. However, for lower values of the agglomeration parameter μ_1, no significative variations are evident. The physical meaning of this behavior can be traced in the fact that the concentration of both agglomerated CNTs remains almost unaltered even when the FG-CNTs distribution varies. The results collected in Table 8, calculated for $\mu_1 = 0.1$, suggest that a decrease in the natural frequencies value can be achieved for higher values of μ_2. Also for this case, the highest frequency variation is observed for lower values of p.

Once the eigenvalues of the shell under consideration are derived for several material configurations, the corresponding eigenvectors are then calculated. In Fig. 13, the first nine mode shapes are represented, accounting for the FGM power distribution of Eqn. (51) with $p = 5$. In addition, the agglomeration of CNTs is modelled for $\mu_1 = 0.7$ and $\mu_2 = 1$. For each mode, the deflection of the structure is calculated employing the EDZ4 theory, starting from the generalized displacement field components and considering the reconstruction of the three-dimensional displacements profile according to Eqn. (15).

Similar parametric investigations are performed on an arbitrarily-shaped revolution paraboloid. The isogeometric mapping of the physical domain is reported in Fig. 14, taking into account the generalized blending functions of Eqn. (101). Unlike previous examples, for the present structure the lamination scheme accounts for two thick layers reinforced with agglomerated FG-CNTs, while the central core is made of triclinic material (118). Finally, two laminae of graphite-epoxy ($\rho^{(k)} = 1450\ \mathrm{kg}/\mathrm{m}^3$) with general orientation are located in the external sides of the structure. The mechanical properties of the material at issue are expressed in terms of the orthotropic engineering constants, as reported below:

$$\begin{aligned} &E_1^{(k)} = 137.90\ \text{GPa} \qquad G_{23}^{(k)} = 6.21\ \text{GPa} \qquad \nu_{23}^{(k)} = 0.49 \\ &E_2^{(k)} = E_3^{(k)} = 8.96\ \text{GPa} \quad G_{12}^{(k)} = G_{13}^{(k)} = 7.10\ \text{GPa} \quad \nu_{12}^{(k)} = \nu_{13}^{(k)} = 0.30 \end{aligned} \tag{119}$$

The results are reported in Table 9 and Table 10, and they are shown in Fig. 15. In Table 9 mode frequencies are calculated for different values of μ_1, setting $\mu_2 = 1$ for all simulations. Furthermore, the eigenvalues of the problem under consideration are derived for the case of isotropic layers without FG-CNTs. These numerical investigations highlight the effect of the presence of agglomerated CNTs within the matrix on the dynamic response. On the other hand, the natural frequencies are also calculated under the assumption of completely agglomerated nanoparticles, namely $\mu_1 = \mu_2 = 1$, thus showing the impact of CNT agglomeration on the vibrational response of the shell. The investigation is made for different values of parameter p to illustrate the effect of the through-the-thickness distribution. Also for this case, a uniform distribution ($p = 0$) of agglomerated CNTs yields the highest natural frequencies, while for $p = 10$ a noticeable variation is seen only when $\mu_1 = \mu_2 = 1$. On the other hand, the same study is performed in Table 10 for the case $\mu_1 = 0.1$, where the natural frequencies for different values of the agglomeration parameter μ_2 are shown. Then, the results for the first four modes are depicted in Fig. 16. Unlike the previous simulations, in this case a variation of natural frequencies is observed even for higher values of p. Furthermore, a variation in the dynamic response of the shell is seen even for lower values of μ_2, indicating that both dispersed and agglomerated CNTs contribute to the modification of the material properties of the matrix.

11. Conclusions

In the present work, higher order theories have been used to derive a refined model for the evaluation of the natural frequencies of laminated anisotropic doubly-curved shell structures employing a generalized expression of the unknown displacement field variable along the thickness direction. Then, generalized shape functions have been used to interpolate the variables in a non-uniform rectangular computational grid. The lamination schemes consist of generally anisotropic layers and isotropic matrices reinforced by agglomerated CNTs, distributed according to a five-parameters power law. Thanks to the adoption of the GDQ method for the derivation of a numerical solution, extensive parametric investigations have been performed, showing that the agglomeration of nanofibers can reduce the efficiency of the reinforcing phase. Furthermore, the through-the-thickness CNT distribution may provide stretching deformations even in lower modes, therefore a higher order polynomial is required to match three-dimensional numerical predictions. It is shown that the present higher order theory can be adopted to derive with a reduced computational effort the vibrational response of anisotropic FGM-reinforced doubly-curved shell panels, therefore it can be a valid tool which can support the design process.

CRediT authorship contribution statement

Francesco Tornabene: Writing – review & editing, Writing – original draft, Validation, Supervision, Software, Methodology, Investigation, Formal analysis, Data curation, Conceptualization. **Matteo Viscoti:** Writing – original draft, Validation, Investigation. **Rossana Dimitri:** Writing – review & editing, Validation, Supervision, Methodology, Investigation, Formal analysis.

Declaration of competing interest

The authors declare that they have no known competing financial interests or personal relationships that could have appeared to influence the work reported in this paper.

Data availability

No data was used for the research described in the article.

Appendix I

In the following equation, the complete expression can be found of the three-dimensional stiffness coefficients $E_{ij}^{(k)} = C_{ij}^{(k)}$ for *i, j* = 1, ..., 6 which occur in Eqn. (37) for the case of an orthotropic material [11]. As a matter of fact, the elastic constitutive behavior of the orthotropic material is completely described if the nine engineering constants are provided, namely the elastic moduli $E_1^{(k)}, E_2^{(k)}, E_3^{(k)}$, the shear moduli $G_{12}^{(k)}, G_{13}^{(k)}, G_{23}^{(k)}$ and the Poisson's coefficients $\nu_{12}^{(k)}, \nu_{13}^{(k)}, \nu_{23}^{(k)}$.

$$\begin{gathered}
C_{11}^{(k)} = \frac{1-\nu_{23}^{(k)}\nu_{32}^{(k)}}{E_2^{(k)}E_3^{(k)}\Delta^{(k)}}, \quad C_{22}^{(k)} = \frac{1-\nu_{13}^{(k)}\nu_{31}^{(k)}}{E_1^{(k)}E_3^{(k)}\Delta^{(k)}}, \quad C_{33}^{(k)} = \frac{1-\nu_{12}^{(k)}\nu_{21}^{(k)}}{E_1^{(k)}E_2^{(k)}\Delta^{(k)}} \\
C_{12}^{(k)} = \frac{\nu_{12}^{(k)}+\nu_{32}^{(k)}\nu_{13}^{(k)}}{E_1^{(k)}E_3^{(k)}\Delta^{(k)}}, \quad C_{13}^{(k)} = \frac{\nu_{13}^{(k)}+\nu_{12}^{(k)}\nu_{23}^{(k)}}{E_1^{(k)}E_2^{(k)}\Delta^{(k)}}, \quad C_{23}^{(k)} = \frac{\nu_{23}^{(k)}+\nu_{21}^{(k)}\nu_{13}^{(k)}}{E_1^{(k)}E_2^{(k)}\Delta^{(k)}} \\
C_{44}^{(k)} = G_{13}^{(k)}, \quad C_{55}^{(k)} = G_{23}^{(k)}, \quad C_{66}^{(k)} = G_{12}^{(k)} \\
C_{14}^{(k)} = C_{15}^{(k)} = C_{16}^{(k)} = C_{24}^{(k)} = C_{25}^{(k)} = C_{26}^{(k)} = C_{63}^{(k)} = C_{64}^{(k)} = C_{65}^{(k)} = C_{43}^{(k)} = C_{45}^{(k)} = C_{53}^{(k)} = 0
\end{gathered} \tag{A.1}$$

where the quantity $\Delta^{(k)}$ reads as follows:

$$\Delta^{(k)} = \frac{1-\nu_{12}^{(k)}\nu_{21}^{(k)}-\nu_{23}^{(k)}\nu_{32}^{(k)}-\nu_{13}^{(k)}\nu_{31}^{(k)}-2\nu_{21}^{(k)}\nu_{32}^{(k)}\nu_{13}^{(k)}}{E_1^{(k)}E_2^{(k)}E_3^{(k)}} \tag{A.2}$$

Appendix II

In the present Appendix, the complete expression is reported for the interested reader of coefficients $O_{kr}^{(\tau\eta)\alpha_i\alpha_j}$ with *i, j, k* = 1, 2, 3 and *r* = 1, ..., 9 occurring in Eqn. (44) for a generic τ = 0, ..., *N* + 1 and a generic η = 0, ..., *N* + 1. The relations reported in the following should be evaluated in each point of the computational domain, according to Ref. [76]. Furthermore, the derivatives of the Lamè parameters A_1,A_2 with respect to α_1,α_2 are numerically evaluated with the GDQ method.

$$O_{11}^{(\tau\eta)\alpha_i\alpha_1} = \frac{A_{11(20)}^{(\tau\eta)\alpha_i\alpha_1}}{A_1}\frac{\partial}{\partial\alpha_1} + \frac{A_{12(11)}^{(\tau\eta)\alpha_i\alpha_1}}{A_1A_2}\frac{\partial A_2}{\partial\alpha_1} - \frac{A_{16(20)}^{(\tau\eta)\alpha_i\alpha_1}}{A_1A_2}\frac{\partial A_1}{\partial\alpha_2} + \frac{A_{16(11)}^{(\tau\eta)\alpha_i\alpha_1}}{A_2}\frac{\partial}{\partial\alpha_2} - \frac{A_{14(20)}^{(\tau\eta)\alpha_i\alpha_1}}{R_1} + A_{14(10)}^{(\tau\bar{\eta})\alpha_i\alpha_1} \tag{A.3}$$

$$O_{12}^{(\tau\eta)\alpha_i\alpha_1} = \frac{A_{12(11)}^{(\tau\eta)\alpha_i\alpha_1}}{A_1}\frac{\partial}{\partial\alpha_1} + \frac{A_{22(02)}^{(\tau\eta)\alpha_i\alpha_1}}{A_1A_2}\frac{\partial A_2}{\partial\alpha_1} - \frac{A_{26(11)}^{(\tau\eta)\alpha_i\alpha_1}}{A_1A_2}\frac{\partial A_1}{\partial\alpha_2} + \frac{A_{26(02)}^{(\tau\eta)\alpha_i\alpha_1}}{A_2}\frac{\partial}{\partial\alpha_2} - \frac{A_{24(11)}^{(\tau\eta)\alpha_i\alpha_1}}{R_1} + A_{24(01)}^{(\tau\bar{\eta})\alpha_i\alpha_1} \tag{A.4}$$

$$O_{13}^{(\tau\eta)\alpha_i\alpha_1} = \frac{A_{16(20)}^{(\tau\eta)\alpha_i\alpha_1}}{A_1}\frac{\partial}{\partial\alpha_1} + \frac{A_{26(11)}^{(\tau\eta)\alpha_i\alpha_1}}{A_1A_2}\frac{\partial A_2}{\partial\alpha_1} - \frac{A_{66(20)}^{(\tau\eta)\alpha_i\alpha_1}}{A_1A_2}\frac{\partial A_1}{\partial\alpha_2} + \frac{A_{66(11)}^{(\tau\eta)\alpha_i\alpha_1}}{A_2}\frac{\partial}{\partial\alpha_2} - \frac{A_{46(20)}^{(\tau\eta)\alpha_i\alpha_1}}{R_1} + A_{46(10)}^{(\tau\bar{\eta})\alpha_i\alpha_1} \tag{A.5}$$

$$O_{14}^{(\tau\eta)\alpha_i\alpha_1} = \frac{A_{16(11)}^{(\tau\eta)\alpha_i\alpha_1}}{A_1}\frac{\partial}{\partial\alpha_1} + \frac{A_{26(02)}^{(\tau\eta)\alpha_i\alpha_1}}{A_1A_2}\frac{\partial A_2}{\partial\alpha_1} - \frac{A_{66(11)}^{(\tau\eta)\alpha_i\alpha_1}}{A_1A_2}\frac{\partial A_1}{\partial\alpha_2} + \frac{A_{66(02)}^{(\tau\eta)\alpha_i\alpha_1}}{A_2}\frac{\partial}{\partial\alpha_2} - \frac{A_{46(11)}^{(\tau\eta)\alpha_i\alpha_1}}{R_1} + A_{46(01)}^{(\tau\bar{\eta})\alpha_i\alpha_1} \tag{A.6}$$

$$O_{15}^{(\tau\eta)\alpha_i\alpha_1} = \frac{A_{14(20)}^{(\tau\eta)\alpha_i\alpha_1}}{A_1}\frac{\partial}{\partial\alpha_1} + \frac{A_{24(11)}^{(\tau\eta)\alpha_i\alpha_1}}{A_1A_2}\frac{\partial A_2}{\partial\alpha_1} - \frac{A_{46(20)}^{(\tau\eta)\alpha_i\alpha_1}}{A_1A_2}\frac{\partial A_1}{\partial\alpha_2} + \frac{A_{46(11)}^{(\tau\eta)\alpha_i\alpha_1}}{A_2}\frac{\partial}{\partial\alpha_2} - \frac{A_{44(20)}^{(\tau\eta)\alpha_i\alpha_1}}{R_1} + A_{44(10)}^{(\tau\bar{\eta})\alpha_i\alpha_1} \tag{A.7}$$

$$O_{16}^{(\tau\eta)\alpha_i\alpha_1} = \frac{A_{15(11)}^{(\tau\eta)\alpha_i\alpha_1}}{A_1}\frac{\partial}{\partial\alpha_1} + \frac{A_{25(02)}^{(\tau\eta)\alpha_i\alpha_1}}{A_1A_2}\frac{\partial A_2}{\partial\alpha_1} - \frac{A_{56(11)}^{(\tau\eta)\alpha_i\alpha_1}}{A_1A_2}\frac{\partial A_1}{\partial\alpha_2} + \frac{A_{56(02)}^{(\tau\eta)\alpha_i\alpha_1}}{A_2}\frac{\partial}{\partial\alpha_2} - \frac{A_{45(11)}^{(\tau\eta)\alpha_i\alpha_1}}{R_1} + A_{45(01)}^{(\tau\bar{\eta})\alpha_i\alpha_1} \tag{A.8}$$

$$O_{17}^{(\tau\eta)\alpha_i\alpha_1} = \frac{A_{14(10)}^{(\bar{\tau}\eta)\alpha_i\alpha_1}}{A_1}\frac{\partial}{\partial\alpha_1} + \frac{A_{24(01)}^{(\bar{\tau}\eta)\alpha_i\alpha_1}}{A_1A_2}\frac{\partial A_2}{\partial\alpha_1} - \frac{A_{46(10)}^{(\bar{\tau}\eta)\alpha_i\alpha_1}}{A_1A_2}\frac{\partial A_1}{\partial\alpha_2} + \frac{A_{46(01)}^{(\bar{\tau}\eta)\alpha_i\alpha_1}}{A_2}\frac{\partial}{\partial\alpha_2} - \frac{A_{44(10)}^{(\bar{\tau}\eta)\alpha_i\alpha_1}}{R_1} + A_{44(00)}^{(\bar{\tau}\bar{\eta})\alpha_i\alpha_1} \tag{A.9}$$

$$O_{18}^{(\tau\eta)\alpha_i\alpha_1} = \frac{A_{15(10)}^{(\bar{\tau}\eta)\alpha_i\alpha_1}}{A_1}\frac{\partial}{\partial\alpha_1} + \frac{A_{25(01)}^{(\bar{\tau}\eta)\alpha_i\alpha_1}}{A_1A_2}\frac{\partial A_2}{\partial\alpha_1} - \frac{A_{56(10)}^{(\bar{\tau}\eta)\alpha_i\alpha_1}}{A_1A_2}\frac{\partial A_1}{\partial\alpha_2} + \frac{A_{56(01)}^{(\bar{\tau}\eta)\alpha_i\alpha_1}}{A_2}\frac{\partial}{\partial\alpha_2} - \frac{A_{45(10)}^{(\bar{\tau}\eta)\alpha_i\alpha_1}}{R_1} + A_{45(00)}^{(\bar{\tau}\bar{\eta})\alpha_i\alpha_1} \tag{A.10}$$

$$O_{19}^{(\tau\eta)\alpha_i\alpha_1} = \frac{A_{13(10)}^{(\bar{\tau}\eta)\alpha_i\alpha_1}}{A_1}\frac{\partial}{\partial\alpha_1} + \frac{A_{23(01)}^{(\bar{\tau}\eta)\alpha_i\alpha_1}}{A_1A_2}\frac{\partial A_2}{\partial\alpha_1} - \frac{A_{36(10)}^{(\bar{\tau}\eta)\alpha_i\alpha_1}}{A_1A_2}\frac{\partial A_1}{\partial\alpha_2} + \frac{A_{36(01)}^{(\bar{\tau}\eta)\alpha_i\alpha_1}}{A_2}\frac{\partial}{\partial\alpha_2} - \frac{A_{34(10)}^{(\bar{\tau}\eta)\alpha_i\alpha_1}}{R_1} + A_{34(00)}^{(\bar{\tau}\bar{\eta})\alpha_i\alpha_1} \tag{A.11}$$

$$O_{21}^{(\tau\eta)\alpha_i\alpha_2}=\frac{A_{11(20)}^{(\tau\eta)\alpha_i\alpha_2}}{A_1A_2}\frac{\partial A_1}{\partial\alpha_2}+\frac{A_{12(11)}^{(\tau\eta)\alpha_i\alpha_2}}{A_2}\frac{\partial}{\partial\alpha_2}+\frac{A_{16(20)}^{(\tau\eta)\alpha_i\alpha_2}}{A_1}\frac{\partial}{\partial\alpha_1}-\frac{A_{16(11)}^{(\tau\eta)\alpha_i\alpha_2}}{A_1A_2}\frac{\partial A_2}{\partial\alpha_1}-\frac{A_{15(11)}^{(\tau\eta)\alpha_i\alpha_2}}{R_2}+A_{15(10)}^{(\tau\bar{\eta})\alpha_i\alpha_2} \tag{A.12}$$

$$O_{22}^{(\tau\eta)\alpha_i\alpha_2}=\frac{A_{12(11)}^{(\tau\eta)\alpha_i\alpha_2}}{A_1A_2}\frac{\partial A_1}{\partial\alpha_2}+\frac{A_{22(02)}^{(\tau\eta)\alpha_i\alpha_2}}{A_2}\frac{\partial}{\partial\alpha_2}+\frac{A_{26(11)}^{(\tau\eta)\alpha_i\alpha_2}}{A_1}\frac{\partial}{\partial\alpha_1}-\frac{A_{26(02)}^{(\tau\eta)\alpha_i\alpha_2}}{A_1A_2}\frac{\partial A_2}{\partial\alpha_1}-\frac{A_{25(02)}^{(\tau\eta)\alpha_i\alpha_2}}{R_2}+A_{25(01)}^{(\tau\bar{\eta})\alpha_i\alpha_2} \tag{A.13}$$

$$O_{23}^{(\tau\eta)\alpha_i\alpha_2}=\frac{A_{16(20)}^{(\tau\eta)\alpha_i\alpha_2}}{A_1A_2}\frac{\partial A_1}{\partial\alpha_2}+\frac{A_{26(11)}^{(\tau\eta)\alpha_i\alpha_2}}{A_2}\frac{\partial}{\partial\alpha_2}+\frac{A_{66(20)}^{(\tau\eta)\alpha_i\alpha_2}}{A_1}\frac{\partial}{\partial\alpha_1}-\frac{A_{66(11)}^{(\tau\eta)\alpha_i\alpha_2}}{A_1A_2}\frac{\partial A_2}{\partial\alpha_1}-\frac{A_{56(11)}^{(\tau\eta)\alpha_i\alpha_2}}{R_2}+A_{56(10)}^{(\tau\bar{\eta})\alpha_i\alpha_2} \tag{A.14}$$

$$O_{24}^{(\tau\eta)\alpha_i\alpha_2}=\frac{A_{16(11)}^{(\tau\eta)\alpha_i\alpha_2}}{A_1A_2}\frac{\partial A_1}{\partial\alpha_2}+\frac{A_{26(02)}^{(\tau\eta)\alpha_i\alpha_2}}{A_2}\frac{\partial}{\partial\alpha_2}+\frac{A_{66(11)}^{(\tau\eta)\alpha_i\alpha_2}}{A_1}\frac{\partial}{\partial\alpha_1}-\frac{A_{66(02)}^{(\tau\eta)\alpha_i\alpha_2}}{A_1A_2}\frac{\partial A_2}{\partial\alpha_1}-\frac{A_{56(02)}^{(\tau\eta)\alpha_i\alpha_2}}{R_2}+A_{56(01)}^{(\tau\bar{\eta})\alpha_i\alpha_2} \tag{A.15}$$

$$O_{25}^{(\tau\eta)\alpha_i\alpha_2}=\frac{A_{14(20)}^{(\tau\eta)\alpha_i\alpha_2}}{A_1A_2}\frac{\partial A_1}{\partial\alpha_2}+\frac{A_{24(11)}^{(\tau\eta)\alpha_i\alpha_2}}{A_2}\frac{\partial}{\partial\alpha_2}+\frac{A_{46(20)}^{(\tau\eta)\alpha_i\alpha_2}}{A_1}\frac{\partial}{\partial\alpha_1}-\frac{A_{46(11)}^{(\tau\eta)\alpha_i\alpha_2}}{A_1A_2}\frac{\partial A_2}{\partial\alpha_1}-\frac{A_{45(11)}^{(\tau\eta)\alpha_i\alpha_2}}{R_2}+A_{45(10)}^{(\tau\bar{\eta})\alpha_i\alpha_2} \tag{A.16}$$

$$O_{26}^{(\tau\eta)\alpha_i\alpha_2}=\frac{A_{15(11)}^{(\tau\eta)\alpha_i\alpha_2}}{A_1A_2}\frac{\partial A_1}{\partial\alpha_2}+\frac{A_{25(02)}^{(\tau\eta)\alpha_i\alpha_2}}{A_2}\frac{\partial}{\partial\alpha_2}+\frac{A_{56(11)}^{(\tau\eta)\alpha_i\alpha_2}}{A_1}\frac{\partial}{\partial\alpha_1}-\frac{A_{56(02)}^{(\tau\eta)\alpha_i\alpha_2}}{A_1A_2}\frac{\partial A_2}{\partial\alpha_1}-\frac{A_{55(02)}^{(\tau\eta)\alpha_i\alpha_2}}{R_2}+A_{55(01)}^{(\tau\bar{\eta})\alpha_i\alpha_2} \tag{A.17}$$

$$O_{27}^{(\tau\eta)\alpha_i\alpha_2}=\frac{A_{14(10)}^{(\bar{\tau}\eta)\alpha_i\alpha_2}}{A_1A_2}\frac{\partial A_1}{\partial\alpha_2}+\frac{A_{24(01)}^{(\bar{\tau}\eta)\alpha_i\alpha_2}}{A_2}\frac{\partial}{\partial\alpha_2}+\frac{A_{46(10)}^{(\bar{\tau}\eta)\alpha_i\alpha_2}}{A_1}\frac{\partial}{\partial\alpha_1}-\frac{A_{46(01)}^{(\bar{\tau}\eta)\alpha_i\alpha_2}}{A_1A_2}\frac{\partial A_2}{\partial\alpha_1}-\frac{A_{45(01)}^{(\bar{\tau}\eta)\alpha_i\alpha_2}}{R_2}+A_{45(00)}^{(\bar{\tau}\bar{\eta})\alpha_i\alpha_2} \tag{A.18}$$

$$O_{28}^{(\tau\eta)\alpha_i\alpha_2}=\frac{A_{15(10)}^{(\bar{\tau}\eta)\alpha_i\alpha_2}}{A_1A_2}\frac{\partial A_1}{\partial\alpha_2}+\frac{A_{25(01)}^{(\bar{\tau}\eta)\alpha_i\alpha_2}}{A_2}\frac{\partial}{\partial\alpha_2}+\frac{A_{56(10)}^{(\bar{\tau}\eta)\alpha_i\alpha_2}}{A_1}\frac{\partial}{\partial\alpha_1}-\frac{A_{56(01)}^{(\bar{\tau}\eta)\alpha_i\alpha_2}}{A_1A_2}\frac{\partial A_2}{\partial\alpha_1}-\frac{A_{55(01)}^{(\bar{\tau}\eta)\alpha_i\alpha_2}}{R_2}+A_{55(00)}^{(\bar{\tau}\bar{\eta})\alpha_i\alpha_2} \tag{A.19}$$

$$O_{29}^{(\tau\eta)\alpha_i\alpha_2}=\frac{A_{13(10)}^{(\bar{\tau}\eta)\alpha_i\alpha_2}}{A_1A_2}\frac{\partial A_1}{\partial\alpha_2}+\frac{A_{23(01)}^{(\bar{\tau}\eta)\alpha_i\alpha_2}}{A_2}\frac{\partial}{\partial\alpha_2}+\frac{A_{36(10)}^{(\bar{\tau}\eta)\alpha_i\alpha_2}}{A_1}\frac{\partial}{\partial\alpha_1}-\frac{A_{36(01)}^{(\bar{\tau}\eta)\alpha_i\alpha_2}}{A_1A_2}\frac{\partial A_2}{\partial\alpha_1}-\frac{A_{35(01)}^{(\bar{\tau}\eta)\alpha_i\alpha_2}}{R_2}+A_{35(00)}^{(\bar{\tau}\bar{\eta})\alpha_i\alpha_2} \tag{A.20}$$

$$O_{31}^{(\tau\eta)\alpha_i\alpha_3}=\frac{A_{11(20)}^{(\tau\eta)\alpha_i\alpha_3}}{R_1}+\frac{A_{12(11)}^{(\tau\eta)\alpha_i\alpha_3}}{R_2}+\frac{A_{14(20)}^{(\tau\eta)\alpha_i\alpha_3}}{A_1}\frac{\partial}{\partial\alpha_1}+\frac{A_{15(11)}^{(\tau\eta)\alpha_i\alpha_3}}{A_2}\frac{\partial}{\partial\alpha_2}+A_{13(10)}^{(\tau\bar{\eta})\alpha_i\alpha_3} \tag{A.21}$$

$$O_{32}^{(\tau\eta)\alpha_i\alpha_3}=\frac{A_{12(11)}^{(\tau\eta)\alpha_i\alpha_3}}{R_1}+\frac{A_{22(02)}^{(\tau\eta)\alpha_i\alpha_3}}{R_2}+\frac{A_{24(11)}^{(\tau\eta)\alpha_i\alpha_3}}{A_1}\frac{\partial}{\partial\alpha_1}+\frac{A_{25(02)}^{(\tau\eta)\alpha_i\alpha_3}}{A_2}\frac{\partial}{\partial\alpha_2}+A_{23(01)}^{(\tau\bar{\eta})\alpha_i\alpha_3} \tag{A.22}$$

$$O_{33}^{(\tau\eta)\alpha_i\alpha_3}=\frac{A_{16(20)}^{(\tau\eta)\alpha_i\alpha_3}}{R_1}+\frac{A_{26(11)}^{(\tau\eta)\alpha_i\alpha_3}}{R_2}+\frac{A_{46(20)}^{(\tau\eta)\alpha_i\alpha_3}}{A_1}\frac{\partial}{\partial\alpha_1}+\frac{A_{56(11)}^{(\tau\eta)\alpha_i\alpha_3}}{A_2}\frac{\partial}{\partial\alpha_2}+A_{36(10)}^{(\tau\bar{\eta})\alpha_i\alpha_3} \tag{A.23}$$

$$O_{34}^{(\tau\eta)\alpha_i\alpha_3}=\frac{A_{16(11)}^{(\tau\eta)\alpha_i\alpha_3}}{R_1}+\frac{A_{26(02)}^{(\tau\eta)\alpha_i\alpha_3}}{R_2}+\frac{A_{46(11)}^{(\tau\eta)\alpha_i\alpha_3}}{A_1}\frac{\partial}{\partial\alpha_1}+\frac{A_{56(02)}^{(\tau\eta)\alpha_i\alpha_3}}{A_2}\frac{\partial}{\partial\alpha_2}+A_{36(01)}^{(\tau\bar{\eta})\alpha_i\alpha_3} \tag{A.24}$$

$$O_{35}^{(\tau\eta)\alpha_i\alpha_3}=\frac{A_{14(20)}^{(\tau\eta)\alpha_i\alpha_3}}{R_1}+\frac{A_{24(11)}^{(\tau\eta)\alpha_i\alpha_3}}{R_2}+\frac{A_{44(20)}^{(\tau\eta)\alpha_i\alpha_3}}{A_1}\frac{\partial}{\partial\alpha_1}+\frac{A_{45(11)}^{(\tau\eta)\alpha_i\alpha_3}}{A_2}\frac{\partial}{\partial\alpha_2}+A_{34(10)}^{(\tau\bar{\eta})\alpha_i\alpha_3} \tag{A.25}$$

$$O_{36}^{(\tau\eta)\alpha_i\alpha_3}=\frac{A_{15(11)}^{(\tau\eta)\alpha_i\alpha_3}}{R_1}+\frac{A_{25(02)}^{(\tau\eta)\alpha_i\alpha_3}}{R_2}+\frac{A_{45(11)}^{(\tau\eta)\alpha_i\alpha_3}}{A_1}\frac{\partial}{\partial\alpha_1}+\frac{A_{55(02)}^{(\tau\eta)\alpha_i\alpha_3}}{A_2}\frac{\partial}{\partial\alpha_2}+A_{35(01)}^{(\tau\bar{\eta})\alpha_i\alpha_3} \tag{A.26}$$

$$O_{37}^{(\tau\eta)\alpha_i\alpha_3}=\frac{A_{14(10)}^{(\bar{\tau}\eta)\alpha_i\alpha_3}}{R_1}+\frac{A_{24(01)}^{(\bar{\tau}\eta)\alpha_i\alpha_3}}{R_2}+\frac{A_{44(10)}^{(\bar{\tau}\eta)\alpha_i\alpha_3}}{A_1}\frac{\partial}{\partial\alpha_1}+\frac{A_{45(01)}^{(\bar{\tau}\eta)\alpha_i\alpha_3}}{A_2}\frac{\partial}{\partial\alpha_2}+A_{34(00)}^{(\bar{\tau}\bar{\eta})\alpha_i\alpha_3} \tag{A.27}$$

$$O_{38}^{(\tau\eta)\alpha_i\alpha_3}=\frac{A_{15(10)}^{(\bar{\tau}\eta)\alpha_i\alpha_3}}{R_1}+\frac{A_{25(01)}^{(\bar{\tau}\eta)\alpha_i\alpha_3}}{R_2}+\frac{A_{45(10)}^{(\bar{\tau}\eta)\alpha_i\alpha_3}}{A_1}\frac{\partial}{\partial\alpha_1}+\frac{A_{55(01)}^{(\bar{\tau}\eta)\alpha_i\alpha_3}}{A_2}\frac{\partial}{\partial\alpha_2}+A_{35(00)}^{(\bar{\tau}\bar{\eta})\alpha_i\alpha_3} \tag{A.28}$$

$$O_{39}^{(\tau\eta)\alpha_i\alpha_3}=\frac{A_{13(10)}^{(\bar{\tau}\eta)\alpha_i\alpha_3}}{R_1}+\frac{A_{23(01)}^{(\bar{\tau}\eta)\alpha_i\alpha_3}}{R_2}+\frac{A_{34(10)}^{(\bar{\tau}\eta)\alpha_i\alpha_3}}{A_1}\frac{\partial}{\partial\alpha_1}+\frac{A_{35(01)}^{(\bar{\tau}\eta)\alpha_i\alpha_3}}{A_2}\frac{\partial}{\partial\alpha_2}+A_{33(00)}^{(\bar{\tau}\bar{\eta})\alpha_i\alpha_3} \tag{A.29}$$

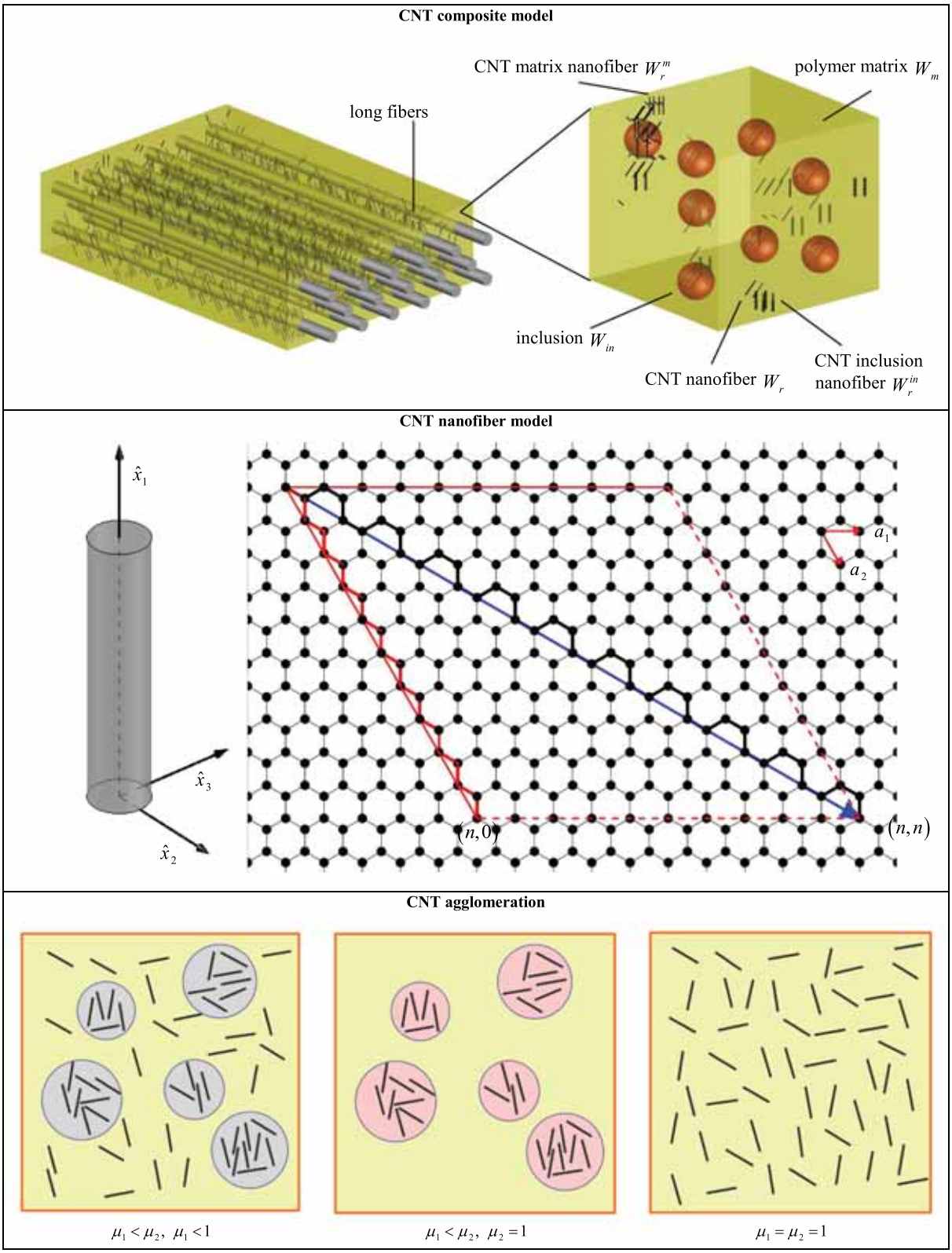

Fig. 1. Micromechanical model of an isotropic matrix reinforced with long fibers and dispersed CNTs taking into account the effect of the agglomeration of nanofibers.

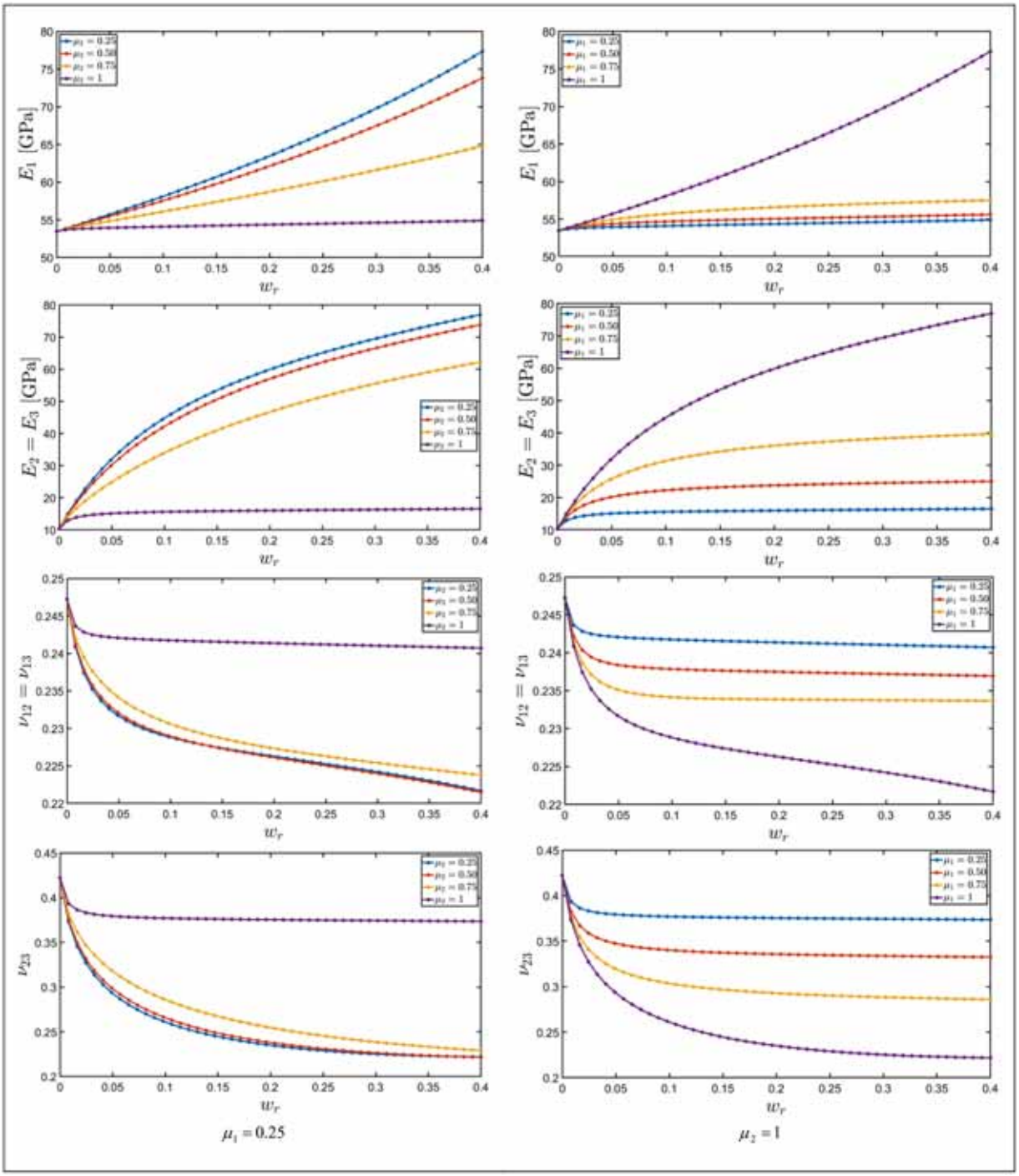

Fig. 2. Variation of the engineering constants of a polymer matrix reinforced with a dispersion of armchair CNT (10, 10) taking into account the effect of the agglomeration parameters μ_1,μ_2 of the dispersion. For the computation, a volume fraction equal to $w_f = 0.85$ is considered for long fibers.

<table>
<tr><th colspan="2">Rectangular plate</th></tr>
<tr><td colspan="2">Reference surface equation in principal coordinates
$\mathbf{r}\left(\alpha_1,\alpha_2\right)=\alpha_1\mathbf{e}_1+\alpha_2\mathbf{e}_2$</td></tr>
<tr><td>3D FEM model
C3D20 brick elements - 1530765 DOFs</td><td>2D GDQ model
LGL distribution - $I_N\times I_M=25\times 25$</td></tr>
<tr><td>  </td><td> 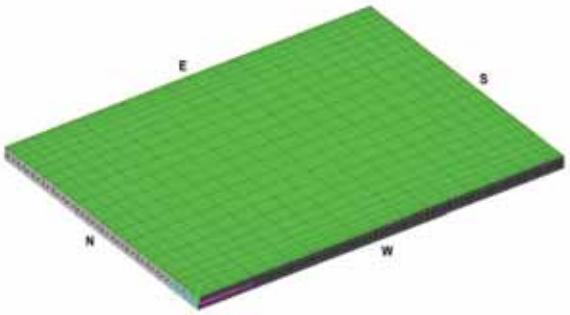
</td></tr>
<tr><td colspan="2">Geometric input: $\left(\alpha_1,\alpha_2\right)\in\left[\alpha_1^0,\alpha_1^1\right]\times\left[\alpha_2^0,\alpha_2^1\right]$, $\alpha_1^0=\alpha_2^0=0$, $\alpha_1^1=L_x=2.00$ m, $\alpha_2^1=L_y=1.50$ m
$h_1^0=h_2^0=h_4^0=h_5^0=0.01$ m, $h_3^0=0.015$ m</td></tr>
<tr><td colspan="2">Material properties: $\left(70/30/45/20/50\right)$
1st layer: CNT composite,
2nd layer: trigonal material,
3rd layer: CNT composite,
4th layer: trigonal material,
5th layer: CNT composite</td></tr>
</table>

Fig. 3. Mechanical and geometric properties of a laminated rectangular plate made of CNT composite and generally anisotropic materials.

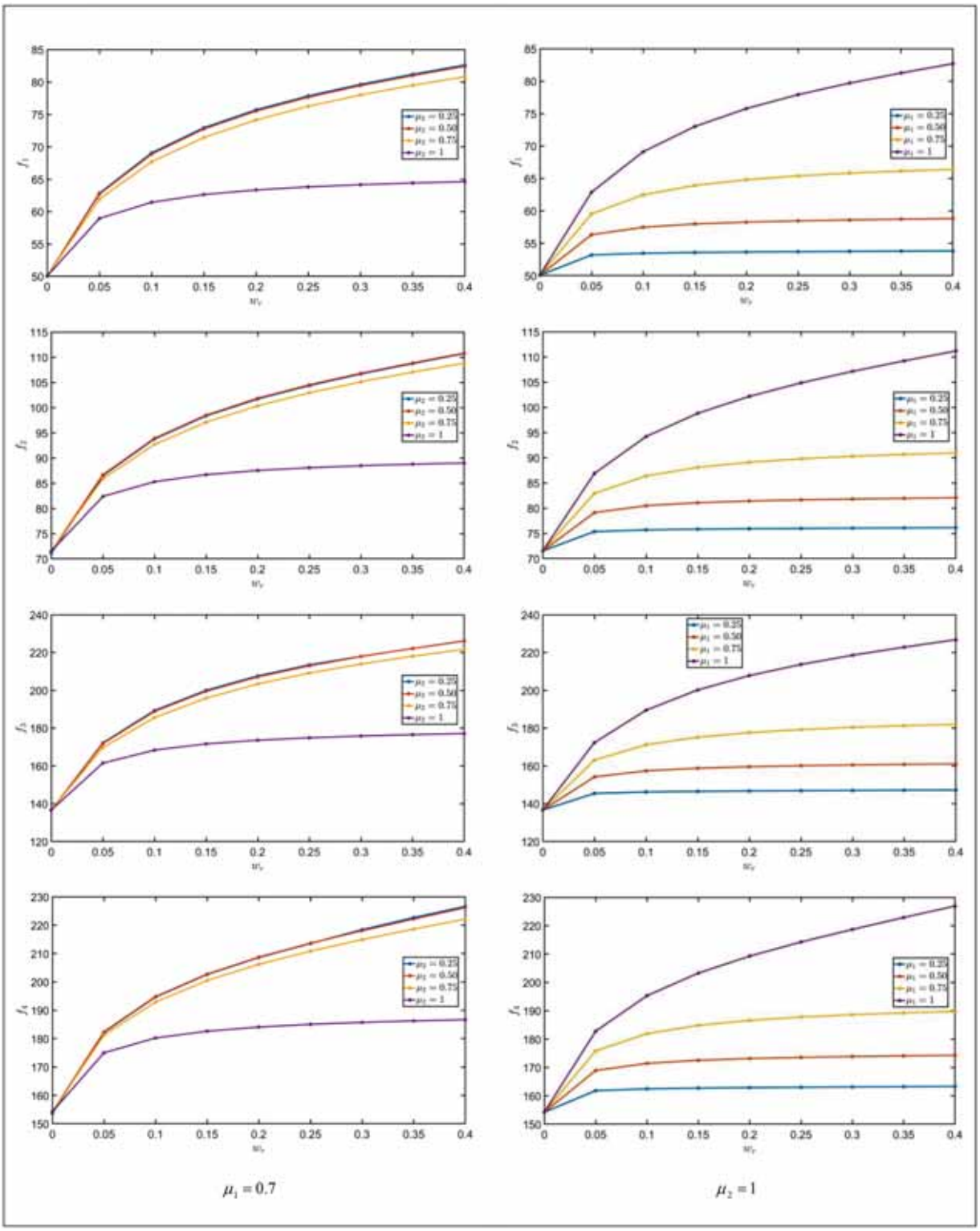

Fig. 4. Parametric investigation on the first natural frequencies of a rectangular plate made of generally anisotropic materials reinforced with a uniform dispersion of CNT within the isotropic matrix. The influence of the agglomeration parameters on the natural frequencies have been outlined for different values of the nanofiber concentration.

Rectangular plate

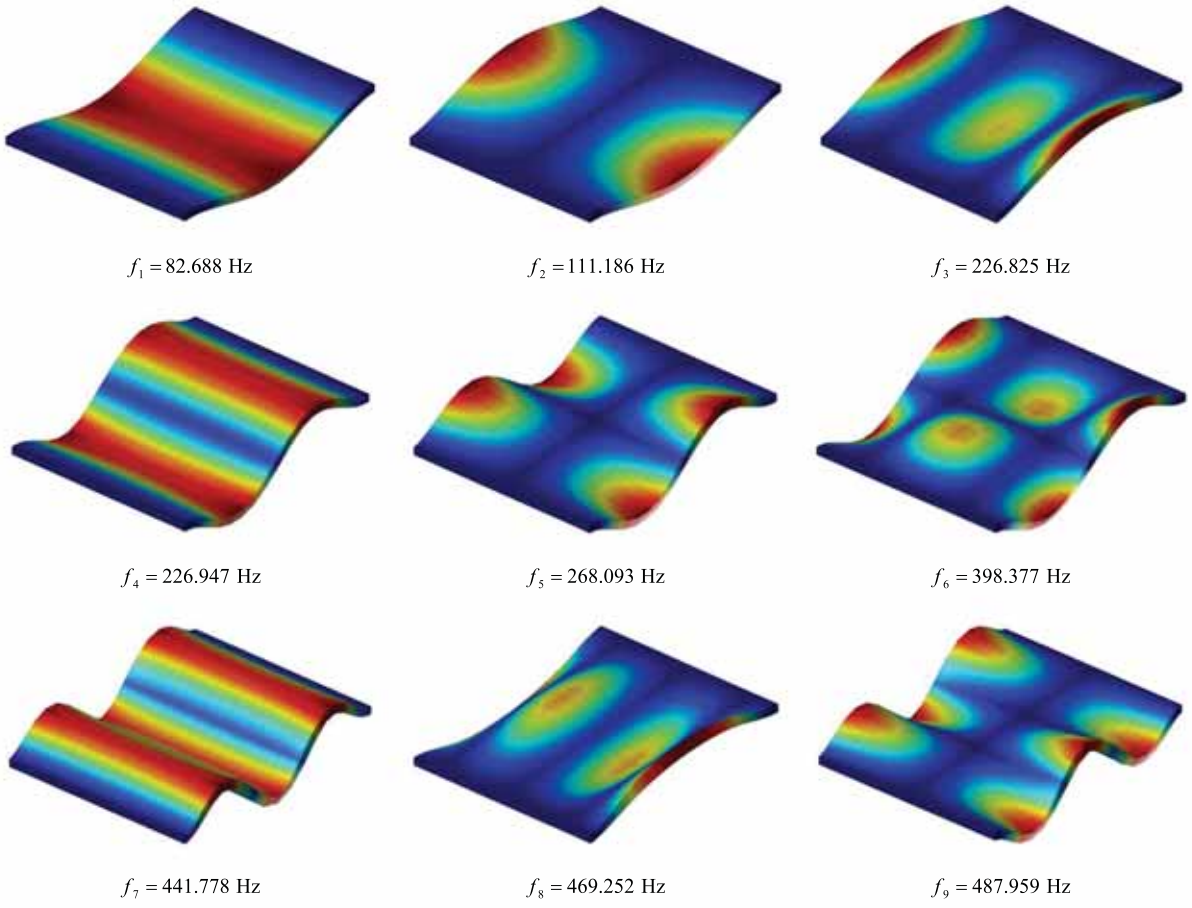

HSDT: EDZ4
Discrete Points: LGL with $I_N = I_M = 25$ - 9522 DOFs

Lamination Scheme: $(70/30/45/20/50)$, $h_1^0 = h_2^0 = h_4^0 = h_5^0 = 0.01$ m, $h_3^0 = 0.015$ m
Laminae Material Sequence: 1st CNT composite, 2nd trigonal material, 3rd CNT composite, 4th trigonal material, 5th CNT composite
Composite CNT parameters: $w_f = 0.85$, $w_r = 0.4$, $\mu_1 = 1$, $\mu_2 = 1$

Fig. 5. Mode shapes of a laminated rectangular plate reinforced with a uniform dispersion of CNTs within the isotropic matrix. They have been calculated with the EDZ4 displacement field assumption.

Hyperbolic paraboloid

Reference surface equation in principal coordinates

$$\mathbf{r}(\alpha_1,\alpha_2)=\left(\frac{k^{\alpha_1}\tan\alpha_1}{2}+\frac{k^{\alpha_2}\tan^2\alpha_2}{4}\sin\alpha_1\right)\mathbf{e}_1-\frac{k^{\alpha_2}\tan^2\alpha_2}{2}\mathbf{e}_2+\left(\frac{k^{\alpha_1}\tan^2\alpha_1}{4}-\frac{k^{\alpha_2}\tan^2\alpha_2}{4}\cos\alpha_1\right)\mathbf{e}_3$$

3D FEM model C3D20 brick elements - 1530765 DOFs	**2D GDQ model** LGL distribution - $I_N \times I_M = 25\times 27$
	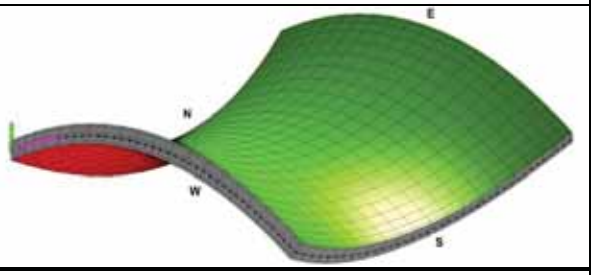

Geometric input: $(\alpha_1,\alpha_2)\in\left[\alpha_1^0,\alpha_1^1\right]\times\left[\alpha_2^0,\alpha_2^1\right]$, $\alpha_1^0=\alpha_2^0=-\pi/6$, $\alpha_1^1=\alpha_2^1=\pi/6$

$k^{\alpha_1}=2$, $k^{\alpha_2}=2.5$, $h_1^0=h_2^0=h_4^0=h_5^0=0.01$ m, $h_3^0=0.015$ m

Material properties: $(70/30/45/20/50)$

1st layer: CNT composite,
2nd layer: trigonal material,
3rd layer: CNT composite
4th layer: trigonal material,
5th layer: CNT composite

Fig. 6. Mechanical and geometric properties of a laminated hyperbolic paraboloid made of CNT composite and generally anisotropic materials.

Hyperbolic paraboloid

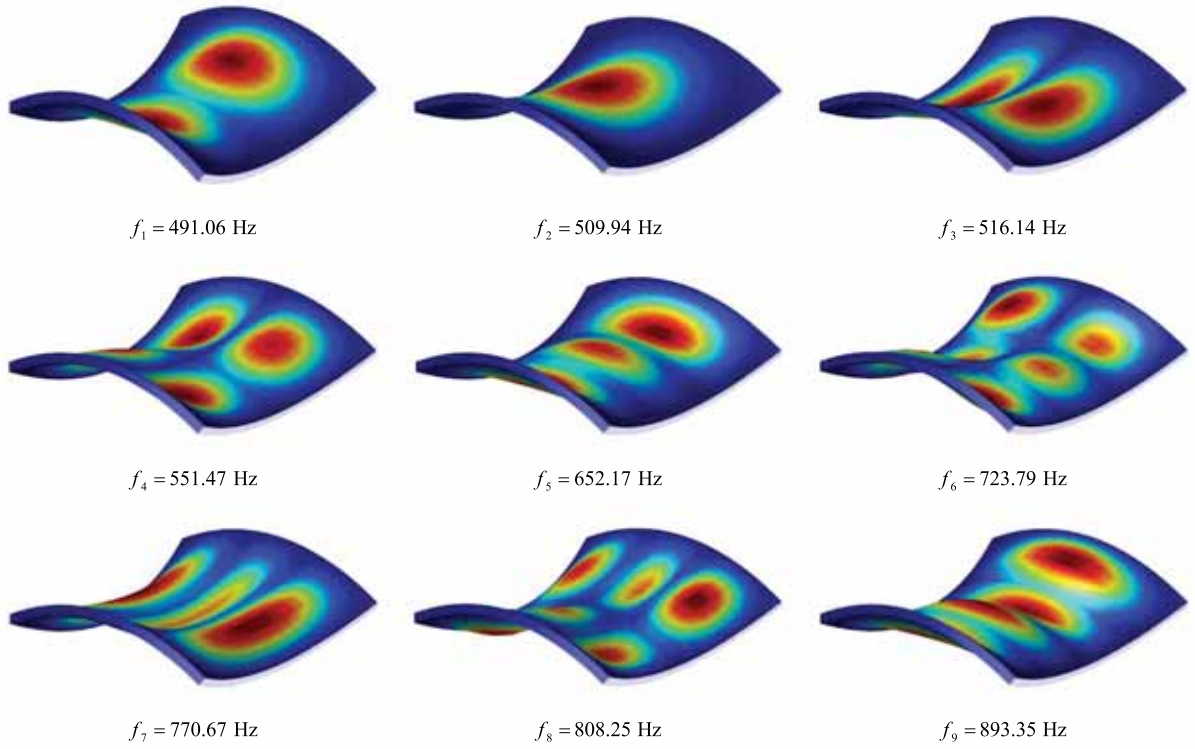

$f_1=491.06$ Hz $f_2=509.94$ Hz $f_3=516.14$ Hz

$f_4=551.47$ Hz $f_5=652.17$ Hz $f_6=723.79$ Hz

$f_7=770.67$ Hz $f_8=808.25$ Hz $f_9=893.35$ Hz

HSDT: EDZ4

Discrete points: LGL distribution with $I_N=I_M=25$ - 9522 DOFs

Lamination scheme: $(70/30/45/20/50)$, $h_1^0=h_2^0=h_4^0=h_5^0=0.01$ m, $h_3^0=0.015$ m

Laminae material sequence: 1st CNT composite, 2nd trigonal material, 3rd CNT composite, 4th trigonal material, 5th CNT composite

Composite CNT parameters: $w_f=0.85$, $w_r=0.2$, $\mu_1=0.75$, $\mu_2=1$

Fig. 7. Mode shapes of a laminated hyperbolic paraboloid reinforced with a uniform dispersion of CNTs within the isotropic matrix. They have been calculated with the EDZ4 displacement field assumption.

Catenoid

Reference surface equation in principal coordinates

$$\mathbf{r}(\alpha_1,\alpha_2)=a\cosh\left(\frac{\alpha_1}{a}\right)\cos\alpha_2\ \mathbf{e}_1-a\cosh\left(\frac{\alpha_1}{a}\right)\sin\alpha_2\ \mathbf{e}_2+a\sinh\alpha_1\ \mathbf{e}_3$$

3D FEM model

C3D20 brick elements - 1530765 DOFs

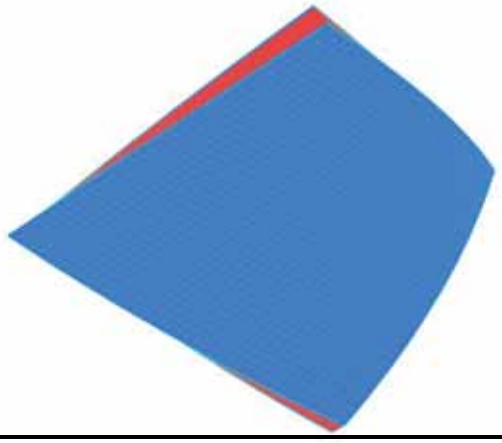

2D GDQ model

LGL distribution . $I_N\times I_M=25\times 27$

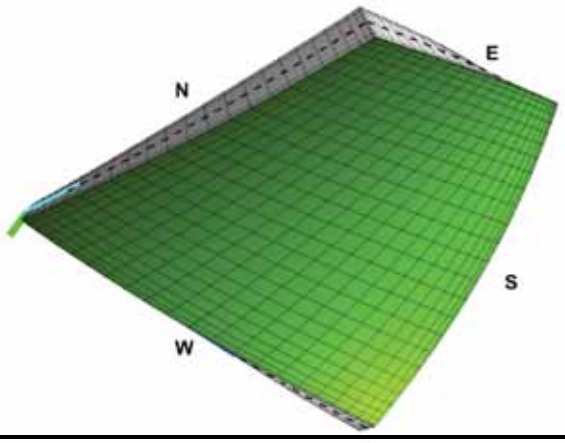

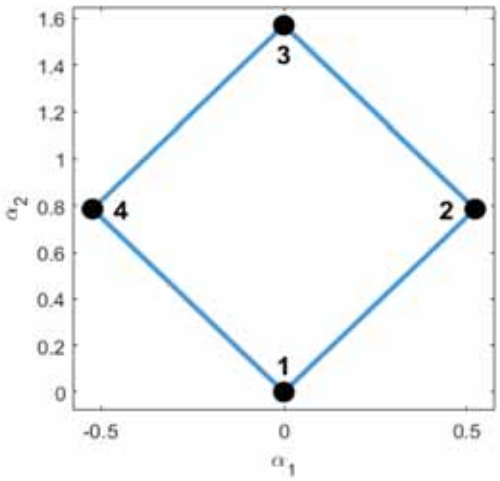

Edge 1-2

knots → 0.0,0.0,0.0,0.0,1.0,1.0,1.0,1.0

weigths → 1.0,1.0,1.0,1.0

control points → $(0.000000,0.000000),(0.174533,0.261799),(0.349066,0.523599),(0.523599,0.785398)$

Edge 2-3

knots → 0.0,0.0,0.0,1.0,1.0,1.0

weigths → 1.0,1.0,1.0

control points → $(0.523599,0.785398),(0.349066,1.047198),(0.174533,1.308997),(0.000000,1.570796)$

Edge 3-4

knots → 0.0,0.0,0.0,0.0,1.0,1.0,1.0,1.0

weigths → 1.0,1.0,1.0,1.0

control points → $(0.000000,1.570796),(-0.174533,1.308997),(-0.349066,1.047198),(-0.523599,0.785398)$

Edge 4-1

knots → 0.0,0.0,0.0,0.0,1.0,1.0,1.0,1.0

weigths → 1.0,1.0,1.0,1.0

control points → $(-0.523599,0.785398),(-0.349066,0.523599),(-0.174533,0.261799),(0.000000,0.000000)$

Geometric input: $a=0.95$ m , $h_1^0=h_3^0=0.01$ m, $h_2^0=0.07$ m

Material properties: $\left(70/\text{FG-CNT}^{PM}_{CNT(5P)(a=1/b=0/c=d=1/p)}/40\right)$

1st layer: triclinic material,

2nd layer $\text{FG-CNT}^{PM}_{CNT(5P)}$,

3rd layer: triclinic material

Boundary springs: Super elliptic distribution $(\bar{\lambda}=1)$,

$\bar{\xi}_m=0$ (W-N), $\bar{\xi}_m=1$ (E-S), $\bar{\xi}_m=\mathbf{0.47}$, $p=1000$,

$k_{1f}^{(k)\xi_1^0}=k_{1f}^{(k)\xi_1^1}=k_{2f}^{(k)\xi_1^0}=k_{2f}^{(k)\xi_1^1}=k_{3f}^{(k)\xi_1^0}=k_{3f}^{(k)\xi_1^1}=1\times10^{21}$ N/m^3,

$k_{1f}^{(k)\xi_2^0}=k_{1f}^{(k)\xi_2^1}=k_{2f}^{(k)\xi_2^0}=k_{2f}^{(k)\xi_2^1}=k_{3f}^{(k)\xi_2^0}=k_{3f}^{(k)\xi_2^1}=1\times10^{21}$ N/m^3

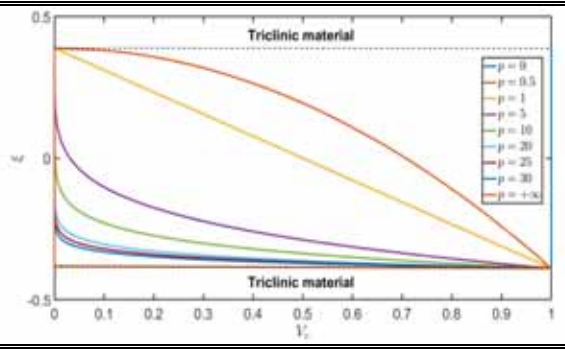

Fig. 8. Mechanical and geometric properties of a laminated catenoid of arbitrary shape made of FG-CNT and generally anisotropic materials.

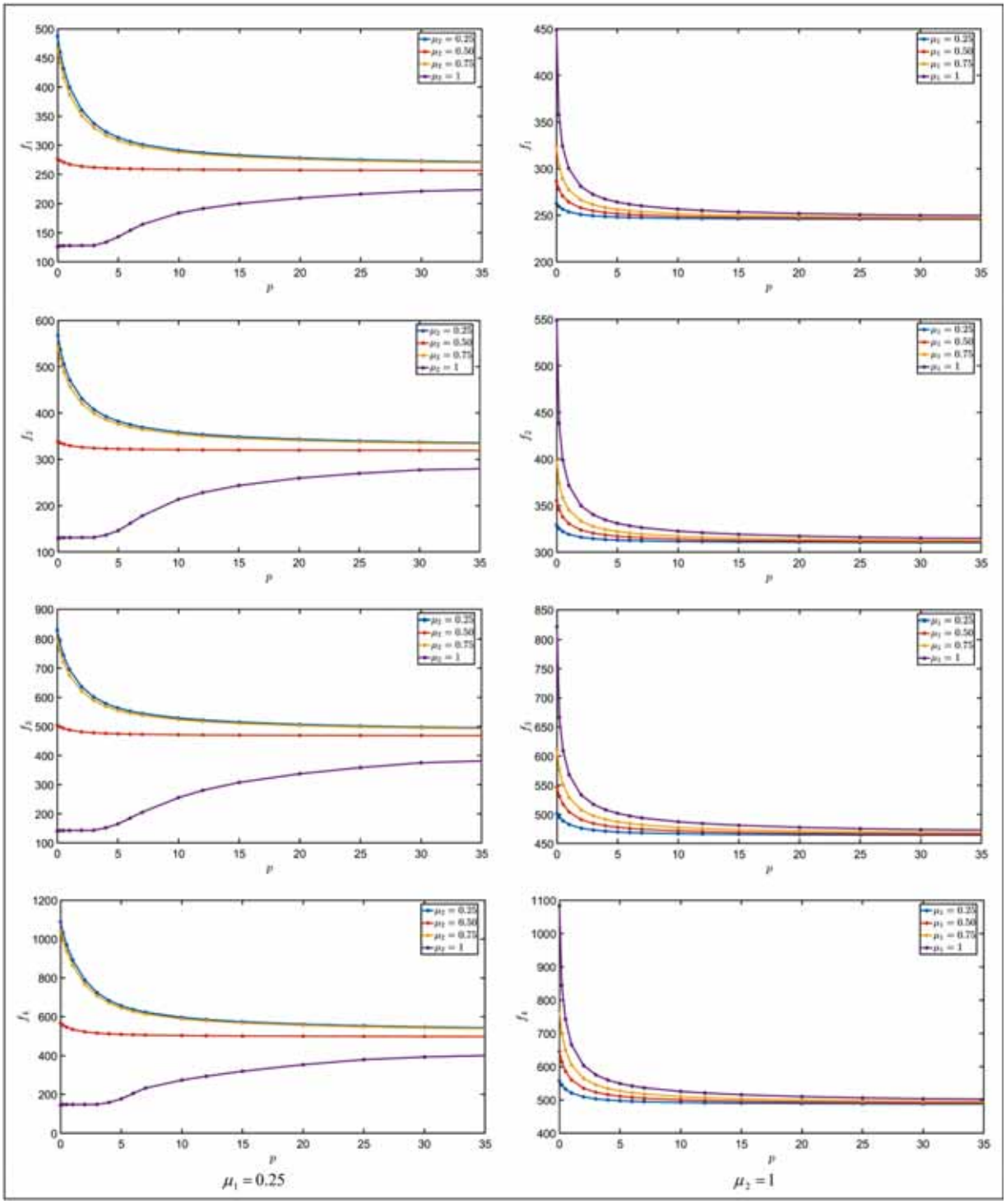

Fig. 9. Parametric investigation on the first natural frequencies of a catenoid of arbitrary shape made of generally anisotropic materials reinforced with a dispersion of FG-CNTs within the isotropic matrix. The influence of the agglomeration parameters on the natural frequencies have been outlined for different values of the through-the-thickness distribution exponents.

Catenoid

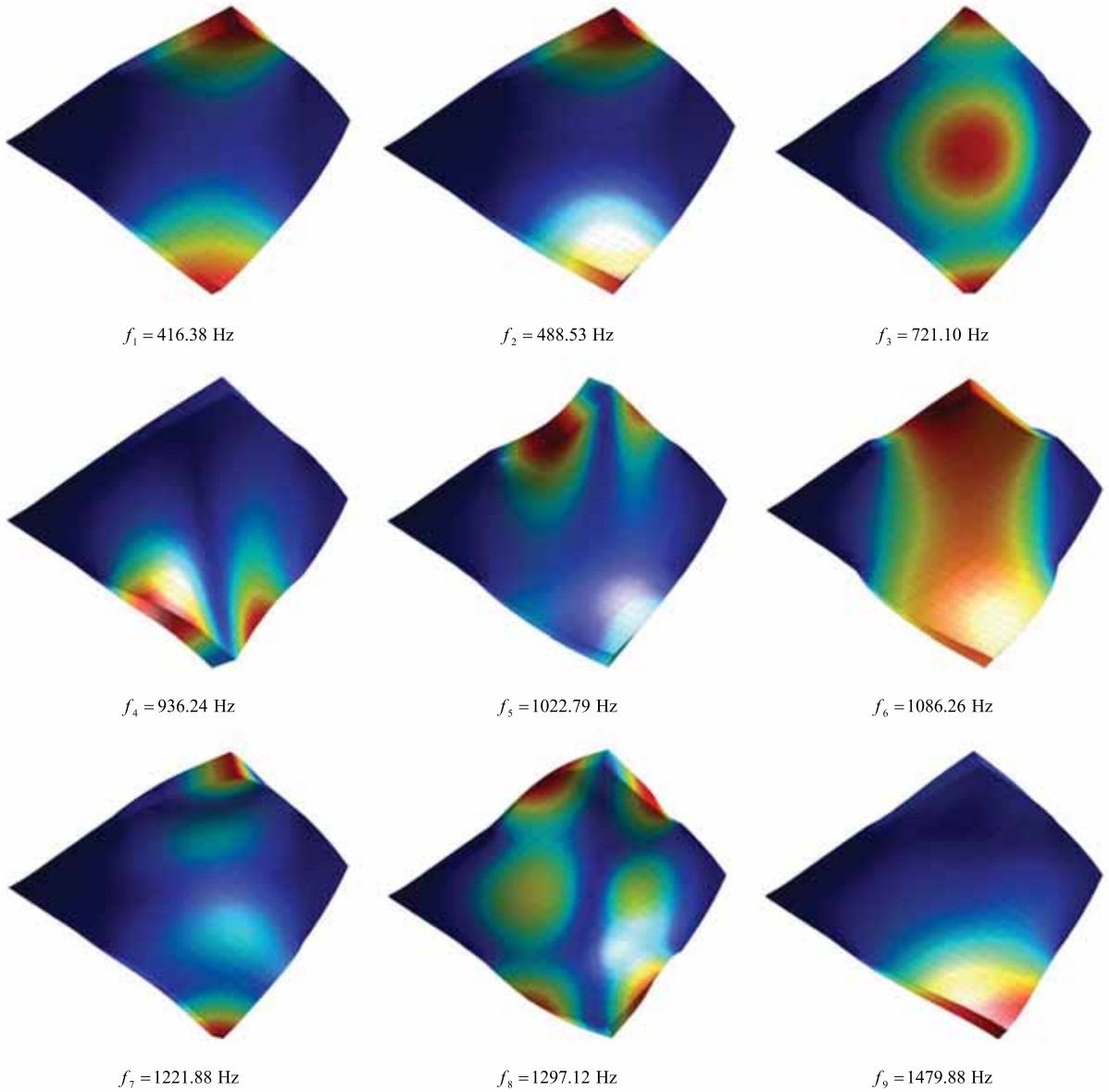

HSDT: EDZ4

Discrete Points: LGL distribution with $I_N \times I_M = 25 \times 27$ - 10350 DOFs

Lamination Scheme: $\left(70 / \text{FG-CNT}^{PM}_{CNT(5P)(a=1/b=0/c=d=1/p=0.5)} / 40\right)$, $h_1^0 = h_3^0 = 0.01$ m, $h_2^0 = 0.07$ m

Laminae Material Sequence: 1st layer: triclinic material, 2nd layer: $\text{FG-CNT}^{PM}_{CNT(5P)}$, 3rd layer: triclinic material

FG-CNT parameters: $w_f = 0$, $w_r = 0.25$, $\mu_1 = 0.25$, $\mu_2 = 0.5$

Fig. 10. Mode shapes of a laminated catenoid of arbitrary shape reinforced with a dispersion of FG-CNTs within the isotropic matrix. They have been calculated with the EDZ4 displacement field assumption.

Helicoid

Reference surface equation in principal coordinates

$$\mathbf{r}\left(\alpha_1,\alpha_2\right)=a\cosh\left(\frac{\alpha_1}{a}\right)\cos\alpha_2\ \mathbf{e}_1-a\cosh\left(\frac{\alpha_1}{a}\right)\sin\alpha_2\ \mathbf{e}_2+a\sinh\alpha_1\ \mathbf{e}_3$$

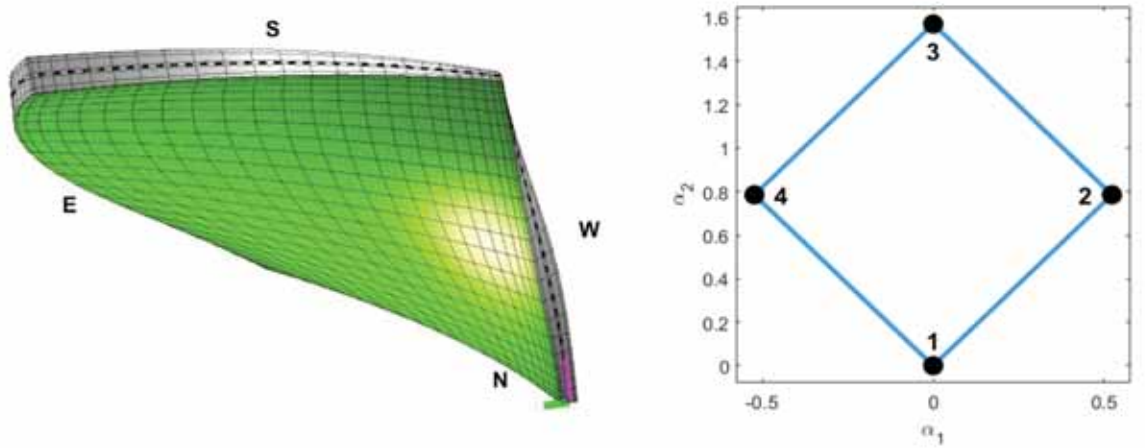

Edge 1-2

knots → 0.0,0.0,0.0,0.0,1.0,1.0,1.0,1.0

weigths → 1.0,1.0,1.0,1.0

control points → $(0.000000,0.000000),(0.174533,0.261799),(0.349066,0.523599),(0.523599,0.785398)$

Edge 3-4

knots → 0.0,0.0,0.0,0.0,1.0,1.0,1.0,1.0

weigths → 1.0,1.0,1.0,1.0

control points → $(0.000000,1.570796),(-0.174533,1.308997),(-0.349066,1.047198),(-0.523599,0.785398)$

Edge 2-3

knots → 0.0,0.0,0.0,1.0,1.0,1.0

weigths → 1.0,1.0,1.0

control points → $(0.523599,0.785398),(0.349066,1.047198),(0.174533,1.308997),(0.000000,1.570796)$

Edge 4-1

knots → 0.0,0.0,0.0,0.0,1.0,1.0,1.0,1.0

weigths → 1.0,1.0,1.0,1.0

control points → $(-0.523599,0.785398),(-0.349066,0.523599),(-0.174533,0.261799),(0.000000,0.000000)$

Thickness variation: $h_k\left(\alpha_1,\alpha_2\right)=h_k^0\left(1+\delta_1\phi_1\left(\alpha_1,\alpha_2\right)+\delta_2\phi_2\left(\alpha_1,\alpha_2\right)+\delta_3\phi_3\left(\alpha_1,\alpha_2\right)+\delta_4\phi_4\left(\alpha_1,\alpha_2\right)+\bar{\delta}\right),\ k=1,...,l$

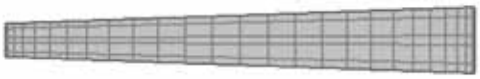

$\phi_1\left(\alpha_1,\alpha_2\right)=\left(\sin\left(\pi\left(n_1\bar{\alpha}_1+\alpha_{1m}\right)\right)\right)^{p_1}\quad \delta_1=1,\ n_1=1,\ p_1=2,\ \alpha_{1m}=0$

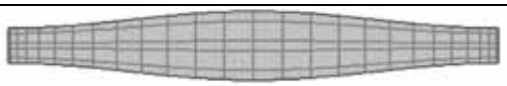

$\phi_2\left(\alpha_1,\alpha_2\right)=\bar{\alpha}_2^{p_2}\quad \delta_2=1,\ p_2=2$

Geometric Inputs:

$a=1.00$ m, $h_1^0=h_3^0=h_5^0=0.01$ m, $h_2^0=h_4^0=0.02$ m

Material Properties:

$\left(70/\text{FG-CNT}^{PM}_{CNT(5P)(a=1/b=0/c=d=1/p)}/65/\text{FG-CNT}^{CNT(5P)(a=1/b=0/c=d=1/p)}_{PM}/50\right)$

1st layer: trigonal material, 2nd layer: $\text{FG-CNT}^{PM}_{CNT(5P)}$,

3rd layer: trigonal material, 4th layer: $\text{FG-CNT}^{CNT}_{PM(5P)}$,

5th layer: trigonal material

$\left(w_f=0,\ w_r=0.25\right)$

Boundary Springs

In plane: Super elliptic distribution

$\left(\bar{\xi}_m=1,\ \bar{\xi}_m=0.47,\ n=1000\right)$

Out of plane: constant distribution $\left(\bar{\lambda}=1\right)$

$k_{1f}^{(k)\bar{\xi}_{s2}^1}=1\times10^{21}$ N/m^3, $k_{2f}^{(k)\bar{\xi}_{s2}^1}=1\times10^{21}$ N/m^3, $k_{3f}^{(k)\bar{\xi}_{s2}^1}=1\times10^{21}$ N/m^3

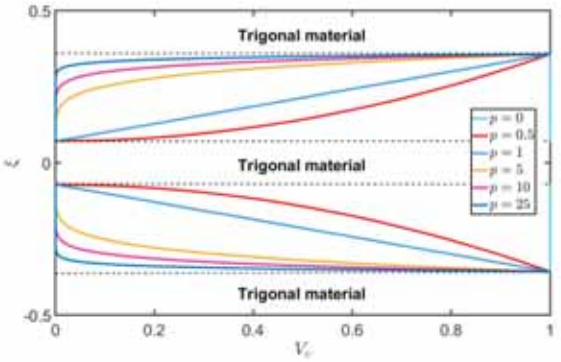

Fig. 11. Mechanical and geometric properties of a laminated helicoid of arbitrary shape made of FG-CNT and generally anisotropic materials.

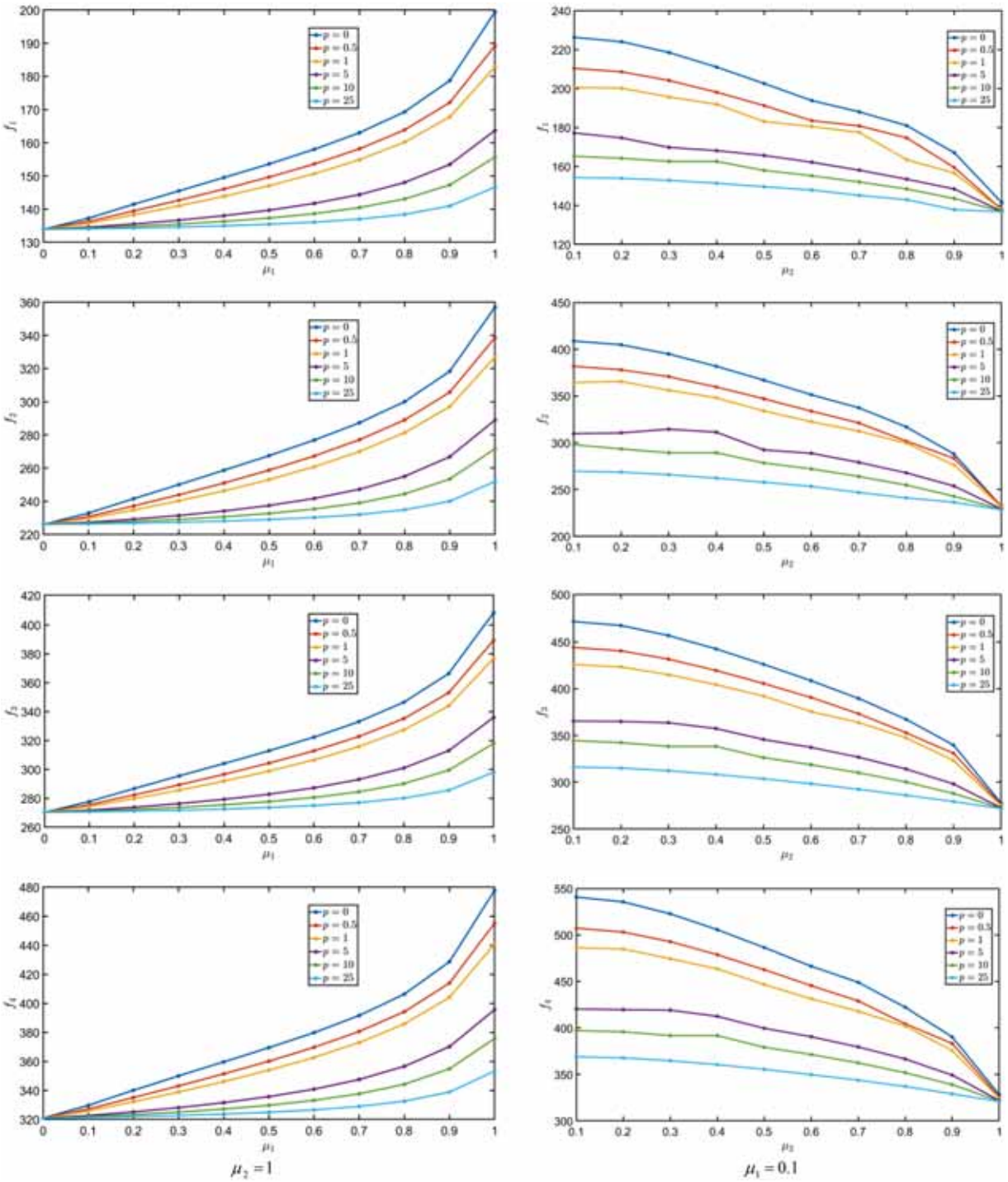

Fig. 12. Parametric investigation on the first natural frequencies of a catenoid of arbitrary shape made of generally anisotropic materials reinforced with a dispersion of FG-CNT within the isotropic matrix. The influence of the agglomeration parameters on the natural frequencies have been outlined for different values of the through-the-thickness distribution exponents.

Helicoid

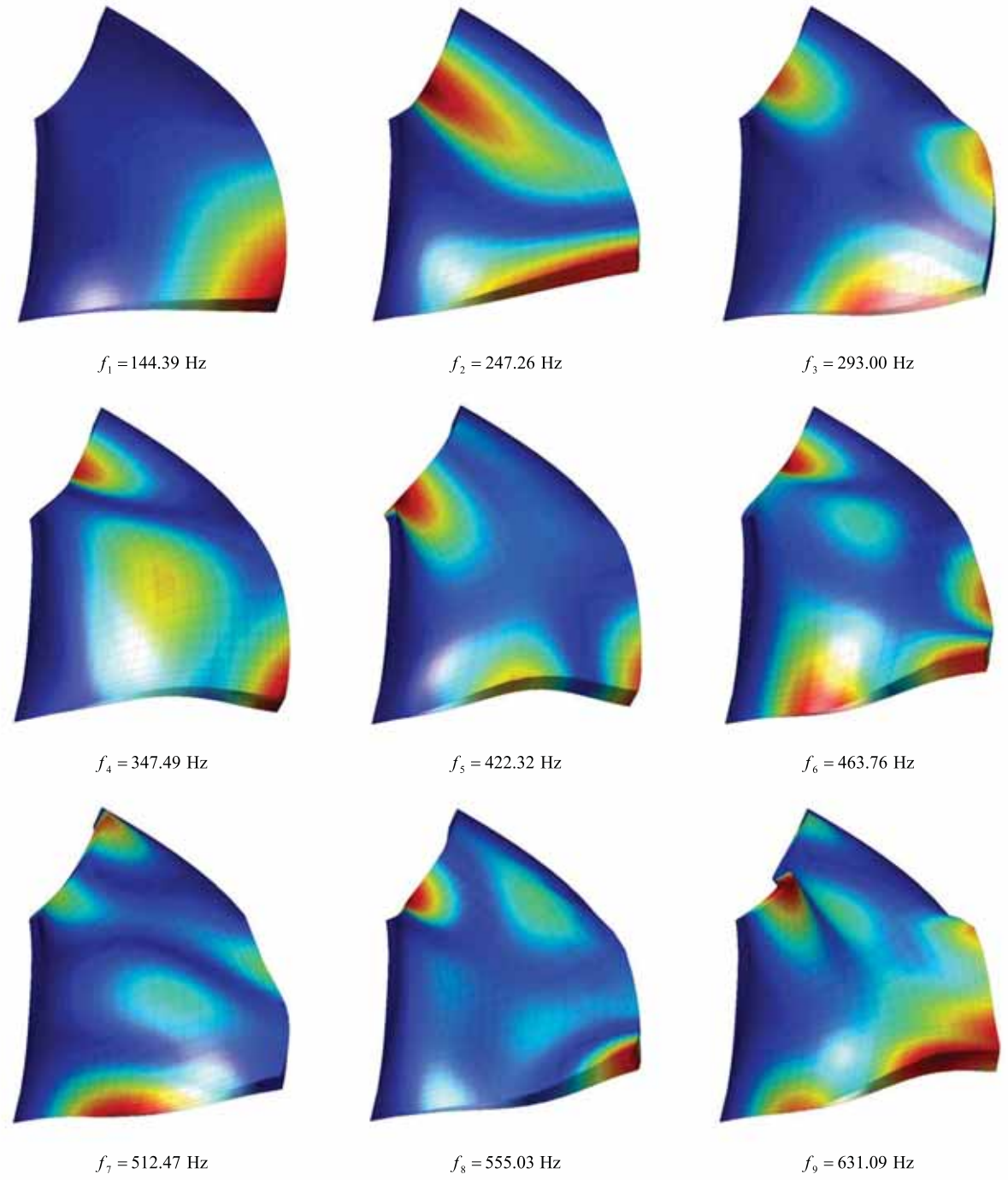

HSDT: EDZ4
Discrete points: LGL distribution with $I_N \times I_M = 25 \times 27$ - 10350 DOFs

Lamination scheme: $\left(70 / \text{FG-CNT}^{PM}_{CNT(5P)(a=1/b=0/c=d=1/p=5)} / 65 / \text{FG-CNT}^{CNT(5P)(a=1/b=0/c=d=1/p=5)}_{PM} / 50\right)$, $h_1^0 = h_3^0 = h_5^0 = 0.01$ m, $h_2^0 = h_4^0 = 0.02$ m
Laminae material sequence: 1st CNT composite, 2nd trigonal material, 3rd CNT composite, 4th trigonal material, 5th CNT composite
FG-CNT parameters: $w_f = 0$, $w_r = 0.25$, $\mu_1 = 0.70$, $\mu_2 = 1$

Fig. 13. Mode shapes of a laminated helicoid of arbitrary shape reinforced with a dispersion of FG-CNTs within the isotropic matrix. They have been calculated with the EDZ4 displacement field assumption.

Revolution paraboloid

$\left(\mathrm{B}^{\mathrm{K}}_{\mathrm{SSS}}\mathrm{FB}^{\mathrm{K}}_{\mathrm{SSS}}\mathrm{C}\right)$

Reference surface equation in principal coordinates

$$\mathbf{r}\left(\alpha_1,\alpha_2\right)=\alpha_1\cos\alpha_2\ \mathbf{e}_1-\alpha_1\sin\alpha_2\ \mathbf{e}_2+a\alpha_1^n\ \mathbf{e}_3$$

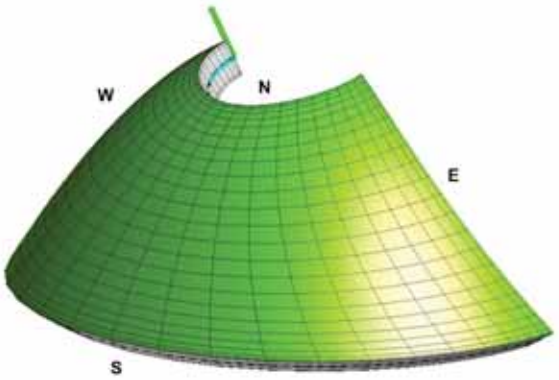

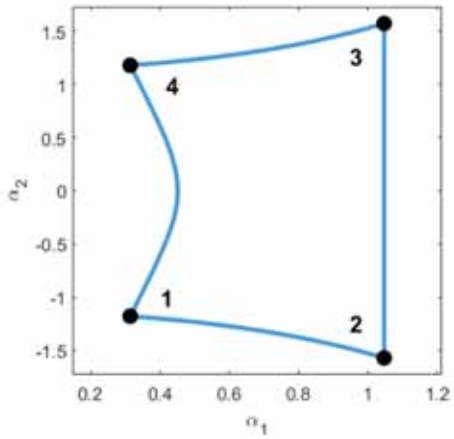

Edge 1-2

knots → 0.0,0.0,0.0,1.0,1.0,1.0

weigths → 1.0,1.0,1.0

control points → $(0.314159,-1.178097),(0.748652,-1.279479),(1.047198,-1.570796)$

Edge 3-4

knots → 0.0,0.0,0.0,1.0,1.0,1.0

weigths → 1.0,1.0,1.0

control points → $(1.047198,1.570796),(0.748652,1.279479),(-0.349066,1.047198)$

Edge 2-3

knots → 0.0,0.0,0.0,0.0,0.0,0.5,1.0,1.0,1.0,1.0,1.0

weigths → 1.0,1.0,1.0,1.0,1.0

control points → $(1.047198,-1.570796),(1.047198,-1.047198),(1.047198,0.000000),(1.047198,1.047198)(1.047198,1.570796)$

Edge 4-1

knots → 0.0,0.0,0.0,0.0,0.0,0.5,1.0,1.0,1.0,1.0,1.0

weigths → 1.0,1.0,1.0,1.0,1.0

control points → $(0.314159,1.178097),(0.405789,0.589049),(0.497419,0.000000),(0.405789,-0.589049)(0.314159,-1.178097)$

Geometric Inputs:

$a=0.80$ m, $n=2$, $h_1^0=h_3^0=h_5^0=0.01$ m, $h_2^0=h_4^0=0.05$ m

Material Properties:

$\left(70/\text{FG-CNT}^{CNT}_{PM(5P)(a=1/b=0/c=d=1/p)}/40/\text{FG-CNT}^{PM(5P)(a=1/b=0/c=d=1/p)}_{CNT}/20\right)$

1st layer: graphite-epoxy, 2nd layer: $\text{FG-CNT}^{CNT}_{PM(5P)}$,

3rd layer: triclinic material, 4th layer: $\text{FG-CNT}^{PM}_{CNT(5P)}$,

5th layer: graphite-epoxy

$\left(w_f=0,\ w_r=0.40\right)$

Boundary Springs:

In plane: Super elliptic distribution

$\left(\bar{\xi}_m=1,\ \bar{\xi}_m=\mathbf{0.47},\ n=1000\right)$

Out of plane: constant distribution $\left(\bar{\lambda}=1\right)$

$k_{1f}^{(k)\xi_2^0}=1\times10^{21}$ N/m^3, $k_{2f}^{(k)\xi_2^0}=1\times10^{21}$ N/m^3, $k_{3f}^{(k)\xi_2^0}=1\times10^{21}$ N/m^3

$k_{1f}^{(k)\xi_2^1}=1\times10^{21}$ N/m^3, $k_{2f}^{(k)\xi_2^1}=1\times10^{21}$ N/m^3, $k_{3f}^{(k)\xi_2^1}=1\times10^{21}$ N/m^3

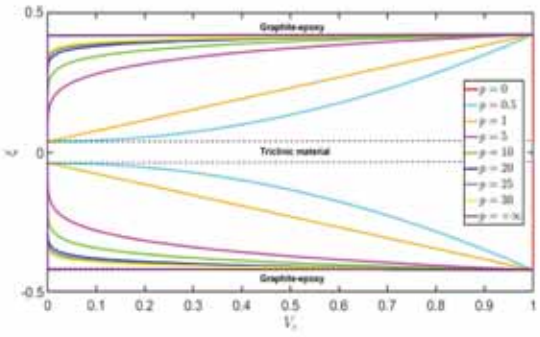

Fig. 14. Mechanical and geometric properties of a laminated revolution paraboloid of arbitrary shape made of FG-CNT and generally anisotropic materials.

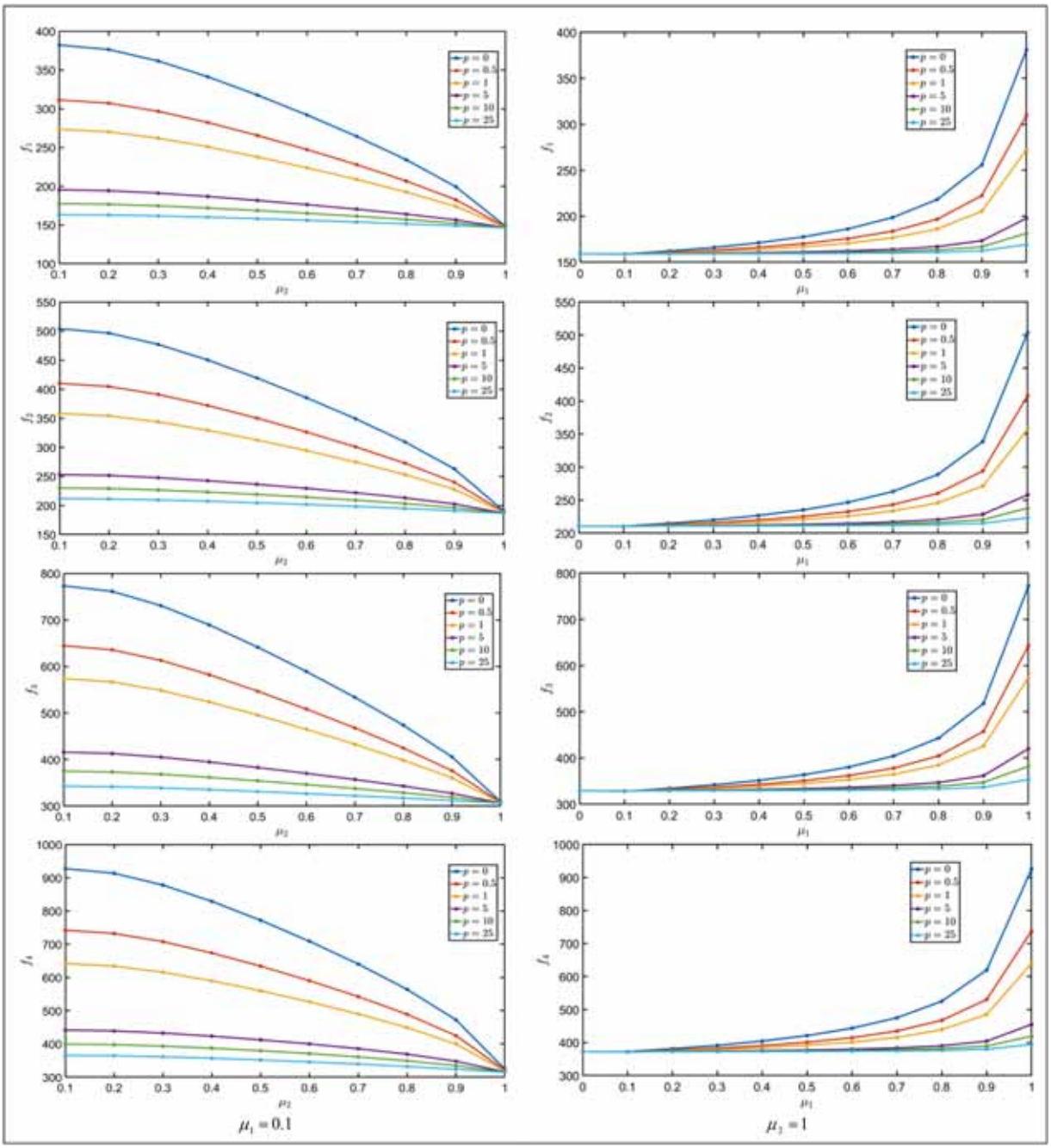

Fig. 15. Parametric investigation on the first natural frequencies of a revolution paraboloid of arbitrary shape made of generally anisotropic materials reinforced with a dispersion of FG-CNT within the isotropic matrix. The influence of the agglomeration parameters on the natural frequencies have been outlined for different values of the through-the-thickness distribution exponents.

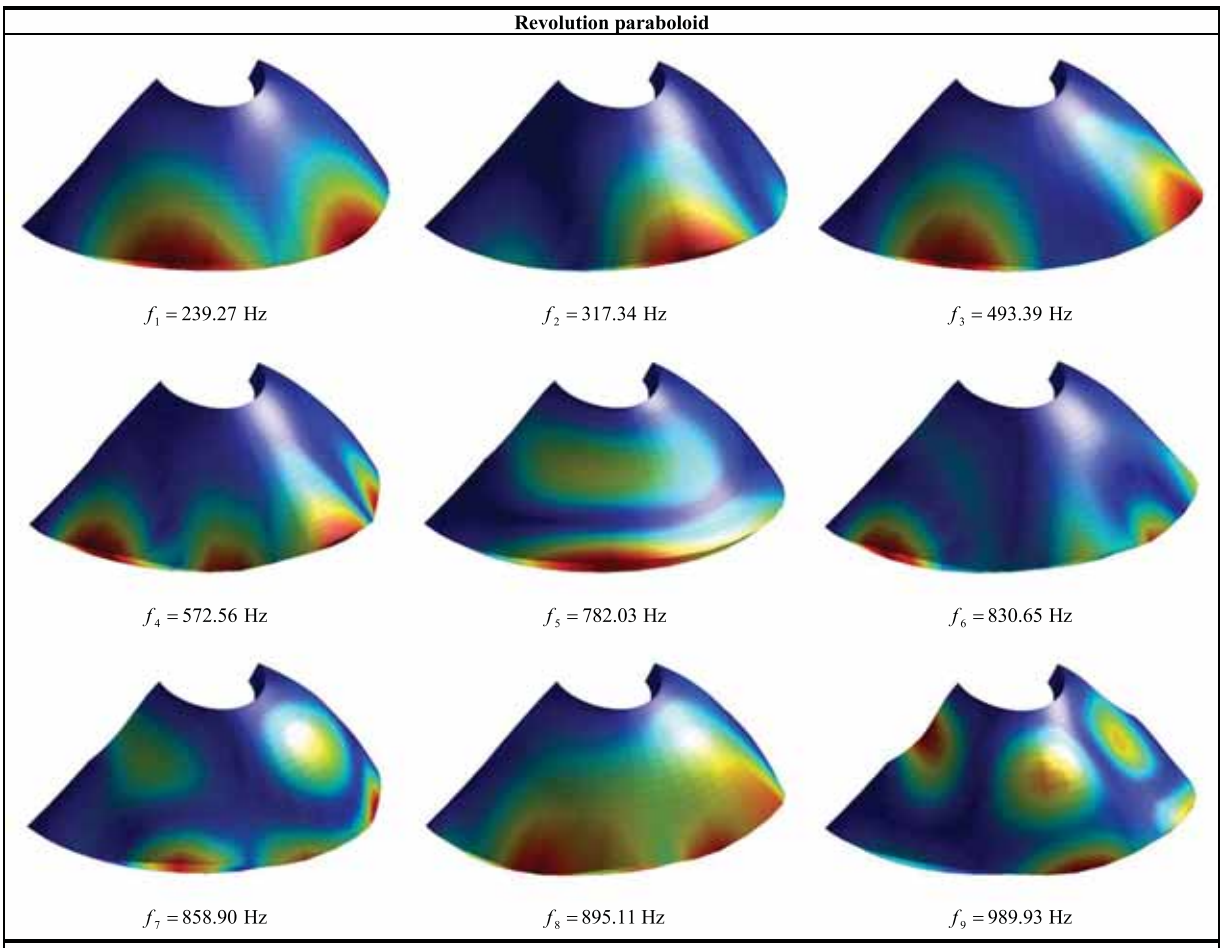

Fig. 16. Mode shapes of a laminated revolution paraboloid of arbitrary shape reinforced with a dispersion of FG-CNTs within the isotropic matrix. They have been calculated with the EDZ4 displacement field assumption.

Table 1
Equivalent Hill elastic moduli for different SWCNTs with various chiral indexes characterized by an armchair configuration (*n, n*).

SWCNT (*n, n*)	$n = 5$	$n = 6$	$n = 10$	$n = 15$	$n = 20$	$n = 50$
k_r[GPa]	536.0	9.9	271.0	181.0	136.0	55.0
l_r[GPa]	184.0	8.4	88.0	58.0	43.0	17.0
m_r[GPa]	132.0	4.4	17.0	5.0	2.0	0.1
n_r[GPa]	2143.0	457.6	1089.0	726.0	545.0	218.0
p_r[GPa]	791.0	27.0	442.0	301.0	227.0	92.0
ρ_r[kg/m^3]	1400	1400	1400	1400	1400	1400

Table 2
Parametric investigation on the first ten mode frequencies of a laminated rectangular plate reinforced with agglomerated CNT composite materials for different values of the nanofibers concentration within the hybrid matrix. Furthermore, the influence of the agglomeration parameters has been pointed out.

Rectangular plate (FCFC)											
w_r	0		0.05	0.10	0.15	0.20	0.25	0.30	0.35	0.40	
Mode f [Hz]	3D FEM	EDZ4	EDZ4							EDZ4	3D FEM
DOFs	1912113	9522	9522							9522	1912113
$\mu_1 = 0.25$, $\mu_2 = 1$											
1	49.610	50.067	53.177	53.450	53.565	53.636	53.689	53.734	53.773	53.809	53.391
2	70.808	71.530	75.351	75.681	75.821	75.908	75.973	76.028	76.076	76.121	75.493
3	135.172	136.708	145.480	146.244	146.568	146.770	146.920	147.045	147.157	147.260	145.992
4	152.497	154.240	161.826	162.468	162.741	162.911	163.040	163.147	163.242	163.331	161.854
5	170.083	172.105	180.694	181.449	181.771	181.973	182.126	182.253	182.367	182.473	180.807
6	254.781	258.318	272.990	274.241	274.775	275.108	275.360	275.570	275.757	275.932	273.171
7	261.034	264.670	282.331	283.859	284.510	284.915	285.220	285.474	285.701	285.911	283.167
8	297.938	302.385	320.651	322.225	322.897	323.318	323.635	323.901	324.138	324.359	320.975
9	335.525	339.581	351.238	352.230	352.661	352.935	353.144	353.322	353.481	353.630	350.287
10	383.089	389.427	414.409	416.550	417.464	418.036	418.467	418.828	419.150	419.450	414.743
$\mu_1 = 0.50$, $\mu_2 = 1$											
1	49.610	50.067	56.310	57.461	57.961	58.250	58.444	58.587	58.701	58.795	58.375
2	70.808	71.530	79.118	80.482	81.073	81.414	81.643	81.812	81.946	82.058	81.435
3	135.172	136.708	154.205	157.397	158.784	159.584	160.122	160.520	160.835	161.097	159.893
4	152.497	154.240	168.940	171.450	172.527	173.145	173.559	173.865	174.107	174.308	172.874
5	170.083	172.105	189.369	192.575	193.976	194.786	195.332	195.736	196.057	196.324	194.739
6	254.781	258.318	286.946	291.926	294.072	295.306	296.135	296.747	297.232	297.636	295.107
7	261.034	264.670	299.653	305.957	308.694	310.274	311.336	312.122	312.745	313.264	310.812
8	297.938	302.385	338.442	344.898	347.701	349.320	350.409	351.215	351.855	352.388	349.337
9	335.525	339.581	362.221	366.171	367.884	368.873	369.539	370.031	370.422	370.747	367.552
10	383.089	389.427	438.354	446.975	450.705	452.855	454.300	455.369	456.217	456.923	452.762
$\mu_1 = 0.75$, $\mu_2 = 1$											
1	49.610	50.067	59.526	62.462	63.918	64.794	65.382	65.807	66.129	66.383	65.940
2	70.808	71.530	82.941	86.384	88.082	89.101	89.783	90.275	90.649	90.943	90.277
3	135.172	136.708	163.113	171.216	175.229	177.642	179.262	180.430	181.318	182.019	180.789
4	152.497	154.240	175.861	181.921	184.862	186.615	187.785	188.625	189.261	189.760	188.247
5	170.083	172.105	198.413	206.759	210.933	213.455	215.151	216.377	217.308	218.044	216.398
6	254.781	258.318	300.722	312.893	318.815	322.345	324.701	326.393	327.674	328.682	326.119
7	261.034	264.670	317.218	333.133	341.002	345.731	348.904	351.194	352.932	354.305	351.893
8	297.938	302.385	356.480	372.822	380.913	385.778	389.042	391.395	393.179	394.584	391.506
9	335.525	339.581	373.249	383.269	388.275	391.304	393.344	394.819	395.940	396.826	393.498
10	383.089	389.427	462.252	483.656	494.162	500.452	504.664	507.697	509.998	511.811	507.697
$\mu_1 = 1$, $\mu_2 = 1$											
1	49.610	50.067	62.873	69.106	72.997	75.764	77.912	79.694	81.256	82.688	82.211
2	70.808	71.530	86.895	94.206	98.819	102.171	104.849	107.143	109.220	111.186	110.415
3	135.172	136.708	172.349	189.510	200.210	207.813	213.713	218.608	222.862	226.825	225.204
4	152.497	154.240	182.788	195.329	203.303	209.284	214.255	218.692	222.897	226.947	225.523
5	170.083	172.105	207.982	226.122	237.699	246.088	252.731	258.357	263.388	268.093	266.253
6	254.781	258.318	314.624	339.712	355.295	366.663	375.865	383.885	391.273	398.377	395.494
7	261.034	264.670	335.357	368.954	389.863	404.706	416.219	425.766	434.122	441.778	439.274
8	297.938	302.385	375.164	406.743	421.684	433.300	443.198	452.192	460.767	469.252	465.428
9	335.525	339.581	384.727	409.993	431.848	447.553	459.885	470.244	479.432	487.959	484.648
10	383.089	389.427	486.654	531.346	559.038	578.754	594.165	607.185	618.944	630.093	625.681

Lamination scheme: $.(70/30/45/20/50)$, $h_1^0 = h_2^0 = h_4^0 = h_5^0 = 0.01\text{m}$, $h_3^0 = 0.015\text{m}$
Material properties: 1st layer: CNT composite, 2nd layer: trigonal material, 3rd layer: CNT composite, 4th layer: trigonal material, 5th layer: CNT composite $(w_f = 0.85)$.
Computational grid: LGL distribution with $I_N = I_M = 25$.

Table 3
Parametric investigation on the first ten mode frequencies of a laminated rectangular plate reinforced with agglomerated CNT composite materials for different values of the nanofibers concentration within the hybrid matrix. Furthermore, the influence of the agglomeration parameters has been pointed out.

Rectangular plate (FCFC)											
w_r	0		0.05	0.10	0.15	0.20	0.25	0.30	0.35	0.40	
Mode f [Hz]	3D FEM	EDZ4	EDZ4							EDZ4	3D FEM
DOFs	1912113	9522	9522							9522	1912113
$\mu_1 = 0.7$, $\mu_2 = 0.7$											
1	49.610	50.022	62.821	69.050	72.939	75.703	77.849	79.631	81.191	82.622	82.211
2	70.808	71.094	86.488	93.771	98.364	101.706	104.378	106.671	108.750	110.720	110.415
3	135.172	136.570	172.195	189.344	200.036	207.633	213.526	217.970	222.129	226.200	225.204
4	152.497	153.669	182.178	194.682	202.630	208.592	213.549	218.419	222.703	226.629	225.523
5	170.083	171.365	207.217	225.296	236.837	245.205	251.835	257.455	262.484	267.192	266.253

(*continued on next page*)

Table 3 (*continued*)

Rectangular plate (FCFC)											
w_r	0		0.05	0.10	0.15	0.20	0.25	0.30	0.35	0.40	
Mode f [Hz]	3D FEM	EDZ4	EDZ4							EDZ4	3D FEM
DOFs	1912113	9522	9522							9522	1912113
6	254.781	257.558	313.683	338.690	354.228	365.564	374.742	382.740	390.109	397.193	395.494
7	261.034	264.387	335.041	368.615	389.508	404.339	415.841	425.380	433.729	441.378	439.274
8	297.938	301.245	374.006	405.324	420.219	431.794	441.656	450.619	459.165	467.621	465.428
9	335.525	338.418	383.397	408.762	430.552	446.218	458.525	468.869	478.048	486.572	484.648
10	383.089	388.361	485.286	529.834	557.459	577.144	592.536	605.531	617.262	628.383	625.681
$\mu_1 = 0.7$, $\mu_2 = 0.8$											
1	49.610	50.022	62.689	68.864	72.74414738	75.510	77.659	79.440	80.997	82.420	81.945
2	70.808	71.094	86.680	93.923	98.51779933	101.863	104.533	106.817	108.878	110.823	110.054
3	135.172	136.570	171.843	188.845	199.5145508	207.117	213.020	217.911	222.158	226.090	224.440
4	152.497	153.669	182.414	194.843	202.7736272	208.721	213.654	218.044	222.186	226.177	224.793
5	170.083	171.365	207.455	225.412	236.9412999	245.317	251.948	257.555	262.556	267.219	265.385
6	254.781	257.558	313.873	338.751	354.2758585	365.609	374.767	382.728	390.039	397.048	394.176
7	261.034	264.387	334.365	367.654	388.5045982	403.348	414.866	424.405	432.736	440.347	437.851
8	297.938	301.245	374.142	405.848	420.6673292	432.185	441.981	450.859	459.299	467.629	463.818
9	335.525	338.418	384.096	408.648	430.4222091	446.112	458.433	468.767	477.910	486.371	483.071
10	383.089	388.361	485.325	529.626	557.2415157	576.952	592.353	605.321	616.985	628.012	623.615
$\mu_1 = 0.7$, $\mu_2 = 0.9$											
1	49.610	50.022	61.910	67.686	71.426	74.138	76.250	77.989	79.485	80.822	80.266
2	70.808	71.094	85.900	92.686	97.103	100.352	102.937	105.118	107.047	108.820	107.793
3	135.172	136.570	169.707	185.616	195.905	203.358	209.164	213.941	218.049	221.720	219.764
4	152.497	153.669	181.241	192.930	200.512	206.197	210.854	214.917	218.634	222.165	220.184
5	170.083	171.365	205.534	222.273	233.336	241.484	247.936	253.336	258.063	262.363	259.932
6	254.781	257.558	311.295	334.734	349.697	360.671	369.460	376.964	383.695	389.975	386.013
7	261.034	264.387	330.184	361.349	381.465	396.021	407.354	416.673	424.686	431.841	428.867
8	297.938	301.245	370.308	402.322	416.552	427.383	436.489	444.586	452.105	459.334	454.081
9	335.525	338.418	382.437	402.883	423.553	438.876	450.925	460.937	469.640	477.502	473.145
10	383.089	388.361	480.527	522.163	548.859	568.181	583.276	595.785	606.718	616.742	610.732
$\mu_1 = 0.7$, $\mu_2 = 1$											
1	49.610	50.022	58.940	61.428	62.623	63.332	63.806	64.148	64.408	64.615	64.105
2	70.808	71.094	82.376	85.302	86.700	87.527	88.078	88.475	88.778	89.018	88.140
3	135.172	136.570	161.504	168.375	171.672	173.627	174.932	175.875	176.593	177.164	175.733
4	152.497	153.669	175.018	180.216	182.660	184.096	185.050	185.734	186.253	186.664	184.594
5	170.083	171.365	197.065	204.109	207.519	209.549	210.908	211.890	212.639	213.234	211.084
6	254.781	257.558	298.834	309.251	314.168	317.061	318.983	320.364	321.414	322.246	318.764
7	261.034	264.387	314.062	327.568	334.038	337.872	340.433	342.281	343.690	344.810	341.978
8	297.938	301.245	353.692	367.560	374.211	378.155	380.790	382.691	384.140	385.292	381.329
9	335.525	338.418	372.239	380.731	384.821	387.252	388.876	390.046	390.936	391.641	387.069
10	383.089	388.361	458.734	476.989	485.676	490.807	494.227	496.691	498.567	500.057	494.549

Lamination scheme: $.(70/30/45/20/50)$, $h_1^0 = h_2^0 = h_4^0 = h_5^0 = 0.01\text{m}$, $h_3^0 = 0.015\text{m}$

Material properties: 1st layer: CNT composite, 2nd layer: trigonal material, 3rd layer: CNT composite, 4th layer: trigonal material, 5th layer: CNT composite $(w_f = 0.85)$.

Computational grid: LGL distribution with $I_N = I_M = 25$.

Table 4
Validation of the higher order ESL displacement field assumption for the free vibration analysis of a fully-clamped hyperbolic paraboloid made of CNT composite layers and generally anisotropic materials.

Hyperbolic paraboloid (CCCC)										
Mode f [Hz]	$w_r = 0.2$					$w_r = 0.4$				
	3D FEM	**FSDT**	**TSDT**	**ED4**	**EDZ4**	**3D FEM**	**FSDT**	**TSDT**	**ED4**	**EDZ4**
DOFs	1530765	3174	6348	7935	9522	1530765	3174	6348	7935	9522
$\mu_1 = 0.25$, $\mu_2 = 1$										
1	429.26	430.75	430.83	432.65	430.05	430.73	432.09	432.17	434.02	431.51
2	439.07	439.18	439.15	440.23	439.35	440.58	440.66	440.64	441.73	440.86
3	442.95	445.36	445.15	446.99	443.96	444.69	446.93	446.73	448.60	445.68
4	473.92	478.70	478.55	480.67	475.38	475.95	480.41	480.27	482.41	477.38
5	573.33	578.79	579.16	581.83	575.16	575.50	580.57	580.95	583.65	577.30
6	616.53	626.71	626.52	629.65	619.20	619.51	629.06	628.89	632.05	622.11
7	639.70	648.35	647.58	651.07	642.15	642.88	650.99	650.26	653.78	645.27
8	681.02	693.04	692.69	696.43	683.91	684.39	695.66	695.34	699.11	687.21
9	785.19	797.89	798.90	802.88	788.22	788.50	800.34	801.34	805.37	791.46
10	787.53	806.47	805.60	810.11	791.95	791.92	809.77	808.96	813.50	796.23
$\mu_1 = 0.50$, $\mu_2 = 1$										
1	454.70	454.85	454.89	457.07	455.29	458.16	458.19	458.22	460.46	458.75
2	468.29	468.01	468.00	469.36	468.45	472.17	471.86	471.85	473.24	472.33
3	473.26	473.81	473.68	475.97	474.02	477.35	477.71	477.59	479.94	478.10

(*continued on next page*)

Table 4 (*continued*)

Hyperbolic paraboloid (CCCC)										
Mode	$w_r = 0.2$					$w_r = 0.4$				
f [Hz]	**3D FEM**	**FSDT**	**TSDT**	**ED4**	**EDZ4**	**3D FEM**	**FSDT**	**TSDT**	**ED4**	**EDZ4**
DOFs	1530765	3174	6348	7935	9522	1530765	3174	6348	7935	9522
4	506.43	507.80	507.71	510.07	507.51	510.85	511.89	511.81	514.22	511.92
5	606.22	607.74	607.93	610.95	607.66	610.75	611.91	612.08	615.17	612.17
6	662.83	666.28	666.22	669.62	664.79	668.96	671.76	671.71	675.17	670.89
7	694.53	697.31	696.89	700.84	696.33	701.81	703.99	703.61	707.64	703.58
8	734.51	738.40	738.19	742.32	736.52	741.71	744.80	744.62	748.83	743.68
9	831.55	835.40	835.93	840.36	833.79	837.87	840.90	841.40	845.91	840.07
10	858.02	865.24	864.80	869.68	861.26	867.28	873.34	872.95	877.91	870.46
$\mu_1 = 0.75$, $\mu_2 = 1$										
1	490.35	489.76	489.75	492.61	491.06	499.50	498.81	498.80	501.77	500.22
2	509.76	509.20	509.19	510.99	509.94	520.18	519.57	519.56	521.44	520.35
3	515.25	514.51	514.43	517.53	516.14	525.91	524.97	524.90	528.13	526.81
4	550.15	549.43	549.34	552.36	551.47	561.27	560.26	560.18	563.30	562.62
5	650.48	649.92	649.93	653.78	652.17	661.86	661.05	661.03	665.02	663.59
6	721.57	720.99	720.90	725.18	723.79	736.09	734.99	734.89	739.31	738.35
7	768.68	767.59	767.36	772.38	770.67	787.30	785.64	785.45	790.63	789.30
8	806.03	804.91	804.74	809.94	808.25	824.22	822.42	822.26	827.63	826.46
9	890.79	889.91	890.00	895.58	893.35	905.88	904.44	904.45	910.22	908.50
10	948.65	948.57	948.29	954.34	952.17	971.11	970.05	969.79	976.03	974.68
$\mu_1 = 1$, $\mu_2 = 1$										
1	552.67	551.83	551.78	555.50	553.44	598.72	597.98	597.94	602.03	599.54
2	580.60	579.83	579.81	582.23	580.74	629.51	628.69	628.68	631.34	629.64
3	586.61	585.26	585.19	589.27	587.61	637.00	635.86	635.79	640.29	638.09
4	624.26	622.89	622.76	626.42	625.83	678.68	677.86	677.74	681.71	680.44
5	728.16	727.11	727.00	731.76	730.09	789.21	788.71	788.59	793.80	791.35
6	816.44	814.78	814.57	819.71	819.00	887.07	886.54	886.33	891.90	889.91
7	890.60	888.12	887.93	894.05	892.81	970.65	969.22	969.04	975.68	973.05
8	926.07	923.42	923.18	929.41	928.57	1008.78	1007.59	1007.36	1014.09	1011.54
9	993.13	991.24	991.00	997.76	996.13	1076.32	1075.79	1075.56	1082.90	1079.63
10	1093.02	1090.97	1090.65	1097.84	1097.19	1190.03	1190.35	1190.06	1197.81	1194.68

Lamination scheme: $.(70\,/30\,/45\,/20\,/50)$, $h_1^0 = h_2^0 = h_4^0 = h_5^0 = 0.01\text{m}$, $h_3^0 = 0.015\text{m}$

Material properties: 1st layer: CNT composite, 2nd layer: triclinic material, 3rd layer: CNT composite, 4th layer: triclinic material, 5th layer: CNT composite $(w_f = 0.85)$.

Computational grid: LGL distribution with $I_N = I_M = 25$.

Table 5
Free vibration analysis of a catenoid of arbitrary shape reinforced with a general distribution of FG-CNT. The effect of the through-the-thickness distribution has been pointed out together with the influence of the agglomeration parameter μ_1.

Catenoid $(B^K_{SSS}B^K_{SSS}B^K_{SSS}B^K_{SSS})$												
p	$p = 0$	$p = 0.2$	$p = 0.5$	$p = 1$	$p = 2$	$p = 5$	$p = 10$	$p = 15$	$p = 20$	$p = 30$	$p = +\infty$	
Mode f [Hz]	EDZ4										EDZ4	3D FEM
$\mu_1 = 0.25$, $\mu_2 = 1$												
1	262.71	259.60	256.65	253.77	250.92	248.11	246.81	246.32	246.06	245.78	245.19	254.02
2	328.83	325.44	322.25	319.14	316.08	313.03	311.62	311.08	310.79	310.49	309.83	315.32
3	501.47	495.05	488.79	482.53	476.20	469.82	466.84	465.70	465.09	464.45	463.08	466.26
4	557.48	544.75	532.53	520.56	508.83	497.37	492.19	490.22	489.18	488.10	485.77	501.72
5	589.15	576.62	564.53	552.59	540.75	529.05	523.71	521.68	520.59	519.46	517.02	534.94
6	683.20	678.76	674.97	671.58	668.49	665.65	664.44	663.99	663.76	663.53	663.03	681.73
7	798.77	782.73	766.95	751.12	735.22	719.33	712.05	709.27	707.80	706.26	702.96	708.43
8	825.82	807.72	789.79	771.73	753.55	735.38	727.06	723.89	722.21	720.45	716.68	721.54
9	975.50	958.25	933.20	908.54	884.28	860.56	849.87	845.82	843.68	841.46	836.67	852.79
10	984.38	969.28	963.24	956.39	942.11	919.71	908.90	904.75	902.56	900.26	895.33	900.93
$\mu_1 = 0.50$, $\mu_2 = 1$												
1	286.37	278.03	270.92	264.29	257.95	251.78	248.94	247.83	247.24	246.60	245.19	254.02
2	355.18	345.74	337.89	330.67	323.79	317.09	313.98	312.76	312.10	311.40	309.83	315.32
3	546.54	531.11	517.39	504.12	490.98	477.80	471.55	469.08	467.74	466.31	463.08	466.26
4	645.74	614.24	586.29	559.95	534.84	510.85	500.00	495.79	493.53	491.13	485.77	501.72
5	674.84	644.36	617.29	591.62	566.86	542.82	531.77	527.46	525.12	522.63	517.02	534.94
6	726.28	709.24	696.86	686.69	677.89	670.09	666.82	665.63	665.01	664.37	663.03	681.73
7	906.63	870.01	836.17	803.04	770.31	738.00	722.99	717.11	713.93	710.55	702.96	708.43
8	945.92	905.44	867.44	830.00	792.94	756.37	739.39	732.74	729.14	725.31	716.68	721.54
9	1039.49	1017.03	999.59	984.09	937.36	888.00	865.74	857.15	852.53	847.63	836.67	852.79
10	1060.59	1038.06	1020.52	989.34	969.55	945.73	924.85	916.26	911.58	906.59	895.33	900.93
$\mu_1 = 0.75$, $\mu_2 = 1$												
1	323.49	303.20	289.26	277.36	266.54	256.38	251.72	249.87	248.85	247.75	245.19	254.02
2	398.56	374.37	358.43	345.19	333.32	322.20	317.07	315.02	313.90	312.68	309.83	315.32

(*continued on next page*)

Table 5 (*continued*)

Catenoid $(B^K_{SSS}B^K_{SSS}B^K_{SSS}B^K_{SSS})$												
p	$p=0$	$p=0.2$	$p=0.5$	$p=1$	$p=2$	$p=5$	$p=10$	$p=15$	$p=20$	$p=30$	$p=+\infty$	
Mode f [Hz]	EDZ4										EDZ4	3D FEM
3	611.02	575.93	550.94	528.73	507.72	487.22	477.46	473.49	471.28	468.86	463.08	466.26
4	768.10	700.37	649.47	604.82	564.17	526.70	509.78	503.05	499.35	495.32	485.77	501.72
5	794.10	727.79	678.61	635.44	595.84	558.79	541.78	534.94	531.14	526.98	517.02	534.94
6	820.56	765.07	733.68	710.77	692.32	676.73	670.35	668.04	666.85	665.62	663.03	681.73
7	1045.43	971.26	913.05	859.43	808.41	759.38	736.48	727.22	722.06	716.43	702.96	708.43
8	1097.28	1017.30	952.52	892.35	835.05	780.12	754.48	744.08	738.28	731.94	716.68	721.54
9	1172.53	1101.49	1058.21	1024.49	994.78	919.94	885.49	871.83	864.30	856.11	836.67	852.79
10	1194.27	1122.84	1079.36	1045.48	997.43	966.91	943.68	930.79	923.38	915.19	895.33	900.93
$\mu_1=1$, $\mu_2=1$												
1	449.02	357.99	324.28	300.52	281.10	264.18	256.66	253.63	251.92	250.02	245.19	254.02
2	549.05	438.41	398.84	371.74	349.95	331.04	322.63	319.24	317.33	315.21	309.83	315.32
3	821.97	666.71	609.47	568.10	533.20	501.76	487.27	481.20	477.71	473.72	463.08	466.26
4	1082.62	843.88	741.81	665.92	603.09	549.18	525.36	515.49	509.78	503.26	485.77	501.72
5	1116.75	871.91	770.20	695.78	634.38	581.33	557.61	547.66	541.86	535.19	517.02	534.94
6	1228.14	925.15	827.89	768.55	725.52	691.57	678.17	673.37	670.90	668.36	663.03	681.73
7	1401.76	1137.65	1023.82	935.05	858.08	789.16	757.61	744.26	736.46	727.47	702.96	708.43
8	1477.09	1197.10	1071.66	973.19	888.10	812.40	777.76	763.01	754.35	744.32	716.68	721.54
9	1733.43	1345.06	1208.02	1119.72	1052.08	964.28	916.49	896.70	885.24	872.11	836.67	852.79
10	1762.08	1367.51	1229.50	1140.82	1072.20	994.90	968.23	953.68	943.53	931.03	895.33	900.93

Lamination scheme: $\left(70/\mathrm{FG}-\mathrm{CNT}^{CNT}_{PM\ (a=1/b=0/c=1/d=1/p)}/40\right)$, $h^0_1=h^0_3=0.01\mathrm{m}$, $h^0_2=0.07\mathrm{m}$, ($w_f=0$, $w_r=0.25$).
Material properties: 1st layer: triclinic material, 2nd layer: FG-CNT, 3rd layer: triclinic material.
Computational grid: LGL distribution with $I_N \times I_M = 25 \times 27$.

Table 6
Free vibration analysis of a catenoid of arbitrary shape reinforced with a general distribution of FG-CNT. The effect of the through-the-thickness distribution has been pointed out together with the influence of the agglomeration parameter μ_2.

Catenoid $(B^K_{SSS}B^K_{SSS}B^K_{SSS}B^K_{SSS})$												
p	$p=0$	$p=0.2$	$p=0.5$	$p=1$	$p=2$	$p=5$	$p=10$	$p=15$	$p=20$	$p=30$	$p=+\infty$	
Mode f [Hz]	EDZ4										EDZ4	3D FEM
$\mu_1=0.25$, $\mu_2=0.25$												
1	487.10	460.41	431.73	399.41	360.34	313.46	291.55	283.05	278.34	273.05	253.32	254.02
2	567.51	537.69	505.95	471.12	430.64	382.29	358.42	348.77	343.34	337.22	315.16	315.32
3	830.58	790.30	745.98	696.16	636.55	563.57	528.67	514.77	506.89	497.83	465.92	466.26
4	1087.89	1032.90	969.91	892.49	788.59	656.14	596.12	573.50	560.96	546.64	496.42	501.72
5	1192.15	1131.20	1060.90	973.88	857.32	711.83	647.29	623.10	609.68	594.30	539.03	534.94
6	1288.26	1216.15	1138.32	1052.01	953.84	839.14	779.36	755.16	741.99	727.94	680.48	681.73
7	1401.48	1335.01	1260.02	1170.50	1051.66	898.78	830.43	804.35	789.58	772.32	708.41	708.43
8	1496.59	1421.77	1337.84	1237.27	1103.51	933.53	859.65	831.93	816.24	797.80	724.73	721.54
9	1772.34	1664.19	1548.33	1422.96	1286.00	1135.87	1042.27	999.04	975.41	948.49	849.69	852.79
10	1817.52	1706.60	1588.57	1460.91	1320.72	1160.10	1063.78	1035.03	1018.31	996.02	900.93	900.93
$\mu_1=0.25$, $\mu_2=0.50$												
1	276.72	273.86	270.75	267.42	263.91	260.27	258.56	257.90	257.55	257.19	253.32	254.02
2	338.62	335.87	332.87	329.64	326.20	322.55	320.80	320.12	319.75	319.37	315.16	315.32
3	504.26	499.34	493.88	487.87	481.40	474.56	471.30	470.03	469.35	468.64	465.92	466.26
4	566.41	556.61	545.87	534.23	521.89	509.02	502.97	500.64	499.40	498.10	496.42	501.72
5	615.41	604.88	593.32	580.77	567.40	553.39	546.76	544.21	542.84	541.41	539.03	534.94
6	716.85	713.85	710.73	707.42	703.82	699.71	697.53	696.62	696.12	695.58	680.48	681.73
7	800.65	787.99	773.91	758.51	742.10	725.11	717.22	714.21	712.62	710.96	708.41	708.43
8	832.89	818.35	802.20	784.54	765.76	746.41	737.48	734.09	732.29	730.41	724.73	721.54
9	995.88	976.23	953.74	929.34	903.57	876.96	864.60	859.86	857.34	854.71	849.69	852.79
10	1002.81	996.62	990.80	979.15	954.61	928.42	916.23	911.55	909.07	906.47	900.93	900.93
$\mu_1=0.25$, $\mu_2=0.75$												
1	466.44	442.37	416.38	386.84	350.95	308.29	288.37	280.59	276.27	271.41	253.32	254.02
2	543.92	517.11	488.53	456.95	420.00	376.13	354.52	345.77	340.84	335.27	315.16	315.32
3	796.88	760.86	721.10	676.03	621.55	555.18	523.38	510.61	503.32	494.93	465.92	466.26
4	1044.38	994.29	936.24	863.88	766.53	644.37	588.84	567.66	555.83	542.26	496.42	501.72
5	1143.40	1087.67	1022.79	941.65	832.99	699.27	639.55	616.87	604.18	589.58	539.03	534.94
6	1221.25	1156.26	1086.26	1008.85	921.43	820.39	768.16	747.12	735.69	723.52	680.48	681.73
7	1350.20	1290.27	1221.88	1138.66	1027.07	885.64	822.07	797.45	783.40	766.92	708.41	708.43
8	1441.76	1374.00	1297.12	1203.36	1077.64	920.16	851.17	824.82	809.79	792.06	724.73	721.54
9	1681.00	1583.70	1479.88	1368.04	1246.58	1114.51	1029.29	988.61	966.14	940.42	849.69	852.79
10	1723.74	1624.00	1518.22	1404.25	1279.85	1138.90	1051.48	1026.15	1010.56	988.65	900.93	900.93
$\mu_1=0.25$, $\mu_2=1$												
1	125.78	127.40	127.61	127.82	128.04	143.09	183.89	200.08	209.52	221.53	253.32	254.02
2	129.14	130.70	130.91	131.13	131.35	146.17	213.62	243.67	259.45	277.20	315.16	315.32

(*continued on next page*)

Table 6 (*continued*)

Catenoid $(B^K_{SSS}B^K_{SSS}B^K_{SSS}B^K_{SSS})$												
p	$p=0$	$p=0.2$	$p=0.5$	$p=1$	$p=2$	$p=5$	$p=10$	$p=15$	$p=20$	$p=30$	$p=+\infty$	
Mode f [Hz]	EDZ4										EDZ4	3D FEM
3	139.99	142.41	142.65	142.90	143.14	165.48	255.61	307.90	337.50	375.19	465.92	466.26
4	144.76	147.19	147.44	147.69	147.94	176.51	273.48	318.69	353.15	392.66	496.42	501.72
5	149.03	189.58	189.74	189.88	189.98	221.29	315.03	347.00	366.44	400.03	539.03	534.94
6	152.52	192.25	192.42	192.56	192.67	234.07	321.00	397.51	449.94	518.89	680.48	681.73
7	165.70	202.01	202.12	202.23	202.33	253.04	355.07	426.75	471.96	531.59	708.41	708.43
8	171.07	202.01	202.40	202.75	203.06	277.45	406.33	489.98	543.80	614.81	724.73	721.54
9	198.40	206.38	206.56	206.71	206.84	281.82	417.11	509.41	570.80	648.01	849.69	852.79
10	216.49	218.74	219.13	219.51	219.87	283.53	422.96	518.09	575.69	666.31	900.93	900.93

Lamination scheme: $\left.\left(70\,/\mathrm{FG}-\mathrm{CNT}^{CNT}_{PM\ (a=1/b=0/c=1/d=1/p)}\ /40\right)\right.$, $h^0_1=h^0_3=0.01\mathrm{m}$, $h^0_2=0.07\mathrm{m}$

Material properties: 1st layer: triclinic material, 2nd layer: FG-CNT ($w_f=0$, $w_r=0.25$), 3rd layer: triclinic material.
Computational grid: LGL distribution with $I_N \times I_M = 25 \times 27$.

Table 7
Free vibration analysis of a helicoidal panel of arbitrary shape reinforced with a general distribution of FG-CNT. The effect of the through-the-thickness distribution has been pointed out for different values of the agglomeration parameter μ_1.

Helicoid $(CFB^K_{SSS}C)$											
f [Hz]	Polymer matrix	$\mu_1=0.1$	$\mu_1=0.2$	$\mu_1=0.3$	$\mu_1=0.4$	$\mu_1=0.5$	$\mu_1=0.6$	$\mu_1=0.7$	$\mu_1=0.8$	$\mu_1=0.9$	$\mu_1=1$
$p=0$											
1	133.92	137.25	141.46	145.50	149.51	153.62	158.02	163.03	169.33	178.76	199.44
2	226.04	232.92	241.53	250.08	258.69	267.54	276.91	287.36	300.09	318.45	357.08
3	270.28	277.66	286.73	295.43	304.04	312.84	322.26	333.00	346.45	366.33	408.47
4	321.01	329.62	340.06	349.95	359.62	369.40	379.77	391.52	406.29	428.57	477.77
5	387.54	398.74	412.76	426.62	440.61	455.09	470.61	488.18	509.96	541.86	609.08
6	419.24	434.35	452.23	469.70	487.07	504.70	523.16	543.47	567.80	602.12	672.36
7	454.58	474.71	498.16	521.29	544.36	567.74	592.02	618.31	649.04	691.09	774.04
8	495.45	515.83	540.30	564.85	589.73	615.29	641.97	669.56	697.03	738.05	838.09
9	559.49	586.23	615.81	634.14	643.11	652.49	664.21	681.73	712.75	761.72	860.68
10	599.49	616.40	628.38	647.81	674.95	701.38	727.67	756.01	790.36	840.07	944.83
$p=0.5$											
1	133.92	136.28	139.43	142.67	146.05	149.65	153.61	158.18	163.88	172.14	189.23
2	226.04	230.83	237.19	243.89	251.04	258.77	267.32	277.10	289.06	305.78	338.72
3	270.28	275.49	282.30	289.28	296.56	304.31	312.85	322.72	335.08	353.00	389.39
4	321.01	327.12	335.04	343.06	351.34	360.09	369.63	380.55	394.15	413.92	455.18
5	387.54	395.39	405.78	416.68	428.27	440.83	454.80	470.94	490.96	519.46	576.56
6	419.24	429.82	443.13	456.98	471.58	487.20	504.28	523.63	546.98	579.10	640.86
7	454.58	468.57	485.89	504.10	523.40	544.10	566.69	592.04	622.07	662.15	736.12
8	495.45	509.56	527.45	546.50	566.97	589.22	613.78	641.52	672.68	707.16	782.43
9	559.49	578.12	600.51	622.65	636.17	644.22	653.14	665.02	684.85	726.72	813.02
10	599.49	613.17	623.53	632.56	650.35	674.72	700.40	727.95	760.30	805.28	894.09
$p=1$											
1	133.92	135.74	138.27	140.96	143.86	147.06	150.66	154.89	160.20	167.78	182.87
2	226.04	229.72	234.75	240.24	246.31	253.10	260.86	270.00	281.35	297.13	326.96
3	270.28	274.30	279.75	285.57	291.84	298.74	306.53	315.69	327.25	343.91	376.84
4	321.01	325.75	332.12	338.84	346.04	353.88	362.67	372.91	385.71	404.06	440.84
5	387.54	393.58	401.84	410.80	420.66	431.68	444.30	459.24	478.00	504.52	555.73
6	419.24	427.38	437.98	449.41	461.90	475.75	491.40	509.64	532.05	562.81	619.77
7	454.58	465.31	479.02	493.97	510.41	528.72	549.42	573.44	602.57	641.50	710.46
8	495.45	506.24	520.33	535.84	553.10	572.54	594.80	620.91	652.54	689.09	750.86
9	559.49	573.78	591.62	610.63	628.99	638.92	646.82	656.54	671.17	703.15	781.99
10	599.49	610.96	620.35	628.02	637.17	656.60	680.92	707.93	739.36	781.79	862.11
$p=5$											
1	133.92	134.57	135.54	136.67	138.03	139.67	141.73	144.39	148.03	153.48	163.71
2	226.04	227.33	229.21	231.44	234.14	237.46	241.69	247.26	255.03	266.88	288.96
3	270.28	271.71	273.80	276.26	279.19	282.75	287.21	293.00	300.94	312.94	335.92
4	321.01	322.70	325.18	328.07	331.51	335.67	340.83	347.49	356.55	370.10	395.60
5	387.54	389.68	392.79	396.48	400.91	406.36	413.25	422.32	434.94	454.20	490.57
6	419.24	422.11	426.13	430.86	436.54	443.50	452.28	463.76	479.61	503.49	547.43
7	454.58	458.32	463.45	469.53	476.87	485.92	497.39	512.47	533.33	564.66	620.99
8	495.45	499.20	504.40	510.59	518.10	527.40	539.28	555.03	577.06	610.62	670.01
9	559.49	564.48	571.21	579.15	588.68	600.30	614.69	631.09	641.83	653.77	683.04
10	599.49	604.33	609.85	614.96	619.98	625.11	630.75	639.43	661.99	698.31	759.44
$p=10$											
1	133.92	134.28	134.83	135.48	136.29	137.32	138.64	140.45	143.08	147.29	155.66
2	226.04	226.75	227.81	229.09	230.67	232.69	235.35	239.02	244.46	253.42	271.66
3	270.28	271.07	272.25	273.68	275.43	277.63	280.51	284.44	290.15	299.37	317.99
4	321.01	321.95	323.35	325.04	327.11	329.70	333.07	337.64	344.24	354.80	375.76
5	387.54	388.72	390.48	392.60	395.22	398.54	402.91	408.93	417.79	432.34	462.04

(*continued on next page*)

Table 7 (*continued*)

Helicoid $(\mathrm{CFB}^{\mathrm{K}}_{\mathrm{SSS}}\mathrm{C})$											
f [Hz]	Polymer matrix	$\mu_1 = 0.1$	$\mu_1 = 0.2$	$\mu_1 = 0.3$	$\mu_1 = 0.4$	$\mu_1 = 0.5$	$\mu_1 = 0.6$	$\mu_1 = 0.7$	$\mu_1 = 0.8$	$\mu_1 = 0.9$	$\mu_1 = 1$
6	419.24	420.83	423.09	425.82	429.18	433.45	439.04	446.71	457.97	476.31	513.11
7	454.58	456.64	459.52	463.00	467.32	472.81	480.04	490.03	504.76	528.86	576.95
8	495.45	497.51	500.42	503.96	508.34	513.94	521.34	531.61	546.89	572.18	623.58
9	559.49	562.24	566.02	570.59	576.22	583.37	592.72	605.46	623.37	640.28	658.93
10	599.49	602.23	605.78	609.51	613.36	617.50	622.10	627.44	634.66	656.70	712.00

Lamination scheme: $.(70\,/\mathrm{FG}-\mathrm{CNT}^{PM}_{CNT(5P)}\,/65\,/\mathrm{FG}-\mathrm{CNT}^{CNT(5P)}_{PM}\,/50),\ \ \mu_2 = 1,\ \ h^0_1 = h^0_3 = h^0_5 = 0.01\mathrm{m},\ \ h^0_2 = h^0_4 = 0.02\mathrm{m}$

Material properties: 1st layer: trigonal material, 2nd layer: FG-CNT ($w_f = 0$, $w_r = 0.25$), 3rd layer: trigonal material, 4th layer: FG-CNT ($w_f = 0$, $w_r = 0.25$), 5th layer: trigonal material.

Computational grid: LGL distribution with $I_N \times I_M = 25 \times 27$.

Table 8

Free vibration analysis of a helicoidal panel of arbitrary shape reinforced with a general distribution of FG-CNT. The effect of the through-the-thickness distribution has been pointed out for different values of the agglomeration parameter μ_2.

Helicoid $(\mathrm{CFB}^{\mathrm{K}}_{\mathrm{SSS}}\mathrm{C})$											
f [Hz]	Polymer matrix	$\mu_2 = 0.1$	$\mu_2 = 0.2$	$\mu_2 = 0.3$	$\mu_2 = 0.4$	$\mu_2 = 0.5$	$\mu_2 = 0.6$	$\mu_2 = 0.7$	$\mu_2 = 0.8$	$\mu_2 = 0.9$	$\mu_2 = 1$
$p = 0$											
1	133.92	226.26	224.04	218.48	211.01	202.57	193.80	188.05	180.97	167.07	141.40
2	226.04	408.71	404.80	394.98	381.77	366.96	351.33	337.43	316.90	288.02	231.91
3	270.28	471.78	467.57	456.94	442.56	426.18	408.61	389.64	367.33	339.77	277.66
4	321.01	540.66	535.54	522.78	505.69	486.47	466.34	449.02	422.19	390.23	328.28
5	387.54	691.70	685.13	668.61	646.25	620.81	593.66	567.75	532.30	486.90	396.30
6	419.24	763.76	756.93	739.77	716.59	690.34	661.99	625.86	590.56	551.55	452.95
7	454.58	874.91	867.01	847.13	820.23	789.48	756.46	721.37	679.68	626.04	471.30
8	495.45	957.15	947.92	924.53	892.24	854.19	812.55	771.21	730.53	671.39	477.28
9	559.49	988.13	977.18	950.02	914.25	875.29	835.13	798.41	758.23	714.77	549.75
10	599.49	1082.11	1071.64	1045.26	1009.72	969.43	926.58	883.17	832.11	767.38	589.50
$p = 0.5$											
1	133.92	210.32	208.56	204.12	198.11	191.21	183.51	180.80	174.67	159.42	137.88
2	226.04	381.74	378.00	370.73	359.58	347.03	333.81	321.14	301.66	283.42	232.55
3	270.28	444.11	440.46	431.67	419.51	405.62	390.67	373.30	352.84	330.97	276.00
4	321.01	507.38	503.05	492.86	478.72	462.60	445.45	428.96	404.37	383.36	325.48
5	387.54	645.43	639.79	626.36	607.69	586.36	563.50	539.66	509.62	475.73	394.35
6	419.24	719.66	713.19	699.67	679.89	657.71	634.37	601.22	570.15	532.23	427.73
7	454.58	822.94	816.63	799.46	776.56	750.21	721.88	689.96	653.71	601.63	469.96
8	495.45	883.30	875.30	854.56	827.00	795.90	762.97	735.13	700.54	647.14	508.13
9	559.49	909.51	900.78	882.15	855.16	824.50	790.88	760.19	744.82	667.71	579.58
10	599.49	1006.95	998.53	977.30	948.60	915.75	880.13	842.80	794.37	739.90	609.58
$p = 1$											
1	133.92	200.60	200.14	195.68	191.88	183.05	180.46	177.48	163.45	156.61	137.71
2	226.04	364.55	365.61	356.11	348.01	334.13	322.51	312.45	299.62	276.27	231.45
3	270.28	425.83	423.35	415.01	404.33	392.17	375.58	363.89	347.46	323.20	274.98
4	321.01	486.27	484.77	474.44	463.62	446.71	431.37	417.90	402.07	375.64	324.43
5	387.54	615.64	612.39	599.61	584.27	564.22	541.92	525.76	501.42	464.02	392.87
6	419.24	690.34	686.47	672.63	653.43	638.75	604.95	586.08	560.42	517.92	425.92
7	454.58	788.18	783.47	768.14	748.37	724.04	693.95	673.20	629.84	583.37	467.14
8	495.45	833.56	827.40	810.10	788.43	760.23	735.75	719.18	658.63	627.10	504.95
9	559.49	867.06	863.33	844.23	821.88	791.20	762.92	748.21	680.90	659.21	575.62
10	599.49	961.05	954.16	935.69	911.46	881.01	846.23	819.95	775.93	720.29	607.19
$p = 5$											
1	133.92	177.20	174.64	169.78	168.11	165.63	162.15	158.11	153.45	148.42	137.02
2	226.04	309.79	310.62	314.49	311.41	292.31	288.74	279.06	267.73	253.86	229.23
3	270.28	365.47	364.95	363.61	357.36	345.73	337.32	326.71	314.16	298.14	272.71
4	321.01	420.32	419.59	419.09	412.52	399.58	390.51	379.60	366.52	349.27	322.01
5	387.54	528.32	525.37	519.49	513.69	495.28	484.07	468.62	450.27	425.75	389.64
6	419.24	590.33	589.65	588.86	572.60	560.35	541.81	523.23	499.85	466.31	421.50
7	454.58	679.03	674.69	651.90	621.67	633.54	613.51	589.84	560.59	521.22	461.04
8	495.45	720.08	714.96	679.12	658.23	677.26	658.05	633.18	601.75	565.02	498.60
9	559.49	768.36	748.08	711.05	694.27	708.85	675.57	663.64	652.35	648.12	567.15
10	599.49	818.88	817.16	809.20	792.71	775.70	752.12	727.06	694.75	656.14	600.95
$p = 10$											
1	133.92	165.21	164.16	162.56	162.56	157.98	155.24	152.00	148.42	143.54	136.84
2	226.04	297.83	293.33	289.27	289.27	278.50	271.99	263.90	254.81	242.81	228.69
3	270.28	344.54	342.38	338.36	338.36	326.27	318.79	310.17	300.22	288.01	272.15
4	321.01	397.06	395.75	391.75	391.75	379.22	371.31	362.39	351.84	338.97	321.40
5	387.54	493.90	490.96	485.26	485.26	467.78	457.05	444.17	429.35	411.58	388.85
6	419.24	549.77	549.81	543.64	543.64	522.09	507.94	492.04	472.76	451.13	420.40
7	454.58	627.38	623.83	615.31	615.31	588.33	571.13	550.57	526.44	497.04	459.55
8	495.45	671.62	668.11	659.67	659.67	631.28	612.56	591.01	566.44	533.91	497.09
9	559.49	677.33	681.14	677.13	677.13	663.04	657.40	648.90	642.49	613.74	565.10
10	599.49	764.99	762.70	754.09	754.09	725.35	706.31	683.10	654.10	628.05	599.24

Lamination scheme: $.\left(70\,/\mathrm{FG}-\mathrm{CNT}^{PM}_{CNT(5P)}\,/65\,/\mathrm{FG}-\mathrm{CNT}^{CNT(5P)}_{PM}\,/50\right),\ \ \mu_1=0.1,\ \ h^0_1=h^0_3=h^0_5=0.01\mathrm{m},\ \ h^0_2=h^0_4=0.02\mathrm{m}$
Material properties: 1st layer: trigonal material, 2nd layer: FG-CNT ($w_f=0$, $w_r=0.25$), 3rd layer: trigonal material, 4th layer: FG-CNT ($w_f=0$, $w_r=0.25$), 5th layer: trigonal material.
Computational grid: LGL distribution with $I_N\times I_M=25\times 27$.

Table 9
Free vibration analysis of a revolution paraboloid of arbitrary shape reinforced with a general distribution of FG-CNT. The effect of the through-the-thickness distribution has been pointed out for different values of the agglomeration parameter μ_1.

Revolution paraboloid $\left(\mathrm{B}^{\mathrm{K}}_{\mathrm{SSS}}\mathrm{FB}^{\mathrm{K}}_{\mathrm{SSS}}\mathrm{C}\right)$											
f [Hz]	Polymer matrix	$\mu_1=0.1$	$\mu_1=0.2$	$\mu_1=0.3$	$\mu_1=0.4$	$\mu_1=0.5$	$\mu_1=0.6$	$\mu_1=0.7$	$\mu_1=0.8$	$\mu_1=0.9$	$\mu_1=1$
$p=0$											
1	146.20	148.25	153.45	159.17	165.72	173.58	183.54	197.10	217.72	256.05	380.09
2	186.82	190.97	199.01	207.63	217.25	228.49	242.41	261.01	288.83	339.96	503.96
3	306.87	310.21	319.86	330.47	342.67	357.39	376.22	402.21	442.39	518.61	771.77
4	313.98	323.76	340.37	358.21	378.10	401.24	429.67	467.26	522.64	621.81	925.98
5	437.48	449.95	469.92	490.19	512.68	539.41	573.27	619.51	689.97	820.89	1240.64
6	456.74	465.73	486.86	511.49	539.86	573.23	614.39	668.91	749.39	892.65	1331.44
7	491.19	500.38	520.66	543.33	569.53	601.02	640.75	694.32	774.13	914.94	1351.72
8	518.38	532.10	554.41	576.71	600.65	628.28	662.71	709.71	783.00	929.77	1433.43
9	541.63	556.29	583.23	612.57	645.50	684.10	731.81	795.06	888.08	1053.82	1562.17
10	602.75	615.36	643.27	675.69	713.74	759.34	816.05	891.02	994.01	1168.92	1762.36
$p=0.5$											
1	146.20	147.46	150.92	154.80	159.30	164.72	171.58	180.95	195.24	221.98	309.42
2	186.82	189.46	194.90	200.88	207.65	215.62	225.50	238.66	258.31	294.37	409.65
3	306.87	309.04	315.66	323.06	331.65	342.06	355.39	373.80	402.40	457.22	643.42
4	313.98	320.26	331.51	343.90	357.91	374.31	394.47	421.02	459.97	529.47	740.74
5	437.48	445.89	460.34	475.46	492.12	511.73	536.50	570.38	622.31	719.58	1035.04
6	456.74	462.34	475.97	492.30	511.85	535.48	565.02	604.30	662.35	766.32	1080.10
7	491.19	497.22	511.06	526.82	545.28	567.64	595.97	634.30	691.70	795.03	1114.12
8	518.38	527.75	543.98	560.84	579.17	600.27	626.31	661.51	715.87	822.37	1200.17
9	541.63	551.29	569.80	590.55	614.31	642.44	677.33	723.66	792.03	914.27	1287.45
10	602.75	610.88	629.39	651.17	677.22	709.04	749.22	802.86	881.67	1021.38	1441.66
$p=1$											
1	146.20	147.08	149.67	152.61	156.04	160.21	165.49	172.69	183.64	204.14	271.70
2	186.82	188.72	192.81	197.40	202.65	208.87	216.60	226.86	242.08	269.81	357.97
3	306.87	308.45	313.49	319.20	325.88	334.01	344.45	358.86	381.23	424.30	573.00
4	313.98	318.54	327.01	336.50	347.38	360.21	376.00	396.71	426.85	480.13	640.43
5	437.48	443.75	455.00	467.15	480.66	496.49	516.34	543.41	584.90	662.99	918.31
6	456.74	460.76	470.78	482.84	497.54	515.70	538.71	569.43	614.67	695.09	934.89
7	491.19	495.63	506.12	518.23	532.56	550.07	572.38	602.65	648.11	730.56	987.13
8	518.38	525.43	538.14	551.74	566.76	584.14	605.51	634.19	678.10	763.33	1067.06
9	541.63	548.79	562.84	578.90	597.58	619.92	647.76	684.73	739.11	836.00	1130.67
10	602.75	608.70	622.52	638.90	658.68	683.12	714.30	756.17	817.76	926.47	1252.79
$p=5$											
1	146.20	146.44	147.28	148.29	149.53	151.10	153.16	156.02	160.41	168.51	194.52
2	186.82	187.38	188.75	190.37	192.35	194.81	197.99	202.31	208.73	220.00	252.88
3	306.87	307.34	309.07	311.14	313.66	316.85	321.06	326.98	336.22	353.88	415.45
4	313.98	315.35	318.17	321.53	325.63	330.73	337.30	346.18	359.16	381.24	440.80
5	437.48	439.48	443.48	448.20	453.88	460.89	469.86	482.05	500.41	534.41	637.16
6	456.74	457.93	461.15	465.10	470.05	476.47	485.12	497.39	516.21	549.62	651.42
7	491.19	492.58	496.15	500.46	505.81	512.62	521.69	534.46	554.20	590.64	703.83
8	518.38	520.67	525.29	530.70	537.15	545.06	555.11	568.66	588.85	625.94	750.28
9	541.63	543.92	548.74	554.55	561.70	570.75	582.63	599.05	623.70	667.17	791.43
10	602.75	604.59	609.16	614.74	621.71	630.70	642.73	659.74	685.82	732.29	865.88
$p=10$											
1	146.20	146.32	146.78	147.35	148.05	148.96	150.19	151.96	154.76	160.04	176.88
2	186.82	187.12	187.86	188.78	189.91	191.37	193.33	196.09	200.35	208.04	230.07
3	306.87	307.12	308.08	309.24	310.69	312.58	315.12	318.78	324.63	335.97	375.04
4	313.98	314.70	316.25	318.13	320.48	323.51	327.56	333.27	342.01	357.50	398.70
5	437.48	438.56	440.77	443.46	446.80	451.07	456.74	464.72	477.00	499.73	570.62
6	456.74	457.37	459.12	461.30	464.06	467.70	472.73	480.11	492.04	514.57	581.20
7	491.19	491.94	493.90	496.31	499.36	503.34	508.77	516.67	529.33	553.58	630.22
8	518.38	519.62	522.19	525.30	529.14	534.02	540.46	549.43	563.14	588.21	668.70
9	541.63	542.87	545.53	548.79	552.90	558.24	565.49	575.91	592.29	622.52	709.56
10	602.75	603.73	606.23	609.32	613.24	618.39	625.48	635.85	652.52	684.00	775.71

Lamination scheme: $\left(70\,/\mathrm{FG}-\mathrm{CNT}^{CNT}_{PM\ (a=1/b=0/c=1/d=1/p)}\ /40\,/\mathrm{FG}-\mathrm{CNT}^{PM}_{CNT\ (a=1/b=0/c=1/d=1/p)}\ /20\right),\ \ h^0_1=h^0_3=h^0_5=0.01\mathrm{m},\ \ h^0_2=h^0_4=0.05\mathrm{m}$
Material properties: 1st layer: graphite-epoxy, 2nd layer: FG-CNT ($w_f=0$, $w_r=0.40$, $\mu_2=1$), 3rd layer: triclinic material, 4th layer: FG-CNT ($w_f=0$, $w_r=0.40$, $\mu_2=1$), 5th layer: graphite-epoxy.
Computational grid: LGL distribution with $I_N\times I_M=25\times 27$.

Table 10
Free vibration analysis of a revolution paraboloid of arbitrary shape reinforced with a general distribution of FG-CNT. The effect of the through-the-thickness distribution has been pointed out for different values of the agglomeration parameter μ_2.

Revolution paraboloid $(B^K_{SSS}FB^K_{SSS}C)$											
f [Hz]	Polymer matrix	$\mu_2 = 0.1$	$\mu_2 = 0.2$	$\mu_2 = 0.3$	$\mu_2 = 0.4$	$\mu_2 = 0.5$	$\mu_2 = 0.6$	$\mu_2 = 0.7$	$\mu_2 = 0.8$	$\mu_2 = 0.9$	$\mu_2 = 1$
$p = 0$											
1	146.20	382.19	376.37	361.52	341.15	317.54	291.80	264.17	234.02	199.17	148.26
2	186.82	504.09	496.44	476.98	450.26	419.27	385.44	349.07	309.27	262.85	190.47
3	306.87	773.20	761.26	730.89	689.31	641.26	589.13	533.57	473.60	405.57	309.38
4	313.98	927.35	913.41	877.88	828.93	771.79	708.88	640.35	563.98	472.52	324.21
5	437.48	1243.57	1223.91	1174.07	1105.81	1026.64	940.25	847.40	745.97	628.62	451.15
6	456.74	1336.13	1315.64	1263.68	1192.50	1109.85	1019.38	921.28	811.59	678.66	468.86
7	491.19	1353.80	1333.66	1282.40	1211.85	1129.58	1039.21	941.38	833.88	704.28	503.56
8	518.38	1438.13	1414.52	1354.28	1271.60	1175.90	1072.05	961.61	843.50	715.90	532.04
9	541.63	1573.82	1550.10	1489.95	1407.40	1311.29	1205.76	1091.18	963.62	809.87	560.70
10	602.75	1773.77	1745.00	1672.54	1573.85	1460.02	1336.79	1206.11	1067.05	901.88	614.96
$p = 0.5$											
1	146.20	311.32	307.16	296.59	282.13	265.40	247.22	227.76	206.62	182.39	147.46
2	186.82	410.01	404.60	390.86	372.03	350.20	326.36	300.71	272.63	239.85	188.97
3	306.87	644.58	635.66	613.04	582.20	546.71	508.43	467.90	424.55	375.94	308.18
4	313.98	742.01	732.31	707.64	673.67	633.99	590.21	542.40	489.00	424.85	320.70
5	437.48	1037.41	1022.58	985.00	933.60	874.13	809.38	739.99	664.51	577.83	446.84
6	456.74	1081.97	1067.70	1031.38	981.28	922.59	857.65	786.56	706.93	611.27	465.66
7	491.19	1118.57	1103.50	1065.41	1013.42	953.28	887.67	816.71	737.64	642.73	500.35
8	518.38	1203.08	1185.01	1139.05	1076.20	1003.83	925.90	844.12	758.60	665.89	527.68
9	541.63	1297.83	1280.46	1236.42	1175.96	1105.49	1027.94	943.46	849.11	735.63	555.68
10	602.75	1443.92	1424.75	1375.94	1308.68	1229.96	1142.91	1047.53	940.35	810.46	610.38
$p = 1$											
1	146.20	273.40	270.16	261.95	250.73	237.76	223.70	208.68	192.42	173.79	147.09
2	186.82	358.38	354.24	343.74	329.34	312.63	294.36	274.68	253.08	227.72	188.23
3	306.87	573.99	566.79	548.56	523.77	495.35	464.82	432.67	398.49	360.36	307.58
4	313.98	641.62	634.28	615.62	589.91	559.83	526.57	490.17	449.34	399.85	318.98
5	437.48	920.45	908.44	878.00	836.37	788.25	735.94	680.00	619.34	549.92	444.60
6	456.74	936.64	925.75	898.05	859.86	815.06	765.40	710.85	649.48	575.25	464.15
7	491.19	991.53	979.46	948.95	907.26	859.00	806.26	749.13	685.64	610.18	498.75
8	518.38	1069.16	1054.52	1017.30	966.48	908.10	845.53	780.25	712.17	637.71	525.36
9	541.63	1140.02	1126.33	1091.62	1043.93	988.32	927.05	860.19	785.39	695.12	553.17
10	602.75	1254.66	1239.70	1201.67	1149.36	1088.25	1020.76	946.81	863.55	762.13	608.15
$p = 5$											
1	146.20	195.43	194.18	191.00	186.65	181.62	176.16	170.29	163.87	156.44	146.45
2	186.82	253.04	251.55	247.75	242.48	236.27	229.36	221.73	213.06	202.43	186.89
3	306.87	415.76	412.71	405.02	394.61	382.77	370.14	356.91	342.84	327.07	306.46
4	313.98	441.63	439.08	432.52	423.34	412.36	399.88	385.71	369.07	347.88	315.77
5	437.48	637.94	633.86	623.21	607.85	588.85	567.07	543.10	516.67	485.60	440.16
6	456.74	654.85	649.67	636.71	619.51	600.40	580.04	557.85	532.54	501.79	461.43
7	491.19	707.80	702.60	689.37	671.18	649.96	626.60	601.15	572.88	539.70	495.64
8	518.38	750.82	744.92	729.87	709.22	685.42	659.82	632.84	603.89	570.34	520.61
9	541.63	797.85	792.32	778.17	758.56	735.38	709.39	680.38	647.03	606.05	548.28
10	602.75	866.88	860.81	845.40	824.27	799.52	771.92	741.09	705.54	662.03	603.96
$p = 10$											
1	146.20	177.43	176.63	174.59	171.79	168.54	164.99	161.17	156.99	152.22	146.33
2	186.82	230.01	229.04	226.55	223.06	218.93	214.27	209.07	203.12	196.00	186.63
3	306.87	374.98	373.06	368.19	361.61	354.10	346.06	337.59	328.55	318.49	306.23
4	313.98	399.41	397.71	393.32	387.09	379.54	370.83	360.83	349.06	334.55	315.12
5	437.48	571.71	568.76	561.04	550.04	536.85	522.13	506.05	488.20	467.17	439.21
6	456.74	584.54	581.37	573.42	562.70	550.31	536.56	521.30	504.09	484.27	460.89
7	491.19	634.17	630.67	621.75	609.43	595.02	579.12	561.82	542.79	521.15	494.98
8	518.38	668.90	665.10	655.43	642.20	626.96	610.45	592.78	573.39	550.58	519.55
9	541.63	715.25	711.48	701.78	688.20	672.00	653.65	633.09	609.65	581.96	547.22
10	602.75	776.39	772.39	762.15	747.87	730.87	711.62	690.03	665.50	637.03	603.08

Lamination scheme: $\left(70\,/\mathrm{FG}-\mathrm{CNT}^{CNT}_{PM\ (a=1/b=0/c=1/d=1/p)}\ /40\,/\mathrm{FG}-\mathrm{CNT}^{PM}_{CNT\ (a=1/b=0/c=1/d=1/p)}\ /20\right)$, $h^0_1 = h^0_3 = h^0_5 = 0.01\mathrm{m}$, $h^0_2 = h^0_4 = 0.05\mathrm{m}$
Material properties: 1st layer: graphite-epoxy, 2nd layer: FG-CNT ($w_f = 0$, $w_r = 0.40$, $\mu_1 = 0.1$), 3rd layer: triclinic material, 4th layer: FG-CNT ($w_f = 0$, $w_r = 0.40$, $\mu_1 = 0.1$), 5th layer: graphite-epoxy.
Computational grid: LGL distribution with $I_N \times I_M = 25 \times 27$.

References

[1] Saleh B, et al. 30 Years of functionally graded materials: an overview of manufacturing methods, applications and future challenges. Engineering 2020; 201:108376.
[2] Garg A, et al. A review of the analysis of sandwich FGM structures. Compos Struct 2021;258:113427.
[3] Eschenauer HA, Olhoff N. Topology optimization of continuum structures: a review. Appl Mech Rev 2001;54:331–90.
[4] Oden JT, Reddy JN. An introduction to the mathematical theory of finite elements. New York: Dover Publications Inc; 1976.
[5] Zienkiewicz O.C., Taylor R.L., The finite element method: solid mechanics, Butterworth Heinemann, Oxford, 2000.
[6] Hughes TJ, Akin JE. Techniques for developing special finite element shape functions with particular reference to singularities. Int J Numer Methods Eng 1980;15:733–51.
[7] Taylor RL. On completeness of shape functions for finite element analysis. Int J Numer Methods Eng 1972;4:17–22.

[8] Hughes TJR, Cottrell JA, Bazilevs Y. Isogeometric analysis: CAD, finite elements, NURBS, exact geometry and mesh refinement. Comput Methods Appl Mech Engineer 2005;194:4135–95.
[9] Piegl L. On NURBS: a survey. IEEE Comput Graph Appl 1991;10:55–71.
[10] Dimitri R. Isogeometric treatment of large deformation contact and debonding problems with T-splines: a review. Curv Layer Struc 2015;2:59–90.
[11] Reddy JN. Mechanics of laminated composite plates and shells. Boca Raton: CRC Press; 2003.
[12] Tornabene F. Hygro-thermo-magneto-electro-elastic theory of anisotropic doubly-curved shells. Esculapio, Bologna 2023.
[13] Reddy JN. An evaluation of equivalent-single-layer and layerwise theories of composite laminates. Compos Struct 1993;25:21–35.
[14] Liew KM, Pan ZZ, Zhang LW. An overview of layerwise theories for composite laminates and structures: development, numerical implementation and application. Compos Struct 2019;216:240–59.
[15] Tornabene F. General higher-order layer-wise theory for free vibrations of doubly-curved laminated composite shells and panels. Mech Advan Mater Struc 2016;23:1046–67.
[16] Robbins Jr DH, Reddy JN. Modelling of thick composites using a layerwise laminate theory. Int J Numer Methods Eng 1993;36:655–77.
[17] Love AEH. A treatise on the mathematical theory of elasticity. Cambridge: Cambridge University Press; 2013.
[18] Mindlin R. Influence of rotatory inertia and shear on flexural motions of isotropic, elastic plates. J Appl Mech 1951;18:31–8.
[19] Reddy JN, Liu C. A higher-order shear deformation theory of laminated elastic shells. Int J Eng Sci 1985;23:319–30.
[20] Tornabene F, Viscoti M, Dimitri R, Reddy JN. Higher Order Theories for the vibration study of doubly curved anisotropic shells with a variable thickness and isogeometric mapped geometry. Compos Struct 2021;267:113829.
[21] Reddy JN, Wang CM, Lee KH. Relationships between bending solutions of classical and shear deformation beam theories. Int J Solids Struct 1997;34:3373–84.
[22] Reddy JN, Wang CM. An overview of the relationships between solutions of the classical and shear deformation plate theories. Compos Sci Technol 2000;60:2327–35.
[23] Wang CM, Lim GT, Reddy JN, Lee KH. Relationships between bending solutions of Reissner and Mindlin plate theories. Engineer Struc 2001;23:838–49.
[24] Tornabene F, Viscoti M, Dimitri R. Generalized higher order layerwise theory for the dynamic study of anisotropic doubly-curved shells with a mapped geometry. Eng Anal Bound Elem 2022;134:147–83.
[25] Tornabene F, Viola E, Fantuzzi N. General higher-order equivalent single layer theory for free vibrations of doubly-curved laminated composite shells and panels. Compos Struct 2013;104:94–117.
[26] Viola E, Tornabene F, Fantuzzi N. Static analysis of completely doubly-curved laminated shells and panels using general higher-order shear deformation theories. Compos Struct 2013;101:59–93.
[27] Avhad PV, Sayyad AS. On the deformation of laminated composite and sandwich curved beams. Curv Layer Struc 2022;9:1–12.
[28] Pagano NJ. Exact solutions for composite laminates in cylindrical bending. J Compos Mater 1969;3:398–411.
[29] Toledano A, Murakami H. A high-order laminated plate theory with improved in-plane responses. Int J Solids Struc 1987;23:111–31.
[30] Murakami H. Laminated composite plate theory with improved in-plane responses. J Appl Mech 1986;53:661–6.
[31] Tessler A, Di Sciuva M, Gherlone M. A refined zigzag beam theory for composite and sandwich beams. J Compos Mater 2009;43:1051–81.
[32] Iurlaro L, et al. Assessment of the refined zigzag theory for bending, vibration, and buckling of sandwich plates: a comparative study of different theories. Compos Struct 2013;106:777–92.
[33] Iurlaro L, et al. Refined zigzag theory for laminated composite and sandwich plates derived from Reissner's Mixed Variational Theorem. Compos Struct 2015;133:809–17.
[34] Washizu K. Variational methods in elasticity and plasticity. Oxford: Pergamon Press; 1975.
[35] Reddy JN. A generalization of two-dimensional theories of laminated composite plates. Commun Appl Numer Methods 1987;3:173–80.
[36] Phan ND, Reddy JN. Analysis of laminated composite plates using a higher-order shear deformation theory. Int J Numer Methods Eng 1985;21:2201–19.
[37] Tornabene F, Viscoti M, Dimitri R. Higher order formulations for doubly-curved shell structures with a honeycomb core. Thin-Walled Struc 2021;164:107789.
[38] Tornabene F, Viscoti M, Dimitri R, Aiello MA. Higher-order modeling of anisogrid composite lattice structures with complex geometries. Engineer Struc 2021;244:112686.
[39] Tornabene F. Free vibration analysis of functionally graded conical, cylindrical shell and annular plate structures with a four-parameter power-law distribution. Comput Methods Appl Mech Eng 2009;198:2911–35.
[40] Tornabene F, Viola E. Free vibration analysis of functionally graded panels and shells of revolution. Meccanica 2009;44:255–81.
[41] Tornabene F, Viola E. Static analysis of functionally graded doubly-curved shells and panels of revolution. Meccanica 2013;48:901–30.
[42] Brischetto S, et al. 3D exact and 2D generalized differential quadrature models for free vibration analysis of functionally graded plates and cylinders. Meccanica 2016;51:2059–98.
[43] Shen HS. Functionally graded materials: nonlinear analysis of plates and shells. Boca Raton: CRC Press; 2016.
[44] Sofiyev AH. Review of research on the vibration and buckling of the FGM conical shells. Compos Struct 2019;211:301–17.
[45] Yousefi AH, Memarzadeh P, Afshari H, Hosseini SJ. Optimization of CNT/polymer/fiber laminated truncated conical panels for maximum fundamental frequency and minimum cost. Mech Based Des Struc Mach 2023;51:3922–44.
[46] Hadj B, Rabia B, Daouadji TH. Influence of the distribution shape of porosity on the bending FGM new plate model resting on elastic foundations. Struc Engineer Mech 2019;72:61–70.
[47] Fu T, Wu X, Xiao Z, Chen Z. Thermoacoustic response of porous FGM cylindrical shell surround by elastic foundation subjected to nonlinear thermal loading. Thin-Walled Struc 2020;156:106996.
[48] Jones RM. Mechanics of composite materials. Boca Raton: CRC Press; 2018.
[49] Tornabene F, et al. Multiscale approach for three-phase CNT/polymer/fiber laminated nanocomposite structures. Polym Compos 2019;40:E102–26.
[50] Hahn HT. Simplified formulas for elastic moduli of unidirectional continuous fiber composites. J Compos, Technol Res 1980;2:5–7.
[51] Tsai S.W., Structural behavior of composite materials, NASACR71 (1964).
[52] Hill R. Theory of mechanical properties of fibre-strengthened materials: I. Elastic behaviour. J Mech Phys Solids 1964;12:199–212.
[53] Odegard GM, et al. Constitutive modelling of nanotube–reinforced polymer composites. Compos Sci Technol 2003;63:1671–87.
[54] Ghasemi AR, Mohammadi MM, Mohandes M. The role of carbon nanofibers on thermo-mechanical properties of polymer matrix composites and their effect on reduction of residual stresses. Engineering 2015;77:519–27.
[55] Aragh BS, Farahani EB, Barati AN. Natural frequency analysis of continuously graded carbon nanotube-reinforced cylindrical shells based on third-order shear deformation theory. Mathem Mech Solids 2013;18:264–84.
[56] Ghasemi AR, et al. Agglomeration effects on the vibrations of CNTs/fiber/polymer/metal hybrid laminates cylindrical shell. Engineering 2019;167:700–16.
[57] Iijima S. Helical microtubules of graphitic carbon. Nature 1991;354:56–8.
[58] Soni SK, Thomas B, Kar VR. A comprehensive review on CNTs and CNT-reinforced composites: syntheses, characteristics and applications. Mater Today Commun 2020;25:101546.
[59] Bakshi SR, Lahiri D, Agarwal A. Carbon nanotube reinforced metal matrix composites-a review. Int Mater Rev 2010;55:41–64.
[60] Yang X, et al. Effect of carbon nanotube (CNT) content on the properties of in-situ synthesis CNT reinforced Al composites. Mater Sci Engineer: A 2016;660:11–8.
[61] Valentino O, et al. Influence of the polymer structure and nanotube concentration on the conductivity and rheological properties of polyethylene/CNT composites. Physica E 2008;40:2440–5.
[62] Shi DL, et al. The effect of nanotube waviness and agglomeration on the elastic property of carbon nanotube-reinforced composites. J Eng Mater Technol 2004;126:250–7.
[63] Shao LH, et al. Prediction of effective moduli of carbon nanotube–reinforced composites with waviness and debonding. Compos Struct 2009;87:274–81.
[64] Seidel GD, Lagoudas DC. Micromechanical analysis of the effective elastic properties of carbon nanotube reinforced composites. Mech Mater 2006;38:884–907.
[65] Abdulrehman MA, Hussein MAM, Marhoon II. Temperature-dependent mechanical properties of Al/Cu nanocomposites under tensile loading via molecular dynamics method. Curv Layer Struc 2022;9:96–104.
[66] Mori T, Tanaka K. Average stress in matrix and average elastic energy of materials with misfitting inclusions. Acta Metallurgica 1973;21:571–4.
[67] Tornabene F, et al. Effect of agglomeration on the natural frequencies of functionally graded carbon nanotube-reinforced laminated composite doubly-curved shells. Engineering 2016;89:187–218.
[68] Nejati M, et al. Static and free vibration analysis of functionally graded conical shells reinforced by carbon nanotubes. Int J. Mech Sci 2017;130:383–98.
[69] Kamarian S, et al. Free vibration analysis of conical shells reinforced with agglomerated carbon nanotubes. Int J Mech Sci 2016;108:157–65.
[70] Banić D, et al. Influence of Winkler-Pasternak foundation on the vibrational behavior of plates and shells reinforced by agglomerated carbon nanotubes. Appl Sci 2017;7:1228.
[71] Medani M, et al. Static and dynamic behavior of (FG-CNT) reinforced porous sandwich plate using energy principle. Steel Comp Struc 2019;32:595–610.
[72] Kiani Y, Dimitri R, Tornabene F. Free vibration of FG-CNT reinforced composite skew cylindrical shells using the Chebyshev-Ritz formulation. Engineering 2018;147:169–77.
[73] Sofiyev AH, et al. Buckling behavior of FG-CNT reinforced composite conical shells subjected to a combined loading. Nanomaterials 2020;10:419.
[74] Li H, et al. Free vibration characteristics of functionally graded porous spherical shell with general boundary conditions by using first-order shear deformation theory. Thin-Walled Struc 2019;144:106331.
[75] Kim K, et al. A method for natural frequency calculation of the functionally graded rectangular plate with general elastic restraints. AIP Adv 2020;10:085203.
[76] Tornabene F, Viscoti M, Dimitri R. Higher order theories for the free vibration analysis of laminated anisotropic doubly-curved shells of arbitrary geometry with general boundary conditions. Compos Struct 2022;297:115740.
[77] Tornabene F, Viscoti M, Dimitri R. Static analysis of anisotropic doubly-curved shells with arbitrary geometry and variable thickness resting on a Winkler-Pasternak support and subjected to general loads. Eng Anal Bound Elem 2022;140:618–73.
[78] Tornabene F, Viscoti M, Dimitri R. Static analysis of anisotropic doubly-curved shell subjected to concentrated loads employing higher order layer-wise theories. Comp Method Engineer Sci 2023;134:1393–468.

[79] Finlayson BA, Scriven LE. The method of weighted residuals-a review. Appl Mech Rev 1966;19:735–48.
[80] Hughes TJ. The finite element method: linear static and dynamic finite element analysis. New York: Dover Publications; 2012.
[81] Avhad PV, Sayyad AS. On the deformation of laminated composite and sandwich curved beams. Curv Layer Struc 2023;9:1–12.
[82] Tornabene F, Fantuzzi N, Ubertini F, Viola E, et al. Strong formulation finite element method based on differential quadrature: a survey. Appl Mech Rev 2015; 67:020801.
[83] Tornabene F, Fantuzzi N, Bacciocchi M. A new doubly-curved shell element for the free vibrations of arbitrarily shaped laminated structures based on weak formulation IsoGeometric analysis. Compos Struct 2017;171:429–61.
[84] Tornabene F, Fantuzzi N, Bacciocchi M. Strong and weak formulations based on differential and integral quadrature methods for the free vibration analysis of composite plates and shells: convergence and accuracy. Eng Anal Bound Elem 2018;92:3–37.
[85] Tornabene F, Viscoti M, Dimitri R. Equivalent single layer higher order theory based on a weak formulation for the dynamic analysis of anisotropic doubly-curved shells with arbitrary geometry and variable thickness. Thin-Walled Struc 2022;174:109119.
[86] Orszag SA. Numerical methods for the simulation of turbulence. Phys Fluids 1969;12:II–250.
[87] Shu C, Richards BE. Application of generalized differential quadrature to solve two-dimensional incompressible Navier-Stokes equations. Int J Numer Methods Fluids 1992;15:791–8.
[88] Shu C. Differential quadrature and its application in engineering. London: Springer; 2000.
[89] Bert CW, Malik M. Differential quadrature method in computational mechanics: a review. Appl Mech Rev 1996;49:1–28.
[90] Wang X. Differential quadrature and differential quadrature-based element methods: theory and applications. Butterworth-Heinem, Waltham 2015.
[91] Tornabene F. Generalized Differential and Integral Quadrature. Esculapio, Bologna 2023.
[92] Dastjerdi S, et al. Nonlocal elasticity analysis of moderately thick porous functionally graded plates in a hygro-thermal environment. Compos Struct 2021; 255:112925.
[93] Fazzolari FA, Viscoti M, Dimitri R, Tornabene F. 1D-Hierarchical Ritz and 2D-GDQ Formulations for the free vibration analysis of circular/elliptical cylindrical shells and beam structures. Compos Struct 2021;258:113338.
[94] Tornabene F, Dimitri R, Viola E. Transient dynamic response of generally-shaped arches based on a GDQ-time-stepping method. Int J Mech Sci 2016;114:277–314.
[95] Dimitri R, Tornabene F, Reddy JN. Numerical study of the mixed-mode behaviour of generally-shaped composite interfaces. Compos Struct 2020;237:111935.
[96] Matbuly MS, Ragb O, Nassar M. Natural frequencies of a functionally graded cracked beam using the differential quadrature method. Appl Math Comput 2009; 215:2307–16.
[97] Szekrenyes A. Application of differential quadrature method to delaminated first-order shear deformable composite plates. Thin-Walled Struc 2021;166:108028.
[98] Razminia K, Razminia A, Baleanu D. Investigation of the fractional diffusion equation based on generalized integral quadrature technique. Appl Math Model 2015;39:86–98.
[99] Shu C, Chew YT, Richards BE. Generalized differential and integral quadrature and their application to solve boundary layer equations. Int J Numer Methods Fluids 1995;21:723–33.
[100] Jang SK, Bert CW, Striz AG. Application of differential quadrature to static analysis of structural components. Int J Numer Methods Eng 1989;28:561–77.
[101] Shu C, et al. Solutions of three-dimensional boundary layer equations by global methods of generalized differential-integral quadrature. Int J Numer Methods Heat Fluid Flow 1996;6:61–75.
[102] Sharma P. Numerical study of grid distribution effect on accuracy of GDQ method of FGPM actuator. Proceedings 2021;45:5706–8.
[103] Shu C, Du H. A generalized approach for implementing general boundary conditions in the GDQ free vibration analysis of plates. Int J Solids Struct 1997; 34:837–46.
[104] Shu C, Du H. Implementation of clamped and simply supported boundary conditions in the GDQ free vibration analysis of beams and plates. Int J Solids Struct 1997;34:819–35.
[105] Tornabene F, Fantuzzi N, Bacciocchi M. DiQuMASPAB: differential quadrature for mechanics of anisotropic shells. Plates, Arch Beams, Esculapio, Bologna 2018.